DEGRADATION MONITORING USING PROBABILISTIC INFERENCE

by

Bulent Alpay

A dissertation submitted in partial fulfillment
of the requirements for the degree of
Doctor of Philosophy
(Nuclear Engineering and Radiological Sciences)
in The University of Michigan
2008

Doctoral Committee:

Professor James Paul Holloway, Chair
Professor Iain D. Boyd
Professor William R. Martin
Professor Tunc Aldemir, The Ohio State University

2008

To my parents

ACKNOWLEDGEMENTS

I would like to thank the faculty and staff in the Department of Nuclear Engineering and Radiological Sciences at the University of Michigan for their assisiance in this journey. I would ike to express my gratitude to Professor James Paul Holloway for his supervision, guidance and commitment. I also would like to thank Professor John C. Lee for giving me the opportunity to advance my knowledge in this area. Special thanks to Ms. Peggy Jo Gramer for assisting me whenever I need it. I would like to especially thank my wife Kasey, for her support in every stage of this endeavor and for making this real.

TABLE OF CONTENTS

LIST OF FIGURES

LIST OF TABLES

LIST OF APPENDICES

CHAPTER 1
INTRODUCTION

In order to increase safety and improve economy and performance in nuclear power plants, the source and extent of component degradations should be identified before failures and breakdowns occur. Having an efficient and robust degradation monitoring system provides valuable information about the onset and progress of degradations to the operator or any decision maker in order to allow better analysis of the current state of the plant and make better decisions on the plant operation. This helps to:

- Prevent loss of safety and sustain the controllability of the plant by taking corrective actions to prevent the failure of the degraded component, to prevent this degradation from triggering another degradation or a failure (tightly coupled events) and to take precautions to reduce the impact of the failure of this component on its environment
- Improve the economy and performance of a plant by optimizing the scheduled maintenance intervals based on real time component degradation information and using an additional prognosis step by which the expected failure time of the degraded component can be predicted, and hence increase the capacity factors.

It is crucial for the next generation of nuclear power plants, which are designed to have a long core life and high fuel burnup, to have a degradation monitoring system. For example, the IRIS (International Reactor Innovative and Secure) reactor, which has an integral configuration was designed to have a three year fuel cycle [1]. If

not detected in advance, degradation of one of the components may result in a failure that can lead to loss of safety or an unanticipated shutdown before the next refueling period. Therefore, it is essential to detect and diagnose the degradations in order to keep the reactor in a safe state, to meet the designed reactor core lifetime and to optimize the scheduled maintenance.

We assume that degradations take place before failures occur, but the time required for a degradation to progress to a failure varies for every component. In Figure 1, we illustrate the evolution of degradation in time. During the nominal operating conditions, the degradation monitoring system is in operation in order to detect degradation. After the onset of degradation, the degradation monitoring system is designed to detect the degradation and isolate the probable components that can lead to that degradation in a multicomponent system. The severity of the degradation should also be identified by estimating the magnitude of the change from the nominal. These three tasks should be performed before the degradation is so severe that there is no time to take any corrective actions, or none of these actions can help prevent the failure of that component and reduce the impact of this failure within the system in a timely manner.

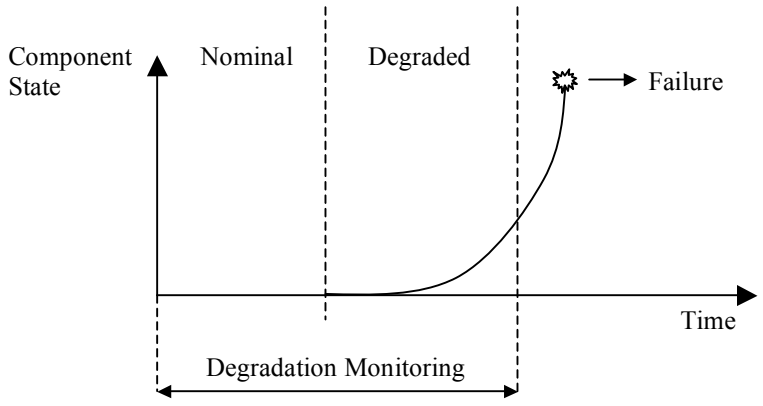

Figure 1. The evolution of degraded component state in time.

Nevertheless not all degradations in the components necessarily result in a failure, but still they may reduce the efficiency and safety margins of the system and therefore they should be monitored.

The nuclear industry, like other large industries, presents challenges on constructing a framework for degradation monitoring. Nuclear power plants are comprised of systems in which many components interact in a very complex way. Some of these components are tightly coupled with each other and may result in cascade failures in the system where the origin of the event may be hard to identify. Since in many instances it is impossible to observe the characteristics of these components directly, observable states are used to infer these characteristics. However, both neutronic and thermal hydraulic design limitations in the nuclear power plants restricts the number of sensors to be used and the choice of sensor locations. Also small component degradations are particularly hard to identify because their signatures in the observations may not be noticeable. An extreme environment in a nuclear power plant can also cause the sensors to degrade in addition to the components, and this may result in inaccurate measurements. The system models in nuclear power plants, which are used to provide analytical redundancy, may also be highly nonlinear and low fidelity. Treating these nonlinearities with approximations in order to obtain a tractable model may introduce additional uncertainty into the identification of component degradations. The substantial modeling errors in low fidelity systems and simultaneous multicomponent degradations may also mask the signature of degradations to be identified.

In this dissertation, our main goal is to develop techniques for degradation monitoring in nuclear power plants by addressing the challenges described above. Our objectives are:

- To construct a unified framework for degradation monitoring based on sequential probabilistic inference using nonlinear filtering for high dimensional and nonlinear systems

- To utilize a reliability degradation database within this framework to:
    - Improve estimation of nominal states for low fidelity system models
    - Design a robust degradation detection and isolation scheme
    - Develop techniques to improve the performance of a filter when it cannot follow an abrupt change due to obliviousness or sample impoverishment
- To develop practical algorithms that work online, in particular by developing a method that can work with relatively few particles
- To test these algorithms for monitoring simultaneous multicomponent degradations.

There have been a variety of methods proposed for the tasks of degradation/fault monitoring. These methods can be analyzed under three broad groups: model-based, knowledge-based and signal processing methods. Model-based methods utilize the process measurements with the model of the monitored plant. These methods use residuals that indicate the inconsistencies between the actual system behavior and the expected system behavior, which is obtained by using the system model. These residuals can be used for detection and diagnostic purposes [2,3]. Model-based techniques like diagnostic observers, parity equations and state/parameter estimation techniques can be used for degradation monitoring. Diagnostic observer [4,5] and sliding mode observer [6] methods are based on reconstructing the outputs of the system from the measurements with the aid of the observers or filters to obtain residuals for detection and isolation of the faults. Parity equations [7-9] are based on simple algebraic projections and geometry. This method computes a residual vector that is zero when no fault is present, and non-zero otherwise, to detect that a fault has occurred. The residual will also be different for different faults, to enable diagnosing which fault has occurred [10]. State estimation techniques are based on estimation of unobservable states by using the observations and the system model. A detailed literature review for state/parameter estimation will be performed in Chapter 2. Recent progress made in system identification (parameter estimation) is discussed in a review paper [11].

Knowledge-based methods are proposed [12,13] for problems when system models are not precisely known. Knowledge about the structure of the process, the functions of systems and components, and qualitative models of the system under various faulty conditions are required to estimate the system dynamics. Heuristic knowledge from the training processes is of great importance. Some of the knowledge-based methods also use certain models built by neural networks, fuzzy systems, or expert systems to map the inputs and outputs of the unknown system [14]. As in model-based methods, residuals are generated to detect and diagnose degradations [15,16].

Signal processing methods like wavelet analysis [17], principal components analysis [18], etc., are based on signal decomposition and are also being used in degradation monitoring. Even though signal processing techniques have superior capability in identifying faults, they have difficulties with noises, disturbances and uncertainties that are not accounted for in the training process; these can make the online signal clusters differ from the expected ones, thus causing errors in fault diagnosis [14].

Hybrid methods are also used for the tasks of degradation monitoring. Alpay and Garcia [19] utilized model-based and data-driven methods in a parallel hybrid modeling structure to minimize modeling uncertainty in order to obtain a sensitive anomaly detection method. Yildiz and Golay [20] combined several artificial intelligence techniques for fault diagnosis and prognosis.

One particular system estimation approach using a discrete cell-to-cell mapping technique [21,22] can account for uncertainties in system modeling and monitored state to generate probabilistic ranking of possible faults. An application of the technique for online risk monitoring [22] of a pressurizer indicates the importance of developing probabilistic techniques for system monitoring and diagnosis.

Since there has been extensive work on the modeling of nuclear power plants, and since high dimensional states and degradations of unknown origin it is relatively harder to utilize knowledge-based and signal processing methods, so we have employed model-

based methods in this dissertation. For the cases when the system model is low fidelity or when degradations change the system parameters, in order to minimize the discrepancy between the real and modeled system behavior, we proposed to utilize a database with the model-based method to construct a hybrid model structure. The "mixing" factor of each data source is determined by using the residuals in a multiple hypothesis testing scheme in this hybrid model. For the model-based part, we focused on state/parameter estimation techniques in a sequential probabilistic inference framework. A detailed review of available techniques for state and parameter estimation is performed in Chapter 2. In Section 2.1 we first describe a general hidden Markov model. We then state our assumptions for degradation monitoring and modify this model by introducing component states, which are the parameters of degradation we need to monitor. In Section 2.2 we derive the framework for recursive Bayesian estimation to solve the sequential probabilistic inference problem. We also define the well-posedness and optimality of the solution to recursive Bayesian estimation problem. Since the optimal solution is intractable, approximate methods seeking suboptimal solutions are reviewed in Section 2.3. In Section 2.4, we address the problem of treating nonlinearity in transforming a probability density function (pdf). We review nonlinear extensions of Kalman filtering and particle filtering, and their approximations for dealing with the nonlinearities in the system model. In Subsection 2.4.2, we investigate the approximation of linearizing the nonlinear system model around the nominal state, which is the basis for extended Kalman filtering (EKF). In Subsection 2.4.3, we review the unscented transform in which an approximation of a pdf is performed by finding a set of points (deterministic sampling) to match certain moments of that pdf, rather than approximating the nonlinear system model. We also derive the unscented Kalman filtering (UKF) based on this approximation, and present an application of degradation monitoring in which we detect and diagnose fouling in steam generators of the IRIS reactor using UKF in Subsection 2.4.3.5. In Subsection 2.4.4 we review particle filtering, which is a sequential Monte Carlo method based on approximating the pdf as in the UKF but instead with stochastic samples. We also derive the sampling importance resampling algorithm on which we base our degradation monitoring technique.

In Chapter 3, we address the inability of a filter to respond to an abrupt change and propose solutions to this problem by introducing another data source, namely a reliability degradation database. In Section 3.1, we construct a joint estimation framework to estimate both the system states and component states (state and parameters). In Subsection 3.2.1, we present the problem of obliviousness in nonlinear extensions of Kalman filtering. We propose an algorithm based on covariance matching in EKF that works adaptively in a multiple hypothesis testing setting. We apply this algorithm for the diagnosis of degradations of multiple components. We test our algorithm with a balance of plant (BOP) model of a boiling water reactor (BWR). We also propose another algorithm to combine a UKF algorithm with the reliability degradation database by solving a multiobjective optimization problem. We present an application of this scheme in degradation monitoring of a fast reactor. In Subsection 3.2.2 we address the sample impoverishment problem in the particle filtering and its negative effect on detection and diagnosis of component degradations. We briefly review different techniques for this problem and in Section 3.3 we propose a novel technique that uses the Metropolis Hastings algorithm, which is a well known Markov chain Monte Carlo (MCMC) method, in order to introduce a reliability degradation database into particle filtering. This technique, which works as a multiple hypothesis testing algorithm, helps the filter to explore the state space to efficiently and accurately estimate the component degradations. In addition to the estimation of the magnitude of degradations, by monitoring the relative likelihoods of the hypotheses this algorithm also determines the degradation mode. In Subsection 3.3.3, we extended this algorithm to be used in degradation detection and isolation by introducing another database for detection and isolation purposes. The schematic of this algorithm is shown in Figure 2.

In Chapter 4, we test our new algorithm with a balance of plant model of a boiling water reactor. In Section 4.1, we describe the system model, and system/component states, which we estimate in our degradation monitoring algorithm. In Subsection 4.1.2, we list the process observation variables and analyze the detectability of degradations through the measurements. We present a representative reliability degradation database, which we

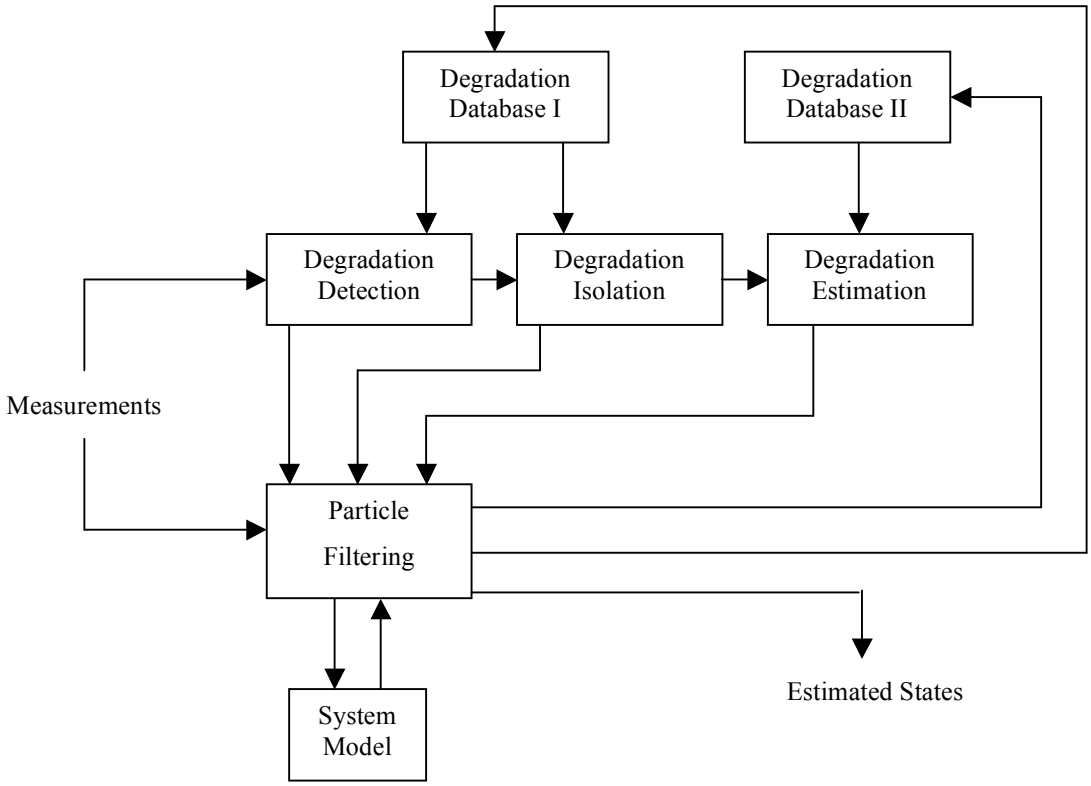

Figure 2. The schematic of the degradation monitoring algorithm.

utilize in constructing the multiple hypotheses to be tested through the Metropolis Hastings algorithm in Section 4.2. In Section 4.3 we analyze the performance of the particle filtering algorithm with respect to the magnitude of modeling noise, sample size and ability to respond to an abrupt change in the component states. We test the degradation detection and isolation part of our algorithm in Section 4.4. We simulate single degradations and simultaneous binary and triple degradations to evaluate the performance of this algorithm. In Section 4.5, we use selected single, binary and triple degradations to test the degradation estimation part of our algorithm.

In summary, our contributions in this dissertation are:

- We develop techniques to modify filtering algorithms in order to utilize additional data sources in detection and estimation of degradations

- We construct a degradation monitoring framework in which we use a novel multiple hypothesis testing algorithm based on the Metropolis Hastings method that utilizes a reliability degradation database:
    - To solve the sample impoverishment problem in particle filtering
    - To improve the performance of particle filtering for small sample size and low fidelity models
    - To construct a degradation detection and isolation algorithm
    - To construct a degradation estimation algorithm:
        - To estimate the magnitude of the degradations
        - To identify degradation modes by which the component degrades.

CHAPTER 2
ESTIMATION THEORY

Estimation in nonlinear, high dimensional systems can be very difficult. In most of the real world applications, linear process models are not available and approximate techniques relying on linearization cannot be used. Simulation techniques based on Monte Carlo sampling are promising, but the computational burden is high. Techniques have therefore been developed to approximate the probability density functions (pdfs), rather than the process model, to reduce the computational cost and to obtain higher order approximations than linearization.

In this chapter, we review various estimation techniques. We concentrate mainly on nonlinear filtering techniques to develop a framework based on sequential probabilistic inference, which is the problem of estimating the hidden variables of a system in an optimal and consistent fashion given noisy or incomplete observations, for real time degradation monitoring.

The structure of this chapter is as follows. In Section 2.1, we define the characteristics of the process model. We use a hidden Markov model structure where the states are unobservable. Within this model we then derive the Bayesian framework for a sequential probabilistic inference problem in Section 2.2. We discuss the possible solutions for recursive Bayesian estimation in Section 2.3. For linear Gaussian system models, we derive the Kalman filter in the Bayesian framework. In Section 2.4, for nonlinear system models we derive two approximate filtering techniques, extended Kalman filtering and unscented Kalman filtering. We also present a new demonstrative example application in which we use unscented Kalman filtering to estimate the fouling of steam generator tubes

in IRIS (International Reactor Innovative and Secure). In Subsection 2.4.4, we present particle filtering as a solution to the recursive Bayesian estimation problem. After testing different problems (some of them are presented in Subsections 2.4.3.5, 3.2.1.2 and 3.2.1.3) by using the extensions of Kalman filtering for our degradation monitoring framework, we instead adopt particle filtering, which provides a better approximation for nonlinear filtering and use this to create new algorithms that can perform better in change estimation by utilizing multiple data sources. In the rest of Section 2.4.4, we review Monte Carlo sampling and sequential importance sampling to derive the sampling importance resampling filter on which we base our degradation monitoring algorithm.

2.1. STOCHASTIC DESCRIPTION OF THE SYSTEM MODEL

We employed a hidden Markov model (HMM) representation. A HMM is a doubly stochastic process with an underlying stochastic process that is not directly observable but can be observed only through another stochastic process that produces the sequence of observations [23]. In our context, the HMM consists of a trivariate process $\{C_t, X_t, Y_t\}$ where C, X and Y are random variables that represent model parameters (component states), system dynamic states and process observations, respectively. The model parameters are treated as constant but uncertain component characteristics, which define the component states of the system. The set of component states $\{C_t\}_{t\geq 0}$ is designated as an unobserved (hidden) stationary first order Markov process on a state space $\mathcal{C}$ with initial probability density $p(c_0)$ where $C_0 \sim p(c_0)$ ($\sim$ denotes that random variable Z is distributed according to a probability density $p(z)$) and Markov transition distribution function $p(c' \mid c)$. When $\mathcal{C}$ is discrete

$$(C_t \mid C_{t-1} = c_{t-1}) \quad \sim \quad p(\cdot \mid c_{t-1}), \tag{2.1}$$

which should be read random variable C_t is distributed according to $p(\cdot \mid c_{t-1})$. The process $\{X_t\}_{t\geq 0}$ is an unobserved first order Markov process on a state space $\mathcal{X}$ with

initial probability density $p(x_0)$ where $X_0 \sim p(x_0)$ and Markov transition distribution function $p(x' \mid x, c)$. When $\mathcal{X}$ is discrete

$$(X_t \mid X_{t-1} = x_{t-1}, C_t = c_t) \quad \sim \quad p(\cdot \mid x_{t-1}, c_t). \tag{2.2}$$

The process $\{X_t\}$ is called the system state of the model; note that this is a function of the component state. Inference has to be carried out only in terms of the observable process $\{Y_t\}$. The observable process $(Y_t \in \mathcal{Y})$ is assumed to be conditionally independent given the bivariate process $\{C_t, X_t\}$ and of marginal distribution $p(y \mid x, c)$. For discrete $\mathcal{Y}$,

$$(Y_t \mid X_t = x_t, C_t = c_t) \quad \sim \quad p(\cdot \mid x_t, c_t). \tag{2.3}$$

This hidden Markov model is illustrated in Figure 3.

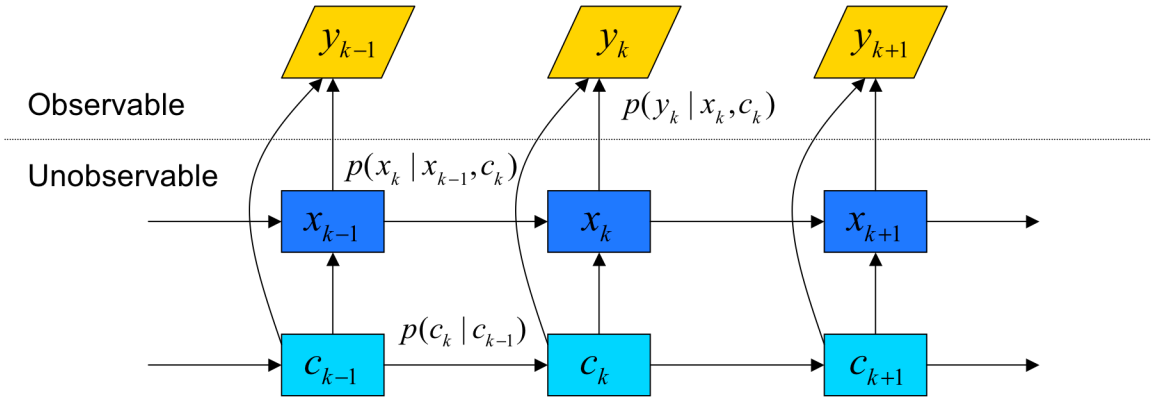

Figure 3. The graphical representation of the HMM.

In order to represent a general physical system within the HMM, we construct the dynamic state space model (DSSM) for a general discrete-time nonlinear system

$$x_k = f\left(x_{k-1}, w_k^x; c_k\right), \tag{2.4}$$

$$y_k = h\left(x_k, v_k; c_k\right). \tag{2.5}$$

where $f(\cdot)$ is the state transition function subject to modeling noise w^x at time step *k*, and $h(\cdot)$ is the observation function subject to sensor noise v. The noise sequences are assumed to be independent and white with known pdfs. We assume that if the component is degraded, the component state undergoes random, discrete transitions. Otherwise, it stays constant and we write the component state

$$c_k = c_{k-1} + w_k^c, \tag{2.6}$$

which is subject to an additive modeling noise w^c. The component transition density $p(c_k \mid c_{k-1})$ is specified by the modeling noise distribution $p(w^c)$, the state transition density $p(x_k \mid x_{k-1}, c_k)$ is determined by the state transition function $f(\cdot)$ and the modeling noise distribution $p(w^x)$, the observation likelihood function $p(y_k \mid x_k, c_k)$ is determined by the observation function $h(\cdot)$ and the measurement noise distribution $p(v)$ at time step *k*. The dynamic state-space model, the initial probability densities of the system and component states and statistics of the noise random variables constitutes the probabilistic model as illustrated in Figure 3.

The key problem to be solved is to find an optimal algorithm to recursively estimate the hidden state variables (x_k, c_k) as the noisy measurements y_k become available.

2.2. RECURSIVE BAYESIAN ESTIMATION

Bayesian analysis, interpreting the probability as a conditional measure of uncertainty, is one of the popular methods to solve inverse problems. In Bayesian inference all of the uncertainties (including states and parameters which are either time-varying or static but unknown) are treated as random variables. The inference is performed within the Bayesian framework given all available information [24]. In a Bayesian framework the posterior density $p(X_k \mid Y_k)$ of the state $X_k = \{x_0, x_1, \ldots, x_k\}$ given all the observations $Y_k = \{y_1, y_2, \ldots, y_k\}$ constitutes the solution to the sequential probabilistic inference

problem (for the present, we do not include the component state C_k in the notation; it can be considered part of the system state X_k for the moment). Our aim is to estimate recursively in time the posterior density $p(X_k \mid Y_k)$ and marginalized posterior density, which is also known as the filtering density $p(x_k \mid Y_k)$ inside the Bayesian framework.

At any time *k*, the posterior density is given by the Bayes' theorem

$$p(X_k \mid Y_k) = \frac{p(Y_k \mid X_k)\, p(X_k)}{p(Y_k)}. \tag{2.7}$$

It is possible to obtain straightforwardly a recursive formula for this density. At first, we rewrite Eq. (2.7) by using $Y_k = \{y_k, Y_{k-1}\}$ and $X_k = \{x_k, X_{k-1}\}$, and then using the definition of conditional probability, we obtain

$$\begin{aligned} p(X_k \mid Y_k) &= \frac{p(y_k, Y_{k-1} \mid X_k)\, p(x_k, X_{k-1})}{p(y_k, Y_{k-1})} \\ &= \frac{p(y_k \mid Y_{k-1}, X_k)\, p(Y_{k-1} \mid y_k, X_k)\, p(x_k, X_{k-1})}{p(y_k \mid Y_{k-1})\, p(Y_{k-1})}. \end{aligned}$$

Since we assumed earlier that the observations are independent given the state, then $p(y_k \mid Y_{k-1}, X_k) = p(y_k \mid X_k)$ and $p(Y_{k-1} \mid y_k, X_k) = p(Y_{k-1} \mid X_k)$. Also, Eq. (2.5) states that the measurements up to time *k-1* depend on the state trajectory up to time *k-1*, so that $p(Y_{k-1} \mid X_k) = p(Y_{k-1} \mid X_{k-1})$ and so

$$p(X_k \mid Y_k) = \frac{p(y_k \mid X_k)\, p(Y_{k-1} \mid X_{k-1})\, p(x_k, X_{k-1})}{p(y_k \mid Y_{k-1})\, p(Y_{k-1})}.$$

In the last step, we use the definition of conditional probability and the first order Markov property of the state to write $p(x_k, X_{k-1}) = p(x_k \mid X_{k-1})\, p(X_{k-1}) = p(x_k \mid x_{k-1})\, p(X_{k-1})$ and

apply Bayes' theorem $p(X_{k-1} \mid Y_{k-1}) = \frac{p(Y_{k-1} \mid X_{k-1}) p(X_{k-1})}{p(Y_{k-1})}$. Rearranging the equation, we obtain a recursive formula for the posterior density as

$$p(X_k \mid Y_k) = p(X_{k-1} \mid Y_{k-1}) \frac{p(y_k \mid x_k) p(x_k \mid x_{k-1})}{p(y_k \mid Y_{k-1})}. \tag{2.8}$$

The filtering density can be written by means of the Bayes' theorem

$$p(x_k \mid Y_k) = \frac{p(Y_k \mid x_k) p(x_k)}{p(Y_k)}. \tag{2.9}$$

We can also construct a recursive formulation for the filtering density. At first, we rewrite Eq. (2.9) by using $Y_k = \{y_k, Y_{k-1}\}$, and then using the definition of conditional probability, we obtain

$$\begin{aligned} p(x_k \mid Y_k) &= \frac{p(y_k, Y_{k-1} \mid x_k) p(x_k)}{p(y_k, Y_{k-1})} \\ &= \frac{p(y_k \mid Y_{k-1}, x_k) p(Y_{k-1} \mid y_k, x_k) p(x_k)}{p(y_k \mid Y_{k-1}) p(Y_{k-1})}. \end{aligned}$$

By using our assumption that the observations are independent given the state, then $p(y_k \mid Y_{k-1}, x_k) = p(y_k \mid x_k)$ and $p(Y_{k-1} \mid y_k, x_k) = p(Y_{k-1} \mid x_k)$. Applying the Bayes' theorem $p(x_k \mid Y_{k-1}) = \frac{p(Y_{k-1} \mid x_k) p(x_k)}{p(Y_{k-1})}$ and rearranging the equation yields

$$p(x_k \mid Y_k) = \frac{p(y_k \mid x_k) p(x_k \mid Y_{k-1})}{p(y_k \mid Y_{k-1})}. \tag{2.10}$$

The prior density $p(x_k \mid Y_{k-1})$, which predicts the state by utilizing the system model is constructed based on the conditional density of x_{k-1} given all the observations, $p(x_{k-1} \mid Y_{k-1})$, prior to time *k* and the state transition function (Eq. (2.4)) as

$$p(x_k \mid Y_{k-1}) = \int p(x_k \mid x_{k-1}) p(x_{k-1} \mid Y_{k-1}) dx_{k-1} \tag{2.11}$$

where

$$p(x_k \mid x_{k-1}) = \int \delta\left(x_k - f\left(x_{k-1}, w_k^x; c_k\right)\right) p\left(w_k^x\right) dw_k^x \,. \tag{2.12}$$

The observation likelihood density is calculated using the observation function (Eq. (2.5))

$$p(y_k \mid x_k) = \int \delta\left(y_k - h(x_k, v_k; c_k)\right) p(v_k) dv_k \,. \tag{2.13}$$

The denominator of Eq. (2.10) is a scalar normalization constant

$$p(y_k \mid Y_{k-1}) = \int p(y_k \mid x_k) p(x_k \mid Y_{k-1}) dx_k \,. \tag{2.14}$$

Equations (2.10) - (2.14) constitute the recursive Bayesian estimation solution to the sequential probabilistic inference problem. Having completed the formulation for recursive Bayesian estimation to solve the sequential probabilistic inference problem, next we define well-posed and optimal nonlinear filtering.

2.2.1. Well-Posed Filtering

Filtering is indeed an inverse problem. Given the history of the observations and the dynamic state space model, we try to find the best estimates of the states. An inverse problem is said to be well-posed if it satisfies: existence, uniqueness and stability [24]. If there is a large disparity in the sensitivity of the solutions to perturbations in initial conditions, inputs, and measurement errors, the filtering problem is ill-posed [25]. These may cause the observation function to be a many to one mapping function, which results in a non-unique solution to this stochastic filtering problem. Sinitsyn [26] defines the main factors that lead to the ill-posedness in filtering problem as insufficient smoothness of the observations, hereditary kernels and the non-Markov behavior of the random processes. For online estimation he introduced the conditionally optimal filtering (COF) idea, which is based on restricting the class of filters in such a way that any filter can be

useful for online estimation. The absolute optimality of estimators are given up for computational simplicity [26].

For high dimensional systems with a limited number of noisy measurements, if the filtering problem is ill-posed then introducing additional data sources and smoothing the measurements may help the filter to find a unique solution. In Chapter 3, we propose to introduce a reliability degradation database into the filtering algorithm in order to find a unique solution for high dimensional systems, especially in estimation of simultaneous component degradations.

2.2.2. Optimal Filtering

The optimality of a filter can be defined through a loss function $L(x,\hat{x})$, where $\hat{x}$ is the state estimate. The loss function is defined such that the larger the estimation error $(x-\hat{x})$, the greater the loss. Given the marginalized posterior density at time step *k*, the expected loss is defined to be

$$\mathrm{E}\left[L(x_k,\hat{x}_k)\,|\,Y_k\right]=\int L(x_k,\hat{x}_k)\,p(x_k\,|\,Y_k)dx_k. \tag{2.15}$$

For the quadratic loss function $L(x_k,\hat{x}_k)=(x_k-\hat{x}_k)(x_k-\hat{x}_k)^T$, the optimal estimate can be derived by minimizing the loss function. By taking the partial derivative with respect to the estimated state $\hat{x}_k$

$$\begin{aligned}\frac{\partial}{\partial\hat{x}_k}\left[\int(x_k-\hat{x}_k)(x_k-\hat{x}_k)^T\,p(x_k\,|\,Y_k)dx_k\right] &= \int\frac{\partial}{\partial\hat{x}_k}(x_k-\hat{x}_k)(x_k-\hat{x}_k)^T\,p(x_k\,|\,Y_k)\,dx_k\\ &= \int -2(x_k-\hat{x}_k)^T\,p(x_k\,|\,Y_k)\,dx_k\\ &= -2\int x_k^T\,p(x_k\,|\,Y_k)\,dx_k+2\int\hat{x}_k^T\,p(x_k\,|\,Y_k)\,dx_k,\end{aligned} \tag{2.16}$$

and by setting Eq. (2.16) to zero, the optimal estimate is found to be the posterior mean

$$\hat{x}_k = \mathrm{E}\left[x_k \mid Y_k\right] = \int x_k p\left(x_k \mid Y_k\right) dx_k, \tag{2.17}$$

which is also called the minimum mean-squared error (MMSE) estimate. This is the most common loss function and for Gaussian posterior densities the mode and median estimates coincide with the mean.

The maximum a posteriori (MAP) estimate tries to find the mode of the marginalized posterior density with the loss function $L\left(x,\hat{x}\right) = \delta\left(x_k - \hat{x}_k\right)$, and then the optimal choice is the mode of the posterior pdf. If the loss function is of the form $L\left(x,\hat{x}\right) = \left|x - \hat{x}\right|$, the optimal estimate is the median of the posterior pdf [27].

Both MMSE and MAP estimates require the calculation of the posterior density, but MAP does not require the calculation of the normalization constant and therefore is less computationally expensive. However, the MAP estimate has a drawback especially for high-dimensional systems. High probability density does not mean high probability mass. A narrow spike with a very small support can have a very high density, but the actual probability of the corresponding state estimate can be very small [24]. For high-dimensional systems especially with high modeling noises, the support of the mode should be analyzed.

2.3. APPROXIMATE METHODS FOR RECURSIVE BAYESIAN ESTIMATION

Equations (2.10) - (2.14) form the basis for the optimal Bayesian solution with respect to any loss function to the sequential probabilistic inference problem. This recursive propagation of the posterior density is only a conceptual solution and in general, it cannot be determined analytically [28]. Under certain constraints solutions exist, e.g., for linear-Gaussian systems Kalman filtering provides the closed form solution. Often the optimal solution is intractable and approximate methods seeking suboptimal solutions are generally used. Some of these approximate methods include:

- Grid-based filtering (GBF) approximates the multi-dimensional integrals with large but finite sums over a uniform grid. This is similar to particle filtering, except in particle filtering the particles are distributed in the state space according to the pdf of the state. Therefore, the computational requirements of the grid-based filtering increase exponentially with the dimension of the state. Since, it is more computationally expensive than particle filtering, this limits its application [29]. Recently, the adaptive grid risk sensitive filter (AGRSF) was introduced by Bhaumik et al. [30] to address the poor numerical efficiency and finite resolution of the grid-based filters. AGRSF is based on setting deterministic grid points in the risk sensitive parts of the state space.
- In Gaussian approximations, the filtering distribution is approximated by a Gaussian (Eq. A.1)

$$p\left(x_k \mid Y_k\right) = N\left(x_k; \bar{x}_k, \left(P_{xx}\right)_k\right). \tag{2.18}$$

The mean $\bar{x}_k$ and the covariance $\left(P_{xx}\right)_k$ of the Gaussian approximation can be computed by matching the first two moments of the filtering distribution. As stated earlier, the Kalman filter (KF) [31] provides the optimal closed form solution for linear Gaussian systems. For nonlinear Gaussian systems, the KF framework can be used if the process and observation models are linearized using a first order truncated Taylor series expansion around the current estimates, which is the basis for extended Kalman filter (EKF) [32]. EKF approximation is valid if all the higher order derivatives of the nonlinear functions are negligible over the monitored region of state variables. This approximation often introduces large errors in the EKF calculated posterior mean and covariance of the transformed Gaussian random variable (GRV), which may lead to suboptimal performance and sometimes divergence of the filter. The unscented Kalman filter (UKF) addresses some of the approximation issues of the EKF in the KF framework. Unlike the EKF, the UKF does not approximate the nonlinear process and observation models; it uses the complete nonlinear models and instead approximates the distribution of the state random variable [33].

- The particle filter (PF) is a statistical, brute force approach to estimation in nonlinear non-Gaussian systems. It was invented to numerically implement the recursive Bayesian estimation formulation of the posterior density. It is a simulation based method to compute the filtering distribution and provides a better approximation than any KF derivatives with the price of an increased level of computational effort [29].

In the rest of this chapter, we focus on Kalman filter derivatives and particle filtering. We first derive the KF within the Bayesian framework. We analyze the approximations introduced in EKF and UKF by propagating the mean and covariance through the nonlinear model and present both of the filtering algorithms. We then derive the PF and its approximations.

2.3.1. Kalman Filtering

The discrete time KF gives the closed form solution to the optimal filtering problem for linear Gaussian systems. Consider the linear dynamic state space model

$$x_k = F_{k,k-1}x_{k-1} + w_k\,, \tag{2.19}$$

$$y_k = H_k x_k + v_k \tag{2.20}$$

where $x_k \in \mathbb{R}^{n_x}$ is the state vector with initial distribution $x_0 \sim N(\bar{x}_0, P_0)$, $y_k \in \mathbb{R}^{n_y}$ is the measurement vector, $F_{k,k-1}$ is the state transition matrix and H_k is the observation matrix; $\{w_k\}$ and $\{v_k\}$ are zero mean white Gaussian noise processes independent of each other with known covariance matrices Q and R, respectively.

$$\begin{aligned} &w_k \sim N(0,Q), \quad v_k \sim N(0,R), \\ &\mathrm{E}\left[w_k w_j^T\right] = Q\delta_{kj}, \quad \mathrm{E}\left[v_k v_j^T\right] = R\delta_{kj}, \quad \mathrm{E}\left[v_k w_j^T\right] = 0. \end{aligned} \tag{2.21}$$

In probabilistic terms the model is

$$p(x_k \mid x_{k-1}) = N(x_k; F_{k,k-1}x_{k-1}, Q), \tag{2.22}$$

$$p(y_k \mid x_k) = N(y_k; H_k x_k, R). \tag{2.23}$$

The optimal filtering equations for the linear model given in Eqs. (2.19)-(2.21) can be evaluated in closed form as

$$\begin{aligned} p(x_k \mid Y_{k-1}) &= N(x_k; \hat{x}_k^-, P_k^-) \\ p(x_k \mid Y_k) &= N(x_k; \hat{x}_k, P_k) \\ p(y_k \mid Y_{k-1}) &= N(y_k; H_k \hat{x}_k^-, S_k) \end{aligned} \tag{2.24}$$

where $\hat{x}_k^-$ is the estimate of x_k before we process the measurement at time k, $\hat{x}_k$ is the estimate of x_k after we process the measurement at time k, P_k^- is the covariance of the estimation error of $\hat{x}_k^-$, and P_k is the covariance of the estimation error of $\hat{x}_k$. The time update equations for the state estimate and its error covariance are

$$\begin{aligned} \hat{x}_k^- &= F_{k,k-1}\hat{x}_{k-1}, \\ P_k^- &= F_{k,k-1}P_{k-1}F_{k,k-1}^T + Q. \end{aligned} \tag{2.25}$$

The measurement update equations are

$$\begin{aligned} \hat{x}_k &= \hat{x}_k^- + K_k(y_k - H_k\hat{x}_k^-), \\ K_k &= P_k^- H_k^T S_k^{-1}, \\ S_k &= H_k P_k^- H_k^T + R, \\ P_k &= P_k^- - K_k S_k K_k^T. \end{aligned} \tag{2.26}$$

The derivation of the KF in the Bayesian framework is presented in Appendix B.

2.4. NONLINEAR EXTENSIONS OF KALMAN FILTERING

In this section, we derive the nonlinear extensions of the Kalman filter. We mainly focus on extended Kalman filter (EKF) and unscented Kalman filter (UKF) and evaluate the validity of their approximations by investigating the propagation of means and covariances in nonlinear equations. We start with discussing the nonlinear transformation of a random variable through linearization which forms the basis for extended Kalman filtering and then through unscented transform to derive unscented Kalman filtering and compare these transformation with the true ones.

2.4.1. General Nonlinear Transformation Problem

Suppose that $x \in \mathbb{R}^{n_x}$, with mean $\bar{x}$, and covariance P_{xx}, is transformed by a general nonlinear function $y = f(x)$. The statistics of y can be calculated once the density of the transformed distribution is determined. In filtering applications, the mean $\bar{y}$ and covariance P_{yy} are the necessary statistics of y to be computed.

It is difficult to transform a probability density function through a nonlinear function. Complexity arises mainly for high dimensional and highly nonlinear systems. If the computational load is a concern, linearization of the nonlinear function around a nominal point is one of the choices despite its low accuracy for highly nonlinear functions. Another choice would be a Monte Carlo type method, which uses random sampling to simulate the prior distribution to be transformed in order to compute the necessary statistics of the transformed one. This forms the basis for particle filtering if performed sequentially. For these types of methods, in order to gain higher accuracy, the number of samples needs to be large, which increases the computational load. Recently, Julier and Uhlmann [34] proposed another method namely unscented transform (UT) for propagation of the necessary statistics with a Monte Carlo like method. The main difference is UT uses deterministic sampling that is specific to the type of the problem by

reducing the computational load based on the choice of number and location of the samples.

2.4.1.1. Propagation of the True Mean

Suppose that x is a GRV with mean $\bar{x}$. By expanding $y = f(x)$ in Taylor series around the mean $x = \bar{x}$

$$\begin{aligned} y &= f(x) \\ &= f(\bar{x}) + D_{\tilde{x}} f + \frac{1}{2!} D_{\tilde{x}}^2 f + \frac{1}{3!} D_{\tilde{x}}^3 f + \dots \end{aligned} \tag{2.27}$$

where $\tilde{x} = x - \bar{x}$, which has zero mean and covariance P_{xx}, and

$$D_{\tilde{x}}^m f = \left(\sum_{j=1}^{n_x} \tilde{x}_j \frac{\partial}{\partial x_j} \right)^m f \Bigg|_{x=\bar{x}}. \tag{2.28}$$

The mean of y can be written as

$$\begin{aligned} \bar{y} &= E\left[f(\bar{x}) + D_{\tilde{x}} f + \frac{1}{2!} D_{\tilde{x}}^2 f + \frac{1}{3!} D_{\tilde{x}}^3 f + \dots \right] \\ &= f(\bar{x}) + E\left[D_{\tilde{x}} f + \frac{1}{2!} D_{\tilde{x}}^2 f + \frac{1}{3!} D_{\tilde{x}}^3 f + \dots \right]. \end{aligned} \tag{2.29}$$

For any integer $m \geq 0$

$$\begin{aligned} E\left[D_{\tilde{x}}^{2m+1} f \right] &= E\left[\left(\sum_{j=1}^{n_x} \tilde{x}_j \frac{\partial}{\partial x_j} \right)^{2m+1} f \Bigg|_{x=\bar{x}} \right] \\ &= 0 \end{aligned} \tag{2.30}$$

because for any symmetric pdf (i.e., let $p(r)$ be the symmetric pdf of r, then $p(r)=p(-r)$ and if m is odd $r^m=-\left(-r\right)^m$) the central odd moments are zero. Rewriting Eq. (2.29)

$$\bar{y}=f\left(\bar{x}\right)+E\left[\frac{1}{2!}D_{\tilde{x}}^2 f+\frac{1}{4!}D_{\tilde{x}}^4 f+\ldots\right]. \tag{2.31}$$

The second order term can also be written as

$$\begin{aligned} E\left[\frac{1}{2!}D_{\tilde{x}}^2 f\right] &= \frac{1}{2}E\left[\left(\sum_{j=1}^{n_x}\tilde{x}_j\frac{\partial}{\partial x_j}\right)^2 f\Bigg|_{x=\bar{x}}\right] \\ &= \frac{1}{2}E\left[\left(\sum_{i,j=1}^{n_x}\tilde{x}_i\tilde{x}_j\frac{\partial^2}{\partial x_i\partial x_j}\right)f\Bigg|_{x=\bar{x}}\right] \\ &= \frac{1}{2}\sum_{i,j=1}^{n_x}E\left[\tilde{x}_i\tilde{x}_j\right]\frac{\partial^2 f}{\partial x_i\partial x_j}\Bigg|_{x=\bar{x}} \\ &= \frac{1}{2}\sum_{i,j=1}^{n_x}\left(P_{xx}\right)_{ij}\frac{\partial^2 f}{\partial x_i\partial x_j}\Bigg|_{x=\bar{x}} \end{aligned} \tag{2.32}$$

Rearranging Eq. (2.31), the true mean of y is

$$\bar{y}=f\left(\bar{x}\right)+\frac{1}{2}\sum_{i,j=1}^{n_x}\left(P_{xx}\right)_{ij}\frac{\partial^2 f}{\partial x_i\partial x_j}\Bigg|_{x=\bar{x}}+\mathrm{E}\left[\frac{1}{4!}D_{\tilde{x}}^4 f+\frac{1}{6!}D_{\tilde{x}}^6 f+\ldots\right]. \tag{2.33}$$

2.4.1.2. Propagation of the True Covariance

The covariance of y is

$$P_{yy}=\mathrm{E}\left[\left(y-\bar{y}\right)\left(y-\bar{y}\right)^T\right]. \tag{2.34}$$

By using Eqs. (2.27) and (2.31), one can write

$$y - \bar{y} = \left[D_{\tilde{x}} f + \frac{1}{2!} D_{\tilde{x}}^2 f + \frac{1}{3!} D_{\tilde{x}}^3 f + \ldots \right] - E\left[\frac{1}{2!} D_{\tilde{x}}^2 f + \frac{1}{4!} D_{\tilde{x}}^4 f + \ldots \right]. \tag{2.35}$$

Substituting Eq. (2.35) into Eq. (2.34) and using the property derived in Eq. (2.30) that odd central moments of a symmetric distribution are zero

$$\begin{aligned} P_{yy} = E\left[D_{\tilde{x}} f \left(D_{\tilde{x}} f \right)^T \right] + E\left[D_{\tilde{x}} f \left(\frac{1}{3!} D_{\tilde{x}}^3 f \right)^T + \frac{1}{2!} D_{\tilde{x}}^2 f \left(\frac{1}{2!} D_{\tilde{x}}^2 f \right)^T + \frac{1}{3!} D_{\tilde{x}}^3 f \left(D_{\tilde{x}} f \right)^T \right] \\ + E\left[\frac{1}{2!} D_{\tilde{x}}^2 f \right] E\left[\frac{1}{2!} D_{\tilde{x}}^2 f \right]^T + \ldots \end{aligned} \tag{2.36}$$

The second order moment can be written as

$$\begin{aligned} E\left[D_{\tilde{x}} f \left(D_{\tilde{x}} f \right)^T \right] &= E\left[\sum_{j=1}^{n_x} \tilde{x}_j \left. \frac{\partial f}{\partial x_j} \right|_{x=\bar{x}} \left(\sum_{k=1}^{n} \tilde{x}_k \left. \frac{\partial f}{\partial x_k} \right|_{x=\bar{x}} \right)^T \right] \\ &= E\left[\sum_{j,k=1}^{n_x} \tilde{x}_j \left. \frac{\partial f}{\partial x_j} \right|_{x=\bar{x}} \left(\left. \frac{\partial f}{\partial x_k} \right|_{x=\bar{x}} \right)^T \tilde{x}_k^T \right] \\ &= \sum_{j,k=1}^{n_x} F_j \left(P_{xx} \right)_{jk} F_k^T \\ &= F P_{xx} F^T \end{aligned} \tag{2.37}$$

where $F = \left. \frac{\partial f}{\partial x} \right|_{x=\bar{x}}$ is the Jacobian matrix at $x = \bar{x}$. Then, the true covariance of y is

$$\begin{aligned} P_{yy} = F P_{xx} F^T + E\left[D_{\tilde{x}} f \left(\frac{1}{3!} D_{\tilde{x}}^3 f \right)^T + \frac{1}{2!} D_{\tilde{x}}^2 f \left(\frac{1}{2!} D_{\tilde{x}}^2 f \right)^T + \frac{1}{3!} D_{\tilde{x}}^3 f \left(D_{\tilde{x}} f \right)^T \right] + \\ E\left[\frac{1}{2!} D_{\tilde{x}}^2 f \right] E\left[\frac{1}{2!} D_{\tilde{x}}^2 f \right]^T + \ldots \end{aligned} \tag{2.38}$$

2.4.2. Linearization

Extended Kalman filtering is based on linearization of the nonlinear system model around the nominal trajectory of the system state.

2.4.2.1. Propagation of the Linearized Mean

A linearization is performed by expanding $y = f\left(x\right)$ in Taylor series around the mean of the GRV $x = \bar{x}$ up to first order

$$\begin{aligned} y &= f\left(x\right) \\ &= f\left(\bar{x}\right) + D_{\tilde{x}} f \end{aligned} \tag{2.39}$$

where $\tilde{x} = x - \bar{x}$. The linearized mean of y can be written as

$$\begin{aligned} \bar{y}_L &= E\left[f\left(\bar{x}\right) + D_{\tilde{x}} f \right] \\ &= f\left(\bar{x}\right) + E\left[D_{\tilde{x}} f \right] \\ &= f\left(\bar{x}\right) \end{aligned} \tag{2.40}$$

by using the property derived in Eq. (2.30) that odd central moments of a symmetric distribution are zero. The linearization matches the true mean of y up to first order.

2.4.2.2. Propagation of the Linearized Covariance

The linearized covariance of y is

$$\left(P_{yy}\right)_L = E\left[\left(y - \bar{y}_L\right)\left(y - \bar{y}_L\right)^T \right] \tag{2.41}$$

Combining Eqs. (2.39) and (2.40), one can write

$$y - \bar{y}_L = D_{\tilde{x}} f \ . \tag{2.42}$$

Substituting Eq. (2.42) into Eq. (2.41)

$$\left(P_{yy}\right)_L = E\left[D_{\tilde{x}} f \left(D_{\tilde{x}} f\right)^T\right]. \tag{2.43}$$

By using the second order moment derived in Eq. (2.37), the linearized covariance of y is given as

$$\left(P_{yy}\right)_L = F P_{xx} F^T . \tag{2.44}$$

The linearization matches the true covariance of y up to third order.

2.4.2.3. Extended Kalman Filtering

Consider the nonlinear system equations

$$x_k = f\left(x_{k-1}, w_k\right), \tag{2.45}$$

$$y_k = h\left(x_k, v_k\right) \tag{2.46}$$

where the noise characteristics are given in Eq. (2.21). For $k = 1,2,\ldots$, the EKF algorithm is:

1. Compute the following Jacobian matrices evaluated at the state estimate, $\hat{x}_{k-1}$

$$\begin{aligned} F_{k-1} &= \left.\frac{\partial f}{\partial x}\right|_{\hat{x}_{k-1}}, \\ L_{k-1} &= \left.\frac{\partial f}{\partial v}\right|_{\hat{x}_{k-1}}. \end{aligned} \tag{2.47}$$

2. Perform the time update of the state estimate and estimation error covariance

$$\hat{x}_k^- = f\left(\hat{x}_{k-1}, 0\right), \tag{2.48}$$

$$P_k^- = F_{k-1} P_{k-1} F_{k-1}^T + L_{k-1} Q L_{k-1}^T . \tag{2.49}$$

3. Compute the following Jacobian matrices evaluated at the state estimate, $\hat{x}_k^-$

$$H_k = \left.\frac{\partial h}{\partial x}\right|_{\hat{x}_k^-}, \qquad M_k = \left.\frac{\partial h}{\partial w}\right|_{\hat{x}_k^-}. \tag{2.50}$$

4. Perform the measurement update of the state estimate and estimation error covariance

$$\hat{x}_k = \hat{x}_k^- + K_k\left[y_k - h\left(\hat{x}_k^-, 0\right)\right], \tag{2.51}$$

$$K_k = P_k^- H_k^T \left(H_k P_k^- H_k^T + M_k R M_k^T\right)^{-1}, \tag{2.52}$$

$$P_k = \left(I - K_k H_k\right) P_k^-. \tag{2.53}$$

In order to reduce the linearization error associated with the EKF, various approaches have been employed. In the iterated EKF, the state estimate $\hat{x}_k^-$ where the Jacobian matrices for the observation equation are computed is refined [29]. In the second order EKF, a second order Taylor series expansion of the nonlinear system equations is performed [32]. In the Gaussian sum filter approach, a non-Gaussian pdf is approximated by a sum of Gaussian pdfs. Since the true pdfs of the modeling and measurement noises can be approximated by a sum of *N* Gaussian pdfs, one can run *N* filters in parallel and then combine them to obtain an estimate [35].

For the cases when the system is highly nonlinear, most of these techniques do not work effectively and can cause the filter to diverge. A recent technique proposed to have a better approximation than EKF and its variations is the unscented Kalman filtering that we present in the next section.

2.4.3. Unscented Transform

Unscented transform is an alternative approximate technique for transforming random variables through a nonlinear function. The idea behind this approach is that it is easier to approximate a probability distribution than it is to approximate an arbitrary nonlinear function or transformation [36].

It is based on finding a set of individual points in the state-space to approximate certain moments of the true pdf of $x \in \mathbb{R}^{n_x}$. Each point is then transformed through a nonlinear function to yield a transformed sample. The necessary statistics are calculated from these transformed samples. The deterministic selection of the sample points separates this algorithm from Monte Carlo type methods, which use random sampling.

The steps in the UT are as follows:

1. Calculate a set of points (sigma points) and weights $\sigma = \left\{ \chi^{(i)}, W^{(i)} \right\}$ that capture the first and second moments (or higher) of the prior random variable.
2. Transform each point through the nonlinear function

$$\gamma^{(i)} = f\left(\chi^{(i)} \right) \qquad i = 0,\ldots,2n_x . \tag{2.54}$$

3. Approximate the posterior statistics as

$$\begin{aligned} \bar{y}_{UT} &= \sum_{i=0}^{2n_x} W^{(i)} \gamma^{(i)}, \\ \left(P_{yy} \right)_{UT} &= \sum_{i=0}^{2n_x} W^{(i)} \left(\gamma^{(i)} - \bar{y}_{UT} \right) \left(\gamma^{(i)} - \bar{y}_{UT} \right)^T . \end{aligned} \tag{2.55}$$

In the next section, the selection framework of the sigma points will be discussed and the set of sigma points for the second order UT will be generated. Then, the approximation of the mean and covariance of the posterior random variable by UT will be analyzed by comparing them with the true mean and covariance.

2.4.3.1. Selection of the Sigma Points

The selection of the sigma points depends on the order of moments to be captured. As the desired order of moments increases, the minimum number of points to capture these statistics increases.

Let $p(x)$ be the pdf of x. The solution of a constraint function $g\left[\sigma, p(x)\right] = 0$ for the set of the sigma points σ contains the information of how many sigma points should be used, where they are located, and what weights are assigned to each point. The solution embraces some degree of freedom in the choice of points, which can be reduced by assigning a cost function $\mathrm{C}\left[\sigma, p(x)\right]$ to the different solutions. The sigma points are obtained by solving

$$\min_{\sigma} \mathrm{C}\left[\sigma, p(x)\right] \quad \text{subject to} \quad g\left[\sigma, p(x)\right] = 0. \tag{2.56}$$

Although sigma points for higher order moments have been calculated [37], only the sigma point selection for second order UT for GRVs will be discussed here.

Suppose that x is a GRV. The distribution of x with an arbitrary mean and covariance can be transformed to the standard Gaussian, which is zero mean and has unit variance. Then, x can be written as

$$x = \bar{x} + Cz \tag{2.57}$$

where z has the standard Gaussian distribution and C is a matrix square root of P_{xx}, $CC^T = P_{xx}$.

The sigma points should capture the first two moments of z in the second order UT. Let $z^{(i)}$ be the i-th component of z. The covariance is

$$E\left[\left(z^{(i)}\right)^2\right]=1 \qquad \forall i \tag{2.58}$$

and since the distribution is symmetric, all odd-ordered moments are zero. The minimum number of points whose distribution obeys these conditions has the structure shown in Figure 4.

There are two types of points. The first type consists of a point at the origin and has a weight $W^{(0)}$. The second type consists of symmetrically distributed *2n* points which lie on the coordinate axes a distance s_1 from the origin and have the same weight $W^{(1)}$. Therefore the second order UT uses $2n_x+1$ sigma points.

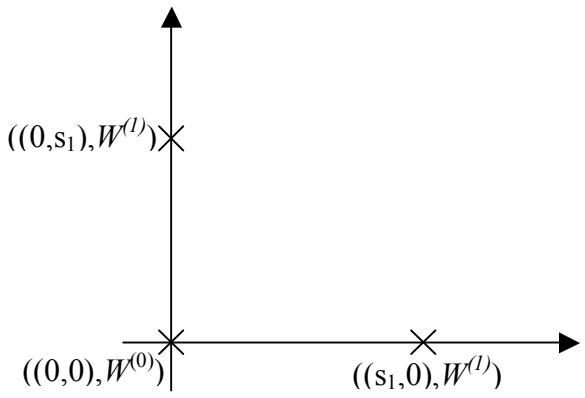

Figure 4. The set of points chosen for a 2-D distribution [38]. Because of the symmetry, the other two sigma points are not shown.

The weights and locations of the points are chosen with regard to the constraint function. There are two constraints: the first one is the covariance of the sigma points should be equal to the identity and the second one is the weights should be normalized, $\sum_i W^{(i)}=1$.

$$g\left[\sigma, p\left(x\right)\right] = \begin{pmatrix} 2W^{(1)}s_1^2 - 1 \\ W^{(0)} + 2n_x W^{(1)} - 1 \end{pmatrix} \tag{2.59}$$

Due to the symmetry of the points it is only necessary to ensure the condition holds in one particular direction. The solution of the constraint equation $g\left[\sigma, p(x)\right] = 0$ is $s_1 = 1/\sqrt{2W^{(1)}}$ and $W^{(0)} = 1 - 2n_x W^{(1)}$. There is a degree of freedom, which corresponds to the value of $W^{(1)}$. By reparameterizing $W^{(1)} \equiv 1/2\left(n_x + \kappa\right)$ with a scaling constant κ and multiplying by C, the sigma points for x are

$$\begin{aligned} \chi^{(0)} &= \bar{x} & W^{(0)} &= \kappa/\left(n_x + \kappa\right) \\ \chi^{(i)} &= \bar{x} + \left(\sqrt{\left(n_x + \kappa\right)P_{xx}}\right)_i & W^{(i)} &= 1/2\left(n_x + \kappa\right) \\ \chi^{(i+n)} &= \bar{x} - \left(\sqrt{\left(n_x + \kappa\right)P_{xx}}\right)_i & W^{(i+n)} &= 1/2\left(n_x + \kappa\right) \end{aligned} \tag{2.60}$$

where $\left(\sqrt{\left(n_x + \kappa\right)P_{xx}}\right)_i$ is the *i*-th row or column of the matrix square root of $\left(n_x + \kappa\right)P_{xx}$ and $W^{(i)}$ is the weight associated with the *i*-th point. The degree of freedom is transferred to the choice of κ which can be eliminated by the cost function. One possible choice for the cost function is to minimize the error between the fourth order moments of the sigma points and the true distribution. For a GRV,

$$E\left[\left(z^{(i)}\right)^4\right] = 3 \qquad \forall i\,. \tag{2.61}$$

Using the symmetry, the cost function is

$$c\left[\sigma, p\left(x\right)\right] = \left|2w^{(1)}s_1^4 - 3\right|, \tag{2.62}$$

which is zero when $w_1 = 3/2s_1^4 = 1/6$ or $\kappa = 3 - n_x$. The cost function minimizes the error in the kurtosis with the set of $2n_x+1$ samples. In order to match the exact kurtosis a different set of sigma points would be needed (fourth order UT) [38].

2.4.3.2. Propagation of the UT Mean

One can approximate the mean $\bar{y}$ of the posteriori distribution by transforming each sigma point using the nonlinear function $y = f(x)$ and taking the weighted sum of the transformed sigma points. The transformed sigma points are computed as

$$\gamma^{(i)} = f\left(\chi^{(i)}\right) \qquad i = 0,\ldots,2n_x \tag{2.63}$$

where $\sigma_i = \left(\sqrt{\left(n_x + \kappa\right) P_{xx}}\right)_i$ and the sigma points are

$$\begin{aligned} \chi^{(0)} &= \bar{x} & W^{(0)} &= \kappa/\left(n_x + \kappa\right) \\ \chi^{(i)} &= \bar{x} + \sigma_i & W^{(i)} &= 1/2\left(n_x + \kappa\right) \\ \chi^{(i+n)} &= \bar{x} - \sigma_i & W^{(i+n)} &= 1/2\left(n_x + \kappa\right) \end{aligned} \tag{2.64}$$

The approximated mean of y, denoted as $\bar{y}_{UT}$, is

$$\bar{y}_{UT} = \sum_{i=0}^{2n_x} W^{(i)} \gamma^{(i)} . \tag{2.65}$$

To compute $\bar{y}_{UT}$, each $\gamma^{(i)}$ in Eq. (2.63) is expanded in Taylor series around $\bar{x}$, yielding

$$\begin{aligned} \bar{y}_{UT} &= \frac{\kappa}{n_x + \kappa} f\left(\bar{x}\right) + \frac{1}{2\left(n_x + \kappa\right)} \sum_{i=1}^{2n_x} \left[f\left(\bar{x}\right) + D_{\sigma_i} f + \frac{1}{2!} D_{\sigma_i}^2 f + \frac{1}{3!} D_{\sigma_i}^3 f + \ldots \right] \\ &= f\left(\bar{x}\right) + \frac{1}{2\left(n_x + \kappa\right)} \sum_{i=1}^{2n_x} \left[D_{\sigma_i} f + \frac{1}{2!} D_{\sigma_i}^2 f + \frac{1}{3!} D_{\sigma_i}^3 f + \ldots \right]. \end{aligned} \tag{2.66}$$

For any integer $m \geq 0$

$$\begin{aligned}
\sum_{i=1}^{2n_x} D_{\sigma_i}^{2m+1} f &= \sum_{i=1}^{2n_x} \left[\left(\sum_{j=1}^{n_x} \sigma_{j,i} \frac{\partial}{\partial x_j} \right)^{2m+1} f \Big|_{x=\bar{x}} \right] \\
&= \sum_{i=1}^{2n_x} \left[\sum_{j=1}^{n_x} \left(\sigma_{j,i} \right)^{2m+1} \frac{\partial^{2m+1}}{\partial x_j^{2m+1}} f \Big|_{x=\bar{x}} \right] \\
&= \sum_{j=1}^{n_x} \left[\sum_{i=1}^{2n_x} \left(\sigma_{j,i} \right)^{2m+1} \frac{\partial^{2m+1}}{\partial x_j^{2m+1}} f \Big|_{x=\bar{x}} \right] \\
&= 0
\end{aligned} \tag{2.67}$$

by using the symmetry of the sigma points as $\sigma_i = -\sigma_{i+n_x}$ for $i = 1, \ldots, n_x$. Therefore, all of the odd terms in Eq. (2.66) will be zero. The second order term in Eq. (2.66) can be written

$$\begin{aligned}
\frac{1}{2\left(n_x + \kappa\right)} \sum_{i=1}^{2n_x} \frac{1}{2} D_{\sigma_i}^2 f &= \frac{1}{4\left(n_x + \kappa\right)} \sum_{i=1}^{2n_x} \left(\sum_{j=1}^{n_x} \sigma_{j,i} \frac{\partial}{\partial x_j} \right)^2 f \Big|_{x=\bar{x}} \\
&= \frac{1}{4\left(n_x + \kappa\right)} \sum_{i=1}^{2n_x} \sum_{j,k=1}^{n_x} \sigma_{j,i} \sigma_{i,k} \frac{\partial^2}{\partial x_j \partial x_k} f \Big|_{x=\bar{x}} \\
&= \frac{1}{2\left(n_x + \kappa\right)} \sum_{j,k=1}^{n_x} \sum_{i=1}^{n_x} \sigma_{j,i} \sigma_{i,k} \frac{\partial^2}{\partial x_j \partial x_k} f \Big|_{x=\bar{x}} .
\end{aligned} \tag{2.68}$$

By using the symmetry of the sigma points as $\sigma_i = -\sigma_{i+n_x}$ for $i = 1, \ldots, n_x$ and substituting $\sigma_{i,j}$ and $\sigma_{i,k}$ we find that

$$\frac{1}{2\left(n_x+\kappa\right)}\sum_{j,k=1}^{n_x}\sum_{i=1}^{n_x}\sigma_{j,i}\sigma_{i,k}\left.\frac{\partial^2 f}{\partial x_j \partial x_k}\right|_{x=\bar{x}} = \frac{1}{2\left(n_x+\kappa\right)}\sum_{j,k=1}^{n_x}\sum_{i=1}^{n_x}\left(\sqrt{\left(n_x+\kappa\right)P_{xx}}\right)_{ji}\left(\sqrt{\left(n_x+\kappa\right)P_{xx}}\right)_{ik}\left.\frac{\partial^2 f}{\partial x_j \partial x_k}\right|_{x=\bar{x}}$$
$$= \frac{1}{2}\sum_{j,k=1}^{n}\left(P_{xx}\right)_{jk}\left.\frac{\partial^2 f}{\partial x_j \partial x_k}\right|_{x=\bar{x}}. \tag{2.69}$$

Eq. (2.66) can be written as

$$\bar{y}_{UT} = f\left(\bar{x}\right)+\frac{1}{2}\sum_{j,k=1}^{n_x}\left(P_{xx}\right)_{jk}\left.\frac{\partial^2 f}{\partial x_j \partial x_k}\right|_{x=\bar{x}}+\frac{1}{2\left(n_x+\kappa\right)}\sum_{i=1}^{2n_x}\left[\frac{1}{4!}D^4_{\sigma_i}f+\frac{1}{6!}D^6_{\sigma_i}f+\ldots\right]. \tag{2.70}$$

The comparison between the true mean of y derived in Eq. (2.33) and the approximation of the mean of y by UT shows that they match up to third order. The scaling constant κ may also be used to minimize the error coming from the higher order terms.

2.4.3.3. Propagation of the UT Covariance

The covariance of y can be approximated by UT using

$$\left(P_{yy}\right)_{UT} = \sum_{i=0}^{2n_x}W^{(i)}\left(\gamma^{(i)}-\bar{y}_{UT}\right)\left(\gamma^{(i)}-\bar{y}_{UT}\right)^T. \tag{2.71}$$

By expanding Eq. (2.63) in Taylor series and combining with Eq. (2.66), one can write

$$\begin{aligned}\left(P_{yy}\right)_{UT} &= \frac{\kappa}{n_x+\kappa}\left(-\frac{1}{2\left(n_x+\kappa\right)}\sum_{j=1}^{2n_x}\left[\frac{1}{2!}D^2_{\sigma_j}f+\ldots\right]\right)\left(-\frac{1}{2\left(n_x+\kappa\right)}\sum_{j=1}^{2n_x}\left[\frac{1}{2!}D^2_{\sigma_j}f+\ldots\right]\right)^T \\ &+\frac{1}{2\left(n_x+\kappa\right)}\sum_{i=1}^{2n_x}\left(\left[D_{\sigma_i}f+\frac{1}{2!}D^2_{\sigma_i}f+\ldots\right]-\frac{1}{2\left(n_x+\kappa\right)}\sum_{j=1}^{2n_x}\left[\frac{1}{2!}D^2_{\sigma_j}f+\ldots\right]\right) \\ &\left(\left[D_{\sigma_i}f+\frac{1}{2!}D^2_{\sigma_i}f+\ldots\right]-\frac{1}{2\left(n_x+\kappa\right)}\sum_{j=1}^{2n_x}\left[\frac{1}{2!}D^2_{\sigma_j}f+\ldots\right]\right)^T.\end{aligned} \tag{2.72}$$

Rearranging Eq. (2.72) we find

$$\begin{aligned}\left(P_{yy}\right)_{UT} &= \frac{\kappa}{n_x+\kappa}\left(\frac{1}{\left(n_x+\kappa\right)^2}\sum_{j=1}^{n_x}\left[\frac{1}{4}D_{\sigma_j}^2 f\left(D_{\sigma_j}^2 f\right)^T+\ldots\right]\right)\\ &+\frac{1}{\left(n_x+\kappa\right)}\sum_{i=1}^{n_x}\left(D_{\sigma_i} f\left(D_{\sigma_i} f\right)^T+\frac{1}{4}D_{\sigma_i}^2 f\left(D_{\sigma_i}^2 f\right)^T\right.\\ &\left.-\frac{1}{2\left(n_x+\kappa\right)}\sum_{j=1}^{n_x}D_{\sigma_i}^2 f\left(D_{\sigma_j}^2 f\right)^T+\frac{1}{4\left(n_x+\kappa\right)^2}\sum_{j=1}^{n_x}D_{\sigma_j}^2 f\left(D_{\sigma_j}^2 f\right)^T+\ldots\right)\\ &=\left[FP_{xx}F^T-\frac{1}{4}FP_{xx}F^T\left(FP_{xx}F^T\right)^T+\ldots\right].\end{aligned} \tag{2.73}$$

The approximation of the covariance of y by UT shows that it matches up with the true covariance to the third order.

2.4.3.4. Unscented Kalman Filtering

For the nonlinear system model described in Eq. (2.45) and Eq. (2.46), for $k=1,2,\ldots$, the UKF algorithm is:

1. First, choose the sigma points as specified in Eq. (2.60)

$$\begin{aligned}\hat{x}_{k-1}^{(0)} &= \hat{x}_{k-1} & W^{(0)} &= \kappa/\left(n_x+\kappa\right)\\ \hat{x}_{k-1}^{(i)} &= \hat{x}_{k-1}+\left(\sqrt{\left(n_x+\kappa\right)\left(P_{xx}\right)_{k-1}}\right)_i & W^{(i)} &= 1/2\left(n_x+\kappa\right)\\ \hat{x}_{k-1}^{(i+n)} &= \hat{x}_{k-1}-\left(\sqrt{\left(n_x+\kappa\right)\left(P_{xx}\right)_{k-1}}\right)_i & W^{(i+n)} &= 1/2\left(n_x+\kappa\right)\end{aligned} \tag{2.74}$$

   where the current best estimate for the mean and covariance of x_{k-1} are $\hat{x}_{k-1}$ and $\left(P_{xx}\right)_{k-1}$.

2. Perform the time update of the state estimate and the estimation error covariance.
   a. Use Eq. (2.45) to propagate the set of sigma points through the state equation.

$$\left(\hat{x}_k^-\right)^{(i)} = f\left(\hat{x}_{k-1}^{(i)}, 0\right). \tag{2.75}$$

b. Combine the $\left(\hat{x}_k^-\right)^{(i)}$ vectors to obtain a priori state estimate at time *k*.

$$\hat{x}_k^- = \sum_{i=0}^{2n_x} W^{(i)} \left(\hat{x}_k^-\right)^{(i)}. \tag{2.76}$$

c. Estimate the corresponding a priori error covariance by adding the error covariance for the modeling noise.

$$\left(P_{xx}^-\right)_k = \sum_{i=0}^{2n_x} W^{(i)} \left(\left(\hat{x}_k^-\right)^{(i)} - \hat{x}_k^-\right)\left(\left(\hat{x}_k^-\right)^{(i)} - \hat{x}_k^-\right)^T + Q\,. \tag{2.77}$$

3. Perform the measurement update of the state estimate and the estimation error covariance

a. Use Eq. (2.46) to obtain the expected measurements with the a priori sigma points

$$\hat{y}_k^{(i)} = h\left(\left(\hat{x}_k^-\right)^{(i)}, 0\right). \tag{2.78}$$

b. Combine the $\hat{y}_k^{(i)}$ vectors to obtain the predicted measurement at time *k*,

$$\hat{y}_k = \sum_{i=0}^{2n_x} W^{(i)} \hat{y}_k^{(i)}\,. \tag{2.79}$$

c. Estimate the corresponding covariance of the predicted measurement by adding the error covariance for the measurement noise

$$\left(P_{yy}\right)_k = \sum_{i=0}^{2n_x} W^{(i)} \left(\hat{y}_k^{(i)} - \hat{y}_k\right)\left(\hat{y}_k^{(i)} - \hat{y}_k\right)^T + R\,. \tag{2.80}$$

d. Estimate the cross covariance between $\hat{x}_k^-$ and $\hat{y}_k$

$$\left(P_{xy}\right)_k = \sum_{i=0}^{2n_x} W^{(i)} \left(\left(\hat{x}_k^-\right)^{(i)} - \hat{x}_k^- \right) \left(\hat{y}_k^{(i)} - \hat{y}_k \right)^T . \tag{2.81}$$

e. The measurement update of the state estimate and estimation error covariance are obtained using the regular Kalman filtering equations

$$\hat{x}_k = \hat{x}_k^- + K_k \left[y_k - \hat{y}_k \right], \tag{2.82}$$

$$K_k = \left(P_{xy}\right)_k \left(P_{yy}\right)_k^{-1}, \tag{2.83}$$

$$\left(P_{xx}\right)_k = \left(P_{xx}^-\right)_k - K_k \left(P_{xy}\right)_k^T . \tag{2.84}$$

The UKF was proposed by Julier and Uhlmann [33] in an attempt to provide a better approximation for nonlinear dynamic state space models than EKF. It is a derivativeless, deterministic sampling based on the Kalman filter structure and consistently outperforms the EKF not only in terms of estimation accuracy, but also in filter robustness and ease of implementation [33].

In the next section we perform an application of the UKF to estimate the degradation in the steam generators (SGs) of IRIS (International Reactor Innovative and Secure).

2.4.3.5. Application: IRIS SG Degradation [39]

As stated in Chapter 1, it is a very important task in nuclear reactors to monitor and diagnose the degradations before serious failures occur. Next generation of nuclear reactors are designed to have a long core life and high fuel burnup. For example, the IRIS reactor was originally designed to have a three year fuel cycle [1]. Since IRIS has an integral configuration where all the primary system components including pumps, steam generators, a pressurizer, and control rod drive mechanisms, are located inside the reactor vessel, a failure in one of these systems may result in loss of safety or interruption of operation. Therefore, especially for the next generation of nuclear reactors, a consistent and efficient degradation monitoring algorithm should be developed to prevent loss of safety and to improve the economy of the reactor.

Estimating the deposition of crud (i.e., corrosion products) on heat transfer surfaces is one of the problems we are interested in. Crud buildup can occur either in the core on the surface of fuel cladding or in the SG both inside and outside of the SG tubing. It impedes the heat transfer and increases the resistance to the fluid flow, resulting in higher pressure drops. In the steam generator, the growth of these deposits causes the thermohydraulic performance to be degraded with time. In the reactor core, these deposits result in degradation in the heat transfer performance, which can lead to local hot spots and cladding failure.

The complex structure and extreme environment in the reactor core and the steam generator limits the placements of the sensors to observe crud buildup. In this application our goal is to detect the SG fouling in IRIS by estimating the crud deposition on the SG tubes.

The IRIS SG is a helical-coil once-through design with the primary fluid flowing outside the tubes. Eight SG modules are located in an annular space between the core barrel and reactor vessel. Feedwater enters the SG through a nozzle in the reactor vessel wall and passes through the lower feed water header. The feedwater enters the SG tubing, and is heated to saturation, boiled to steam, and superheated as it flows upward to the upper steam header [4].

We chose UKF for not only being a better approximation than EKF for highly nonlinear systems, but also its ease of applicability especially when the model is represented by pre-compiled computer codes like RELAP5 [40] in which calculation of Jacobians can be very time consuming and difficult.

We employed a joint estimation approach (described in Section 3.1) in which we augmented the state vector to include both component states c and the system states x as $z = \begin{bmatrix} x & c \end{bmatrix}^T$. The discrete time nonlinear dynamic state space model given in Eqs. (2.4)-(2.6) can be represented in a joint estimation framework as

$$z_k = f\left(z_{k-1}, w_k\right) \tag{2.85}$$

$$y_k = h\left(z_k, v_k\right) \tag{2.86}$$

where $\{w_k\}$ and $\{v_k\}$ are zero mean white Gaussian noise processes independent of each other with known covariance matrices Q and R, respectively. We also augmented the modeling noise vector as

$$w_k = \begin{bmatrix} w_k^x & w_k^c \end{bmatrix}^T \sim N\left(0, Q = \begin{bmatrix} Q_x & 0 \\ 0 & Q_c \end{bmatrix}\right) \tag{2.87}$$

We used RELAP5 as our model. However, RELAP5 does not contain the necessary routines to practice SG fouling applications. We wrote a script to add a crud layer gradually into the RELAP5 model. The script needs the deposition rate and location as inputs and generates the input for RELAP5, which is then run for a time interval where the crud deposition is assumed to be constant. Then the script processes the output of RELAP5 to prepare the input for the next time interval. This loop is terminated when the crud layer no longer changes.

We assumed that crud formation occurs at 10 s after the start of the simulation, rather than through a slow deposition over years of operation. We simulated the fouling of the SG tubes by considering crud buildup uniformly inside the SG tubes as shown in Figure 5.

In our implementation, the plant behavior is observed through the temperature at the outlet of the secondary side. The system states are represented through the pressure distribution inside the secondary side tubes and pressure drop is calculated through these states. The component state to be estimated is the crud layer thickness.

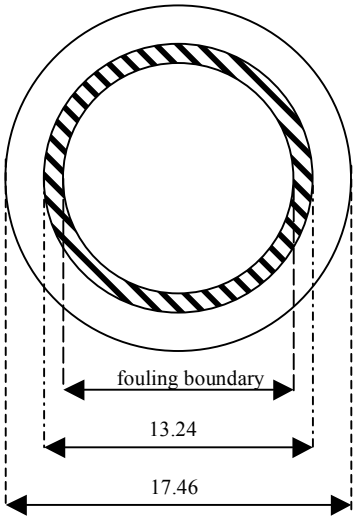

Figure 5. The fouling boundary inside the secondary side tubes.

The stand-alone SG model was constructed by using the RELAP5 model [41] developed by Westinghouse, Polytechnic of Milan and University of Zagreb. We used the same nodalization for the primary and secondary sides of the SG by using the nominal conditions of the SG primary and secondary side inlets as boundary conditions. The nodalization of the stand-alone SG model is given in Figure 6.

The SG tubes in IRIS are assumed to be composed of Inconel Alloy 690. Since the formation and thickness of the crud is not known, we tried our algorithm for different values of thermal conductivity and different thicknesses of the crud. We started our analysis by assuming the thermal conductivity of the crud layer is ~50% less than the thermal conductivity of Inconel Alloy 690 in the operating temperature range. We introduced a 0.5 mm crud layer deposition along the length of the tubes and simulated the measurement, which is the temperature at the outlet of the secondary side with 0.5% noise added. The simulated measurement, and the estimated measurement (through UKF as a state) are shown in Figure 7.

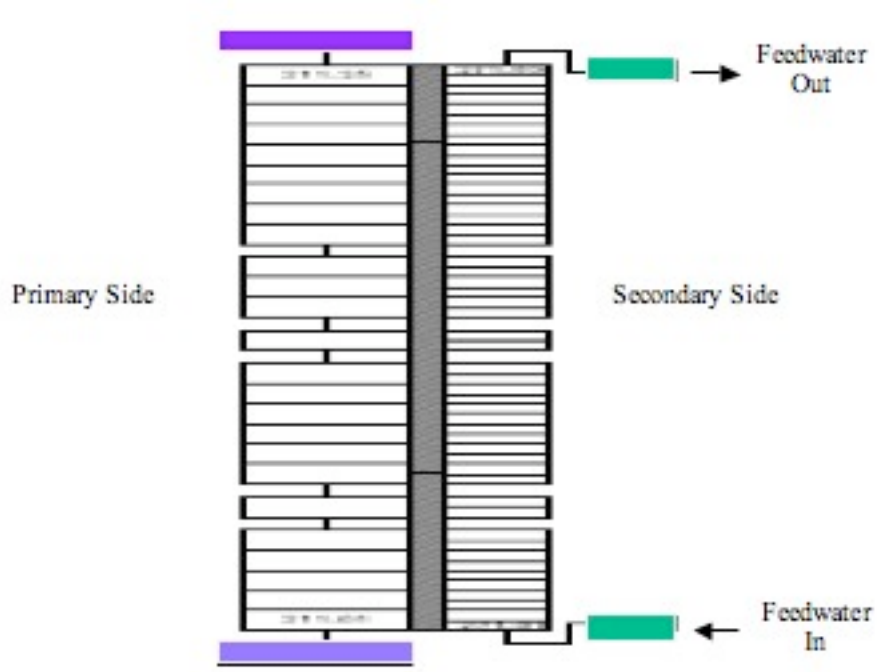

Figure 6. The nodalization of the stand-alone IRIS SG model.

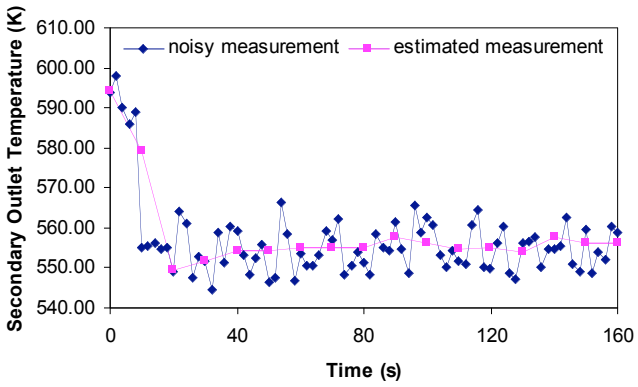

Figure 7. Simulated and estimated measurement for 0.5 mm crud thickness and 50% decrease in thermal conductivity of Inconel.

We applied the UKF to obtain a best estimate of the thickness of the crud layer, considered as a component state [Figure 8(a)], together with a best estimate of the pressure drop along the secondary side [Figure 8(b)].

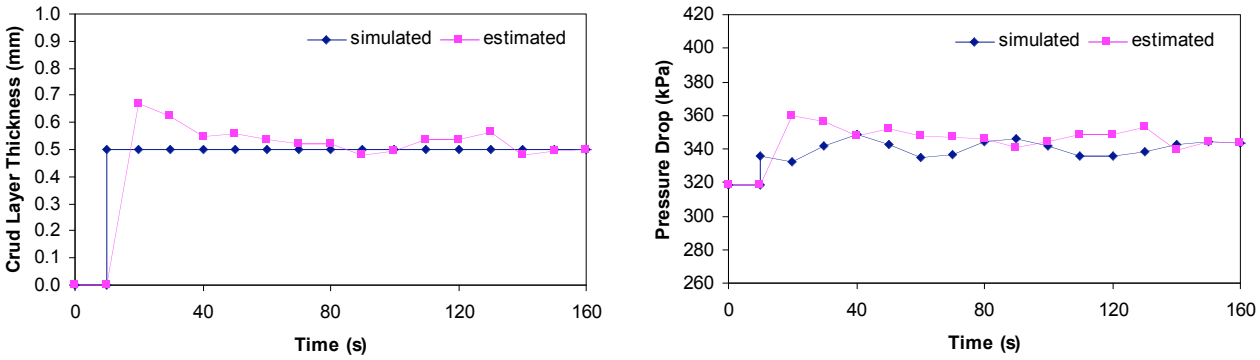

(a) Crud layer thickness

(b) Secondary side pressure drop

Figure 8. Simulated and estimated component and system states for 0.5 mm crud thickness and 50% decrease in thermal conductivity of Inconel.

The UKF algorithm successfully estimates the thickness of the crud layer and the pressure distribution along the secondary side of the SG. A detailed sensitivity analysis can be found in our paper [39].

2.4.4. Particle Filtering

In this section, we derive the particle filtering algorithm that we used to generate our new technique in the rest of this thesis. As explained in the previous sections, for nonlinear systems the extensions of Kalman filter are based on various assumptions to assure tractability. But in general, the dynamic state space model could be high dimensional, highly nonlinear and the states could be non-Gaussian. Particle filtering is a sequential Monte Carlo method alternative to the filtering methods described before. It has a wide range of applicability especially in nonlinear non-Gaussian systems and an easier implementation capability with a price of increased computational effort. After testing different filtering techniques, we chose particle filtering because of its better approximations and wide range of applicability. Our goal is to obtain a general framework for a degradation monitoring algorithm and we believe particle filtering suits our needs.

We start this section by describing Monte Carlo sampling. We discuss how to construct a proposal distribution when we cannot sample from the target distribution. We form the basis for sequential importance sampling (SIS) and explain the weight degeneracy problem in SIS. We finish this section with reviewing sampling importance resampling (SIR) algorithm, which is developed as a remedy for the weight degeneracy problem.

2.4.4.1. Monte Carlo Sampling

The multi-dimensional integrations given in Eqs. (2.11) - (2.14) can be approximated by Monte Carlo sampling. As mentioned in Section 2.3, the computational complexity grows exponentially with the dimension of the integration in the grid based filtering. Monte Carlo methods have an advantage over classical numerical integration, because the relative error, which does not explicitly depend on the state dimension, is of the order of $O\left(N^{-1/2}\right)$ where N is the number of samples.

Consider the computation of an integral at time step k

$$I = \int_{\mathbb{R}^{n_x}} g\left(x_k\right) dx_k. \tag{2.88}$$

To implement Monte Carlo methods, we rewrite the integral in the form

$$I(f) = \int_{\mathbb{R}^{n_x}} f\left(X_k\right) p\left(X_k \mid Y_k\right) dX_k, \tag{2.89}$$

where $g\left(x_k\right) = f\left(X_k\right) p\left(X_k \mid Y_k\right)$ and $p\left(X_k \mid Y_k\right)$ is the posterior density of the state $X_k = \left\{x_1, x_2, \ldots, x_k\right\}$ given all the observations $Y_k = \left\{y_1, y_2, \ldots, y_k\right\}$.

Monte Carlo methods rely on the assumption that we are able to simulate N independent and identically distributed (i.i.d.) random samples, also named particles, $\left\{X_k^{(i)}; i = 1, \ldots, N\right\}$ sampled from $p\left(X_k \mid Y_k\right)$. An empirical estimate of this distribution is then

$$p(X_k \mid Y_k) = \frac{1}{N}\sum_{i=1}^{N}\delta\left(X_k - X_k^{(i)}\right). \tag{2.90}$$

The Monte Carlo estimate of the integral in Eq. (2.89) then becomes

$$\hat{I}_N(f) = \frac{1}{N}\sum_{i=1}^{N} f\left(X_k^{(i)}\right). \tag{2.91}$$

Because the particles are independent, this estimate is unbiased. If the posterior variance of $f(X_k)$, $\sigma^2 = \int_{\mathbb{R}^{n_x}} \left(f(X_k) - I(f)\right)^2 p(X_k \mid Y_k) dX$ is finite, then the variance of $\hat{I}_N(f)$ is equal to σ^2 / N. By the strong law of large numbers

$$\hat{I}_N(f) \underset{N\to+\infty}{\overset{a.s.}{\to}} I(f) \tag{2.92}$$

where $\overset{a.s.}{\to}$ denotes almost sure convergence. Moreover, the central limit theorem yields

$$\sqrt{N}\left(\hat{I}_N(f) - I(f)\right) \underset{N\to+\infty}{\Rightarrow} N\left(0, \sigma^2\right), \tag{2.93}$$

where $\Rightarrow$ denotes convergence in distribution [42]. This means that as $N \to +\infty$, the uncertainty on the approximation will tend to zero.

Even though it may seem that this proposed method is sufficient to approximate integrals like Eq. (2.89), it is usually impossible to sample efficiently from the posterior density $p(X_k \mid Y_k)$, because this density can be multivariate, non-standard and known only up to a proportionality constant [42]. Importance sampling is based on sampling from an alternative density, called the proposal density in order to direct the particles to the regions of importance.

2.4.4.2. Importance Sampling

Let $q(X_k \mid Y_k)$ be a proposal distribution that covers the support of the posterior distribution $p(X_k \mid Y_k)$. Since $p(X_k \mid Y_k)$ is a normalized pdf,

$$\int \frac{p(X_k \mid Y_k)}{q(X_k \mid Y_k)} q(X_k \mid Y_k) dX_k = 1$$

and so dividing Eq. (2.89) by this yields

$$I(f) = \frac{\int f(X_k) W(X_k) q(X_k \mid Y_k) dX_k}{\int W(X_k) q(X_k \mid Y_k) dX_k} \tag{2.94}$$

where $W(X_k)$ is known as the importance weight,

$$W(X_k) = \frac{p(X_k \mid Y_k)}{q(X_k \mid Y_k)}. \tag{2.95}$$

By drawing N i.i.d. particles $\left\{X_k^{(i)}; i = 1, \ldots, N\right\}$ from $q(X_k \mid Y_k)$, the Monte Carlo estimate of the integral is calculated as

$$\hat{I}_N(f) = \frac{\frac{1}{N}\sum_{i=1}^{N} f\left(X_k^{(i)}\right) W\left(X_k^{(i)}\right)}{\frac{1}{N}\sum_{j=1}^{N} W\left(X_k^{(j)}\right)} = \sum_{i=1}^{N} f\left(X_k^{(i)}\right) \tilde{W}\left(X_k^{(i)}\right) \tag{2.96}$$

where

$$\tilde{W}\left(X_k^{(i)}\right) = \frac{W\left(X_k^{(i)}\right)}{\sum_{j=1}^{N} W\left(X_k^{(j)}\right)}.$$

Because $p(X_k \mid Y_k)$ appears in $\tilde{W}\left(X_k^{(i)}\right)$ only in a ratio, we can compute $\tilde{W}\left(X_k^{(i)}\right)$ without knowing the normalized $p(X_k \mid Y_k)$, but can instead use any function that is preoperational to it. The importance sampling estimate $\hat{I}_N(f)$ is biased but consistent, namely the bias vanishes at a rate of $O(N)$ [24]. Under additional assumptions, a central limit theorem with a convergence rate still independent of the dimension of the integrand can be obtained [43].

In this form of the importance sampling, one needs to take all the measurements before estimating the posterior distribution, which increases the computational complexity because one needs to compute the importance weights every time step. This problem can be solved through sequential importance sampling.

2.4.4.3. Sequential Importance Sampling (SIS)

If the proposal distribution is chosen in the following factorized form

$$q(X_k \mid Y_k) = q(X_{k-1} \mid Y_{k-1}) q(x_k \mid X_{k-1}, Y_k), \tag{2.97}$$

we can perform the importance sampling recursively. By iterating we obtain

$$q(X_k \mid Y_k) = q(x_0) \prod_{k=1}^{n} q(x_k \mid X_{k-1}, Y_k). \tag{2.98}$$

In Eq. (2.8) we obtained the following recursive formula for the posterior density

$$p(X_k \mid Y_k) = p(X_{k-1} \mid Y_{k-1}) \frac{p(y_k \mid x_k)\, p(x_k \mid x_{k-1})}{p(y_k \mid Y_{k-1})}.$$

By using this equation and Eq. (2.97), the importance weights can be updated recursively

$$
\begin{aligned}
W\left(X_k^{(i)}\right) &= \frac{p\left(X_k^{(i)} \mid Y_k\right)}{q\left(X_k^{(i)} \mid Y_k\right)} \\
&\propto p\left(X_{k-1}^{(i)} \mid Y_{k-1}\right) \frac{p\left(y_k \mid x_k^{(i)}\right) p\left(x_k^{(i)} \mid x_{k-1}^{(i)}\right)}{q\left(X_{k-1}^{(i)} \mid Y_{k-1}\right) q\left(x_k^{(i)} \mid X_{k-1}^{(i)}, Y_k\right)} \\
&\propto W\left(X_{k-1}^{(i)}\right) \frac{p\left(y_k \mid x_k^{(i)}\right) p\left(x_k^{(i)} \mid x_{k-1}^{(i)}\right)}{q\left(x_k^{(i)} \mid X_{k-1}^{(i)}, Y_k\right)}.
\end{aligned}
\tag{2.99}
$$

Note that, we left out the normalization constant $p\left(y_k \mid Y_{k-1}\right)$ to write this proportionality. In Bayesian filtering we are more interested in the filtering density instead of the posterior density. In the next section, we construct the SIS filtering algorithm.

2.4.4.4. Sequential Importance Sampling Filter

In order to calculate the filtering density, we assume $q\left(x_k \mid X_{k-1}, Y_k\right) = q\left(x_k \mid x_{k-1}, y_k\right)$ (states are first order Markovian). Now, at each time step only $x_k^{(i)}$ needs to be stored and therefore one can discard the state trajectory $X_{k-1}^{(i)}$ and history of measurements Y_{k-1}. The modified importance weights are

$$
W\left(x_k^{(i)}\right) \propto W\left(x_{k-1}^{(i)}\right) \frac{p\left(y_k \mid x_k^{(i)}\right) p\left(x_k^{(i)} \mid x_{k-1}^{(i)}\right)}{q\left(x_k^{(i)} \mid x_{k-1}^{(i)}, y_k\right)}, \tag{2.100}
$$

and the filtering density can be approximated as

$$
p\left(x_k \mid Y_k\right) \approx \sum_{i=1}^{N} W\left(x_k^{(i)}\right) \delta\left(x_k - x_k^{(i)}\right) \tag{2.101}
$$

where the weights are defined in Eq. (2.100). The SIS filtering algorithm consists of recursive propagation of the weights and support points as each measurement is received sequentially [28]. For $k = 1, 2, \ldots$, the SIS filtering algorithm is:

1. For $i = 1, \ldots, N$ sample $x_k^{(i)} \sim q\left(x_k \mid x_{k-1}^{(i)}, y_k\right)$.

2. For $i = 1,\ldots,N$, evaluate the importance weights using Eq. (2.100).

3. Normalize the importance weights $\tilde{W}\left(x_k^{(i)}\right) = \dfrac{W\left(x_k^{(i)}\right)}{\sum_{j=1}^{N} W\left(x_k^{(j)}\right)}$.

The selection of the proposal distribution is the crucial design step in particle filtering, because it can greatly affect the performance of the filter.

It is often convenient to adopt the prior distribution as the proposal distribution

$$q\left(x_k \mid x_{k-1}^{(i)}, y_k\right) = p\left(x_k \mid x_{k-1}^{(i)}\right). \tag{2.102}$$

In this case, the importance weights in Eq. (2.100) satisfy

$$W\left(x_k^{(i)}\right) \propto W\left(x_{k-1}^{(i)}\right) p\left(y_k \mid x_k^{(i)}\right). \tag{2.103}$$

2.4.4.5. Weight Degeneracy Problem

One of the problems with SIS filtering is the degeneracy of the weights. As time increases all but a few particles will have negligible weight. It has been shown [44] that the variance of the importance weights can only increase in time, and therefore it is impossible to avoid weight degeneracy. A suitable measure of degeneracy is the effective sample size N_{eff}, introduced by Kong et.al [45],

$$N_{eff} = \frac{N}{1 + Cov_{q(\cdot|Y_k)}\left(W\left(x_k^{(i)}\right)\right)} = \frac{N}{1 + \mathrm{E}_{q(\cdot|Y_k)}\left(W\left(x_k^{(i)}\right)^2\right)}. \tag{2.104}$$

This cannot be evaluated analytically, because true weights, $W\left(x_k^{(i)}\right)$ are impossible to obtain. Instead, the effective sample size may be estimated by

$$\hat{N}_{eff} = \frac{1}{\sum_{i=1}^{N} W\left(x_k^{(i)}\right)^2}. \tag{2.105}$$

Notice that small N_{eff} indicates severe degeneracy. In order to reduce the effects of the weight degeneracy problem, either we can obtain a better proposal density or we use a resampling step, which is the basis for the sampling importance resampling (SIR) filter.

2.4.4.6. Sampling Importance Resampling Filter

When N_{eff} falls below some threshold, one may use a resampling scheme to eliminate particles that have low importance weights and split particles with high importance weights [46]. The resampling step involves generating a new set of particles at time step *k* by resampling *N* times with replacement from an approximate discrete representation of the filtering distribution given in Eq. (2.101) in the form

$$\hat{p}\left(x_k \mid Y_k\right) = \sum_{i=1}^{N} \frac{1}{N} \delta\left(x_k - x_k^{*(i)}\right) = \sum_{i=1}^{N} \frac{n^{(i)}}{N} \delta\left(x_k - x_k^{(i)}\right) \tag{2.106}$$

where $n^{(i)}$ is the number of copies of the particle $x_k^{(i)}$ in the new set of particles $\left\{x_k^{*(i)}; i = 1,\ldots,N\right\}$ with equal weights, $1/N$. As $N \to +\infty$,

$$\mathrm{E}\left[\left(I(f) - \int_{\mathbb{R}^{n_x}} f\left(x_k\right) \hat{p}\left(X_k \mid Y_k\right) dx_k\right)^2\right]$$

goes to zero [47].

Among many different resampling algorithms three of them are presented here [47]:

1. **Multinomial Resampling**: Generate N uniform numbers, $u^{(i)} \sim U(0,1)$. Use these samples to select $x_k^{*(i)}$ according to the multinomial distribution. That is,

$$x_k^{*(i)} = x\left(F^{-1}\left(u^{(i)}\right)\right) = x_k^{(j)} \tag{2.107}$$

with j such that $u^{(i)} \in \left[\sum_{m=1}^{j-1} W\left(x_k^{(m)}\right), \sum_{m=1}^{j} W\left(x_k^{(m)}\right)\right)$ where F^{-1} denotes the generalized inverse of the cumulative probability distribution of the normalized particle weights.

2. **Stratified Resampling**: Generate N ordered random numbers

$$u^{(i)} = \frac{(i-1) + \tilde{u}^{(i)}}{N} \tag{2.108}$$

where $\tilde{u}^{(i)} \sim U(0,1)$, and use them to select $x_k^{*(i)}$ according to the multinomial distribution.

3. **Systematic Resampling**: Generate N ordered random numbers

$$u^{(i)} = \frac{(i-1) + \tilde{u}}{N} \tag{2.109}$$

where $\tilde{u} \sim U(0,1)$, and use them to select $x_k^{*(i)}$ according to the multinomial distribution.

The resampling step may also introduce new problems into the particle filter. Resampling may limit the parallelization of the algorithm, since the particles may be combined at some point [28]. Since the particles with high importance weights are selected many times, it may lead to a loss of diversity among the particles. This problem is known as sample impoverishment. Solving this problem in a filter to perform degradation monitoring is the primary contribution of this dissertation. This will be the focus of Chapter 3.

In the SIR algorithm proposal distribution is chosen as the prior distribution as given in Eq. (2.102). For $k = 1,2,\ldots$, the SIR filtering algorithm is:

1. For $i = 1,\ldots,N$, sample $x_k^{(i)} \sim p\left(x_k \mid x_{k-1}^{(i)}\right)$.
2. For $i = 1,\ldots,N$, evaluate the importance weights using Eq. (2.103).
3. Normalize the importance weights.
4. Resample with replacement N particles according to the importance weights with one of the resampling algorithms described above.

CHAPTER 3

INTRODUCTION OF A RELIABILITY DEGRADATION DATABASE INTO DEGRADATION MONITORING FRAMEWORK

In the preceding chapter we reviewed various nonlinear filtering techniques. We also presented an application of degradation monitoring in the steam generators of the IRIS reactor. In this chapter we address a very important problem with the filtering techniques, which is the inability of a filter to estimate an abrupt change. Because we model degradations as abrupt changes in the component states, using a filter as a black box for this kind of problem might result in inaccurate estimates of the states. Thus, we propose techniques to improve the filter in order to respond to the changes in the component states.

We start this chapter with the description of the state space model for the degradation monitoring problem in the joint parameter/state estimation framework. In section 3.2 we redefine the problem discussed above for both the extensions of Kalman filter and particle filter. The main issue is that the covariance of the estimate will become small. This is usually a desirable property for an unbiased estimate showing that the filter's belief in the estimate is high. This appears in different ways for different filtering algorithms but the consequence is the same: if there is an abrupt change in one of the states, then it is hard for the filter to respond to that change. This can lead to the filter converging to the wrong state. On the other hand, if our belief to the system model is low, then the problem may be ill-posed, especially for high dimensional systems.

As stated in Chapter 1, our goal in this thesis is twofold. First, we want to generate a general framework for degradation monitoring. Second we want to construct a framework to combine multiple data sources, e.g., reliability degradation database, sensor data, filter estimates, etc. So, generating new techniques as a remedy for the problems mentioned in the previous paragraph by introducing a reliability degradation database unites our goals to obtain a general framework for degradation monitoring. In Section 3.3 we propose to use a reliability degradation database to improve the performance of the filter by exploring the state space in the direction of possible degradations and by eliminating the less likely state transitions using a MCMC move step.

In Subsection 3.3.3 we extend our algorithm to be used in degradation detection and isolation. Our earlier work on degradation monitoring based on parameter (component state) estimation using the extended Kalman filter [48] [49], unscented Kalman filter [50] [39] [51] and particle filtering [52] reinforced our belief in the efficacy of particle filtering in this thesis mainly because of its consistency and efficiency as an estimator.

3.1. STOCHASTIC MODEL FOR DEGRADATION MONITORING

The dynamic system state model for a general discrete-time nonlinear system is given in Eqs. (2.4) – (2.6). We employ a joint estimation framework in which the system and component states are concatenated by utilizing an augmented state vector representation, $z = \begin{bmatrix} x & c \end{bmatrix}^T$. In this framework, the estimations are generated simultaneously, in contrast to dual estimation techniques where two coupled filters are run to estimate both the system and component states. For the Kalman filtering framework, Nelson [53] showed for a range of problems that the joint estimation approach is expected to provide better estimates.

We consider a general physical system, which contains n_c physical components described via component characteristics $c^v \in \mathbb{R}^{n_v}$, i.e., valve flow areas, pump characteristics, etc., which define the component state $c = \begin{bmatrix} c_1 & c_2 & \dots & c_{n_c} \end{bmatrix}^T$ of the

system. There need not be a one-to-one correspondence between the number of actual components in the system and the number of component characteristics. Not only more than one component characteristic may be needed to define a component state, but also one component characteristic may affect more than one component.

The dynamic state space model restructured for our joint estimation framework is

$$z_k = \begin{bmatrix} x_k \\ c_k \end{bmatrix} = \begin{bmatrix} f\left(x_{k-1}, w_k^x; c_k\right) \\ c_{k-1} + w_k^c \end{bmatrix}, \tag{3.1}$$

$$y_k = h\left(z_k\right) + v_k. \tag{3.2}$$

The noise sequences are assumed to be independent and white as described in Eq. 2.87 and to have known pdfs. We treat the component states c_k as constant but uncertain model parameters. If there is a degradation associated with one of the components, then we expect the component state to change abruptly, but stay constant after this change.

In the real plant, the components within a system may degrade due to a random change in their characteristics. The degradation will then affect the system states and monitored process variables. For example, the steam generator tubes may degrade because of crud deposition inside the tubes, which results in changing one of its characteristics, i.e., the flow area. The decrease in the flow area increases the pressure drop and affects the system states, i.e., nodal pressure distribution along the tubes. Also, the degradation deteriorates the heat transfer and consequently decreases the tube outlet temperature, which can be monitored through a sensor.

Small degradations in the components may be harder to detect and isolate compared to larger degradations and failures within the components. The reason is that the signature of small degradations on the process may be lost within noise. One other issue is even if the effect of the degradation on the measurement is identified, for high dimensional systems there could be many component trajectories that can produce the observed change because of the large uncertainties in the system, and that can lead to an ill-posed

filtering problem. Throughout the thesis we assume that analytical redundancy exists, i.e., the influence of the degradation upon the analytical redundancy is observable, and the component degradations are detectable.

As stated in Section 2.1 the component states undergo random, discrete transitions and stay constant between these transitions. Upon the introduction of degradation e.g., within component 1 between time steps *k-1* and *k*, as illustrated in Figure 9, the component state changes according to

$$c_{\deg,k} = c_{nom,k-1} + \Delta c_k + w_k^c \tag{3.3}$$

Since the transition is random, Δc_k is not known. After the degradation occurs, the dynamic state space model given in Eqs. (3.1) and (3.2) is no longer representative of the real plant behavior because of the change in the component state. The challenge is how we can modify the filtering algorithm to explore the state space in order to estimate the states optimally in real time. In the next section, we redefine this problem in a systematic way for different estimation algorithms and review alternative techniques to overcome this problem.

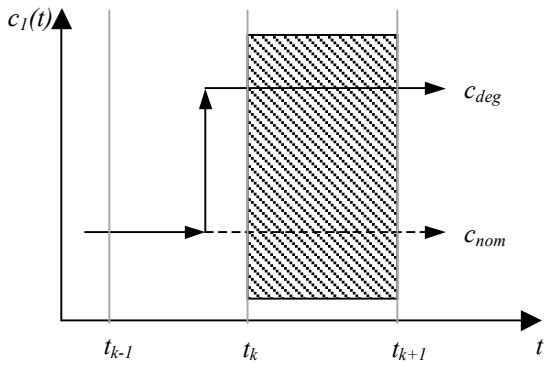

Figure 9. The change in the component state due to degradation.

Before starting this discussion, we rewrite Eqs. (2.10) – (2.14) for the filtering density in the joint estimation framework

$$p(z_k \mid Y_k) = \frac{p(y_k \mid z_k)\, p(z_k \mid Y_{k-1})}{p(y_k \mid Y_{k-1})}. \tag{3.4}$$

The prior density is

$$p(z_k \mid Y_{k-1}) = \int p(z_k \mid z_{k-1}) p(z_{k-1} \mid Y_{k-1})\, dz_{k-1}. \tag{3.5}$$

The state transition density is written by using the definition of conditional probability as

$$p(z_k \mid z_{k-1}) = \frac{p(x_k, c_k, x_{k-1}, c_{k-1})}{p(x_{k-1}, c_{k-1})} = \frac{p(x_k \mid x_{k-1}, c_k, c_{k-1})\, p(x_{k-1}, c_k, c_{k-1})}{p(x_{k-1}, c_{k-1})}.$$

As given in Eq. (3.1), the system state at time *k* is a function of system state at time *k-1* and component state at time *k,* so $p(x_k \mid x_{k-1}, c_k, c_{k-1}) = p(x_k \mid x_{k-1}, c_k)$. Using the definition of the conditional probability again we obtain

$$\begin{aligned} p(z_k \mid z_{k-1}) &= \frac{p(x_k \mid x_{k-1}, c_k)\, p(c_k \mid x_{k-1}, c_{k-1})\, p(x_{k-1}, c_{k-1})}{p(x_{k-1}, c_{k-1})} \\ &= p(x_k \mid x_{k-1}, c_k)\, p(c_k \mid x_{k-1}, c_{k-1}) \end{aligned} \tag{3.6}$$

where for the dynamic state space model given in Eq. (3.1),

$$p(x_k \mid x_{k-1}, c_k) = \int \delta\left(x_k - f\left(x_{k-1}, w_k^x; c_k\right)\right) p\left(w_k^x\right) dw_k^x, \tag{3.7}$$

$$p(c_k \mid x_{k-1}, c_{k-1}) = \int \delta\left(c_k - \left(c_{k-1} + w_k^c\right)\right) p\left(w_k^c\right) dw_k^c. \tag{3.8}$$

The observation likelihood density is calculated using the observation function as

$$p(y_k \mid z_k) = \int \delta\left(y_k - h\left(z_k, v_k\right)\right) p\left(v_k\right) dv_k. \tag{3.9}$$

The denominator of Eq. (3.4) is a scalar normalization constant given by

$$p(y_k \mid Y_{k-1}) = \int p(y_k \mid x_k) p(y_k \mid Y_{k-1})\, dx_k. \tag{3.10}$$

3.2. THE PROBLEM OF CHANGE ESTIMATION IN NONLINEAR FILTERING ALGORITHMS

Filtering techniques suffer from various problems besides the approximations introduced to assure tractability for nonlinear systems. One of these problems is the inability of the filter to respond to abrupt changes in the states. We call abrupt change as any change in the component states that occurs either instantaneously or at least very fast with respect to the sampling period of the measurements [54]. Abrupt changes by no means refer to changes with large magnitude; on the contrary, we are interested in estimation of the small changes.

After running a filter for a long time successfully, the error covariance of estimation gets very small. This prevents the filter from responding to a change in the state because the reduction in the error covariance limits the state space that the filter searches. Assisting the filter to explore the state space is obviously a solution but there is no unique way of doing it. In the next sections, we discuss this problem for different nonlinear filtering algorithms.

3.2.1. Oblivious Nonlinear Kalman Filtering

When the noise inputs to the system are small or when the filter operates over long time intervals, the covariance matrix becomes very small and optimistic. The filter gain therefore becomes small, and the filter relies on old measurements and becomes "oblivious" to new measurements. If an abrupt change occurs, the filter will respond quite sluggishly, yielding poor performance [55,56].

There are a variety of techniques like limited memory filter [55], exponentially age-weighted filter [57], adaptive fading Kalman filter [58] and covariance matching [32] for keeping the filter sensitive to the new measurements. In this dissertation, we suggest a new idea, which is to solve this problem in a multiobjective optimization framework when another data source is present i.e., a reliability degradation database. In the

following subsections we first review covariance matching and analyze its performance in EKF with an application. Then, we show the effects of "obliviousness" in UKF with an application and propose a multiobjective optimization framework to improve the behavior of the filter.

3.2.1.1. Covariance Matching

The basic idea behind the covariance matching techniques is to make the residuals consistent with their statistics. In our paper *Probabilistic Techniques for Diagnosis of Multiple Component Degradations* [48], we developed this technique in an innovative way to construct multiple hypotheses in order to isolate the faulty components and estimate the magnitude of the fault/s. We present this application in the next subsection.

Consider the innovation sequence $\xi_k = \left(y_k - H_k \hat{x}_k^-\right)$, which has a covariance $S_k = H_k P_k^- H_k^T + R$ given in Eq. 2.26. After an abrupt change, the innovation is expected to be large, but its covariance is still small because of the filter's insensitivity to the measurements. Since the actual covariance is expected to be much larger than $S_k = H_k P_k^- H_k^T + R$, in this technique we increase the modeling noise covariance Q in order to increase P_k^- and so match the anticipated value of S_k.

Suppose that the filter estimates $\hat{x}_{k-1}$ and P_{k-1} are available at time *k-1*. The degradation is introduced between time steps *k-1* and *k*. After detecting the degradation, we choose a time lag n_t and calculate the residuals from *k* to $k+n_t-1$ in order to give some statistical smoothing and calculate

$$S_k = \mathrm{E}\left[\xi_{k+l}\xi_{k+l}^T\right] = \frac{1}{n_t}\sum_{l=0}^{n_t-1}\xi_{k+l}\xi_{k+l}^T \tag{3.11}$$

This will produce consistency between the residuals and their statistics. We obtain an equation for Q by setting the covariance of the residual

$$H_k P_k^- H_k^T + R = \mathrm{E}\left[\xi_{k+l}\xi_{k+l}^T\right] \tag{3.12}$$

and so

$$H_k\left(F_{k,k-1}P_{k-1}F_{k,k-1}^T + Q\right)H_k^T + R = \mathrm{E}\left[\xi_{k+l}\xi_{k+l}^T\right] \tag{3.13}$$

finally yielding

$$H_k Q H_k^T = \mathrm{E}\left[\xi_{k+l}\xi_{k+l}^T\right] - H_k F_{k,k-1}P_{k-1}F_{k,k-1}^T H_k^T - R\,. \tag{3.14}$$

If H is of rank less than n_z Eq. (3.14) does not give a unique solution for Q [59].

In the next subsection, we present how we utilized this technique to solve the oblivious filter problem in a multicomponent system.

3.2.1.2. Application: Adaptive EKF with Covariance Matching [48] [49]

We developed an adaptive extended Kalman filtering algorithm for the diagnosis of degradations of multiple components in nuclear power plants. Our diagnostic algorithm uses the measurement residuals to generate a noise input to the uncertain component state in an adaptive Kalman filtering algorithm so that various postulated component degradations may be statistically represented. The diagnostic algorithm has been tested with a balance of plant (BOP) model of a boiling water reactor (BWR).

In this joint estimation framework where $(\cdot)_x$ and $(\cdot)_c$ denote the functions describing the system and component states, respectively, given one measurement residual ξ_k without smoothing we may assume ξ_k^2 is the maximum likelihood estimate [32] of $\mathrm{E}\left[\xi_k\xi_k^T\right]$

$$\xi_k^2 = \mathrm{E}\left[\xi_k\xi_k^T\right] = \left(H_k F_{k,k-1}P_{k-1}F_{k,k-1}^T H_k^T\right)_x + \left(H_k Q H_k^T\right)_x + \left(H_k Q H_k^T\right)_c + R\,. \tag{3.15}$$

The expected covariance of the measurement residual T before recognizing any

component transition

$$T = \left(H_{k-1}F_{k-1,k-2}P_{k-2}F_{k-1,k-2}^{T}H_{k-1}^{T}\right)_{x} + \left(H_{k-1}QH_{k-1}^{T}\right)_{x} + R \tag{3.16}$$

with the recognition that we introduce a finite modeling noise covariance, Q_c to account for modeling errors associated with the component transition.

We assume the measurement residual ξ is a zero-mean Gaussian, so we may evaluate the consistency between the expected value T and observed value ξ_k^2 of residual variance by monitoring the statistic

$$d^* = \xi_k T^{-1} \xi_k^T, \tag{3.17}$$

which is described by a χ^2-distribution [9] with n_y degrees of freedom for n_y observations. If $d^* > \chi_\Omega^2$, where χ_Ω^2 is obtained from a χ^2-table, representing $\Omega\,\%$ desired test significance, then we declare that a modeling deficit exists, i.e., a component state transition has occurred resulting in a statistically significant deviation between observed and predicted process variables. Upon the detection of a system anomaly of unknown origin, we proceed to determine what changes in the component state $c_{k-1} \to \{c = \hat{c}_k\}$ could have resulted in the measurement deficit $\xi_k^2 - T$.

Since we do not know either the type or magnitude of the fault, we estimate the component characteristic uncertainty by considering the impact of each single component fault one at a time. We assume that the covariance of the residual changes at time step k due to the change in the component states resulting $\left(H_k F_{k,k-1} P_{k-1} F_{k,k-1}^T H_k^T\right)_x + \left(H_k Q H_k^T\right)_x + R = T$. Thus, assuming individual component transitions are uncorrelated, we design the noise covariance Q_c to be diagonal so that Eqs. (3.15) and (3.16) yield

$$\left(H_{k-1}QH_{k-1}^{T}\right)_{c} = \xi_k^2 - T\,. \tag{3.18}$$

For component *i*, Eq. (3.18) is used to model the uncertainty in system state modeling as the largest manifestation of the component perturbation, in terms of the *i*-th diagonal element of Q_c

$$q_{c,ii} = \max_{1 \le s \le n_y} \left[\left(\xi_k^2 - T \right)_s / h_{c,si}^2 \right] \tag{3.19}$$

provided that such a perturbation is physically feasible. Here, the component $h_{c,si} = \left(\partial y_s / \partial c_i \right)$ of Jacobian matrix H_c represents the sensitivity coefficient connecting observation y_s to component c_i. The corresponding uncertainty in system state *x* can be specified in an ad hoc manner with $h_{x,sj} = \left(\partial y_s / \partial x_j \right)$ and a diagonal matrix Q_x

$$q_{x,jj} = \max_{1 \le i \le n_c} \left(q_{c,ii} h_{c,si}^2 / h_{x,sj}^2 \right). \tag{3.20}$$

For each component *i*, we construct a hypothesis by replacing only the *i*-th diagonal element of Q_c by $q_{c,ii}$ and updating the Q_x with $q_{x,jj}$. This choice of the elements of $Q = \begin{bmatrix} Q_x & 0 \\ 0 & Q_c \end{bmatrix}$ increases the covariance matrix in Equation (3.15) to introduce additional modeling uncertainty and are tested to determine if the updated covariance matrix Q is thoroughly accounting for the observed modeling deficit $\xi_k^2 - T$ of Eq. (3.18). Allowing for each of n_c components to be either in a faulted or normal operating state, we need to execute a bank of $J = 2^{n_c}$ adaptive filters, which yield a set of *J* multivariate pdfs for the component/system characteristics. We then determine which of the *J* pdfs might represent a component fault and of these, which are significantly different from one another [48]. This determination reduces the original set of *J* feasible component states to a reduced set of *J** unique feasible component states characteristic of faulted component behavior.

The next step is to find which hypotheses are more probable. In order to do that, we first draw a sample from the nominal density $c_{nom}^{(i)} \sim p_{nom}(c \mid y) = \sum_x p_{nom}(x, c \mid y)$ where $i = 1, \ldots, N$. Then for each hypothesis we perform the following, for $hyp = 1, \ldots, J^*$:

1. For $i = 1, \ldots, N$ draw a sample from the pdf $c_{hyp}^{(i)} \sim p_{hyp}(c \mid y) = \sum_x p_{hyp}(x, c \mid y)$.
2. Evaluate the weights for each sample based on the transition/non-transition probabilities obtained from the degradation database [48].
3. Normalize the weights.

This algorithm provides the relative likelihood for each hypothesis.

To demonstrate these algorithms, a low order model of a BOP representative of the Big Rock Point BWR [60] was used. The balance of plant is represented by 11 system variables and observed via five system observation variables. Nine component characteristics were chosen for this demonstration. The details of this model are given in Chapter 4. A binary system fault composed of a 5% increase (from nominal) in the effective flow area of the main steam valve and a simultaneous 10% decrease (from nominal) in the low pressure turbine efficiency was considered in one of the test cases. After detecting the fault in terms of expected residuals and generating 130 different hypotheses (for 9 components, at most 3 simultaneous faults were considered) the performances of the expected hypotheses were calculated and plotted in Figure 10.

Hypothesis A was generated by considering component 2 as constant but uncertain, while Hypothesis B was generated by considering both of the components were constant but uncertain at the time of the fault. Since there was not enough uncertainty inserted into component 1 in Hypothesis A, it needed a longer time to converge to the correct perturbed state. Therefore, Hypothesis B was found to be the correct fault/no fault combination for this test case.

The linearization approximation of the nonlinear system model and the Gaussian assumption of the state variables in the EKF, and the ad hoc approach of Eq. (3.20) that

we employed to calculate the magnitude of the modeling error covariance, prevent the use of these algorithms in a more general framework. Adding additional modeling noise to the states also decreases the precision of the estimates. A more detailed analysis of this application example can be found in [48].

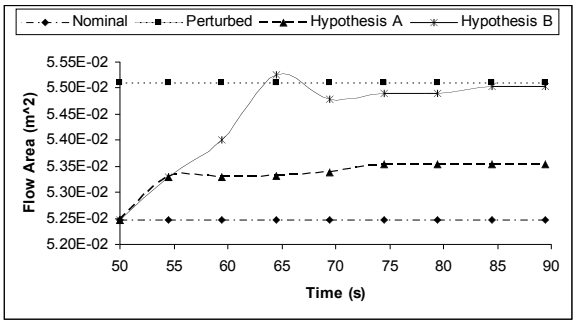

(a) Flow area of the main steam valve (component 1).

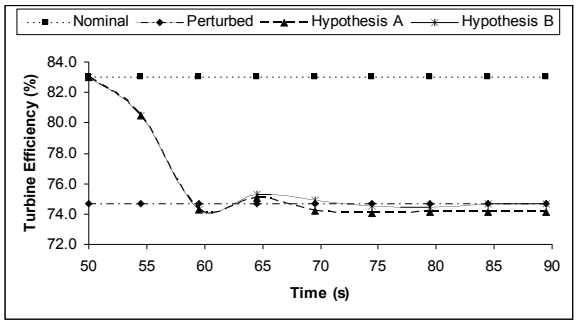

(b) Low pressure turbine efficiency (component 2).

Figure 10. The evolution of two BOP components obtained through the adaptive filter.

3.2.1.3. Application: Multiobjective Optimization with UKF [51]

In this application, we propose to utilize a reliability degradation database compiled from past operational characteristics, tests and maintenance reports for the components of interest to improve the convergence rate of a filter and even to prevent it from diverging for highly nonlinear systems.

To combine the real time filtering algorithm with the reliability database we propose to solve a multiobjective optimization problem. The first objective is to maximize the conditional component state pdf given the measurement history calculated via a filtering estimate of the component. The second objective is to maximize the component state pdf given past operational characteristics derived from the reliability database.

A multiobjective optimization problem usually has no unique, perfect solution. However, one can introduce a set of nondominated, alternative solutions known as the Pareto optimal set [61]. If both of the pdf's are Gaussian, the Pareto optimal points for that

component are the ones between the two means. The mean of the true component state is located between these Pareto optimal points, and the belief on either source of information should be set to estimate it.

We employed the weighted sum method [61] to form the cost function as

$$p\left(c_k \mid Y_k\right) = \alpha p_f\left(c_k \mid Y_k\right) + \left(1-\alpha\right) p_{db}\left(c_k \mid c_{k-1}\right) \tag{3.21}$$

where p_f and p_{db} are conditional pdf's for the component states obtained from UKF and reliability database, respectively. α is a weighting coefficient that expresses the relative "importance" of the objectives and controls their involvement in the cost functional, which can be calculated by direct search, min-max principle [62] or set by expert opinion.

In UKF, at each time step we update the mean of the estimated component state with the one from the reliability database by assuming the conditional mean of the component state can be written as $\mathrm{E}\left[c_k\right] = \alpha \mathrm{E}\left[c_k\right]_f + \left(1-\alpha\right)\mathrm{E}\left[c_k\right]_{db}$.

A sodium-cooled plutonium-uranium metal fueled fast reactor core was chosen to test this algorithm. A simplified model of the plant [63] was employed. The system state is represented through 14 variables, which include normalized neutronic power, six delayed precursor concentrations, four group decay heat fractions, coolant exit and fuel and cladding average temperatures. The components to be estimated are the coolant flow rate and the total reactivity (including feedback). Coolant exit temperature and normalized neutronic power can be measured.

The plant behavior was first monitored during steady state operation. Then a transient was introduced into the constant coolant flow rate $\dot{m}_0$ due to a pump coast-down at t = 200 s in the form of

$$\dot{m}(t) = \dot{m}_0\left(a + be^{-\lambda t}\right) \tag{3.22}$$

where the parameters (*a, b* and λ) are functions of the type of degradation in the pump.

By setting $\dot{m}_0$ = 2583 kg/s and a = 0.08, b = 0.921, λ = 0.069315 [63], we simulated the transient behavior of the plant. We then applied UKF to obtain the best estimates of the system and component states. Although the filter was converged to the nominal values of the states in the steady state operation, in the transient part it could not respond to the change in the system behavior promptly as shown in Figure 11.

In order to improve the convergence characteristics of the filter we used our proposed modified UKF algorithm based on multiobjective optimization. We assumed *a* and *b* are known constants, and λ is a random variable with a Gaussian pdf given in the reliability database. The expected value of λ in the database is 0 for nominal and 0.069315 (true value) for degraded conditions. As a trial, we set our beliefs in the filter and the database to be equal in this algorithm, so $\alpha = 0.5$ was selected somewhat arbitrarily. Then, we updated the best estimate of the coolant flow rate in the filter with the expected value of λ from the reliability database according to $\mathrm{E}\left[\lambda\right] = 0.5 \times \mathrm{E}\left[\lambda\right]_f + 0.5 \times \mathrm{E}\left[\lambda\right]_{db}$ at each time step. We tried the algorithm also with a wrong degradation mode in which the expected value of λ is 0.023105.

Coolant exit temperature is one of the measurements and is plotted in Figure 11 along with its true and estimated (UKF, Modified UKF (True Degradation Mode), Modified UKF (Wrong Degradation Mode)) evolutions in time.

Notice that the UKF by itself follows the nominal plant behavior very well, but at the time of the degradation it is so well converged that it cannot promptly follow the transient during the pump coast-down. On the other hand, the filter combined with the reliability database (even an imperfect database) adjusts much more quickly; it still deviates during the transient, but not as much, and it quickly finds the new steady state after the transient.

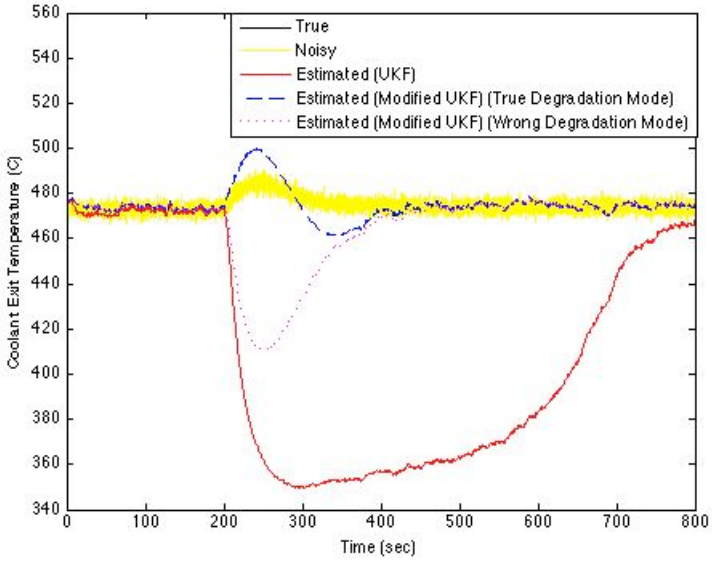

Figure 11. The evolution of true, noisy and estimated coolant exit temperature.

Average fuel and cladding temperatures are given in Figure 12 with their true and estimated (using UKF, Modified UKF (True Degradation Mode), Modified UKF (Wrong Degradation Mode)) evolutions in time.

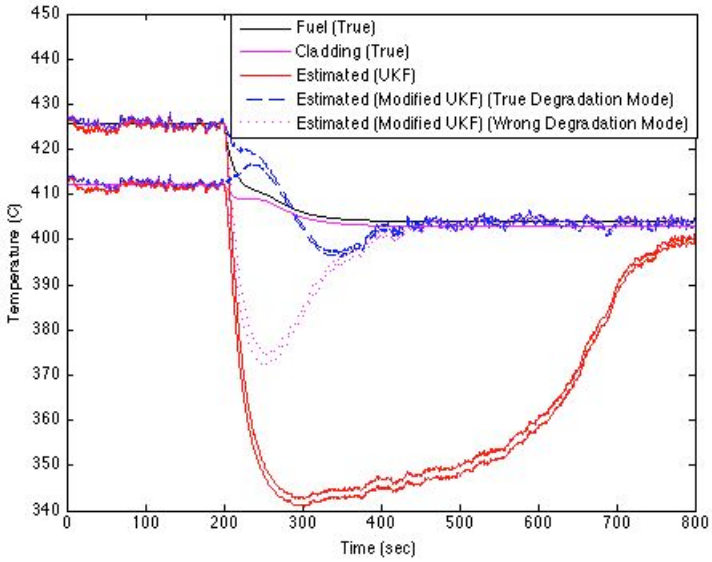

Figure 12. The evolution of true and estimated average fuel and cladding temperatures.

Combining different sources of information (data fusion) in a multiobjective optimization framework improves the performance of the filter. In Figures 11 and 12 we see that the UKF by itself converges to the degraded state quite slowly, but when combined with information from a database, it can converge much more quickly. This is true even when the database is imperfect. Because of this, we will exploit the combination of a database with particle filtering as the main contribution of this thesis to degradation monitoring.

3.2.2. Sample Impoverishment Problem in Particle Filtering

In the particle filtering (PF) sample impoverishment occurs if the region of state space in which the pdf $p(y_k \mid z_k)$ has significant values does not overlap with the pdf $p(z_k \mid Y_{k-1})$. Like in the oblivious nonlinear Kalman filtering, if the variances of the states become very small during the nominal state estimation, then the pdf $p(z_k \mid Y_{k-1})$ will be highly peaked. Degradation occurring in one of the component states alters the pdf $p(y_k \mid z_k)$. After the resampling step this will result in multiplication of only a few particles and elimination of the rest, which leads to sample attrition. Because of this the PF cannot respond to the change in that component state and eventually all of the particles will collapse into a single one. This issue is particularly acute in our case where we use a joint estimation approach that deals with constant parameters e.g., component states, as part of the augmented state vector [64].

This phenomenon is very important for degradation monitoring in nuclear power plants, because a degradation detection, isolation and estimation algorithm should be capable of estimating both the nominal and degraded states with minimal error. If the methods suffer from sample impoverishment, then the estimated states will not be able to represent the real plant behavior, which can result in taking incorrect operational actions and put the reactor in an unsafe state, which may result in an unanticipated shutdown.

There are a couple of techniques to overcome this sample impoverishment problem in particle filters. In the next section, we will first discuss the roughening technique, which

is a PF representation of covariance matching. Then, we will concentrate on a Markov chain Monte Carlo (MCMC) move technique and develop our multiple hypotheses testing algorithm on it.

3.2.2.1. Roughening

Gordon et.al. [46], proposed adding small random disturbances to state particles after the resampling step in addition to any existing modeling noise in order to reduce sample impoverishment. As in the covariance matching technique, there is no unique way to specify the characteristics of the noise. Also, if the state is high dimensional, it is very difficult to apply this technique. Finally, this technique increases the variance of the estimates and the precision of the resulting inferences is inevitably limited [64].

3.2.2.2. Markov Chain Monte Carlo Move Step

Markov chain Monte Carlo (MCMC) methods are powerful algorithms that help to solve most of the Bayesian problems when the data are available in batches [65]. In particular, there is no need for the normalizing constant to be known and the state space can be high dimensional. The applications of MCMC methods involve generating many samples from the posterior distribution of the model parameters by using a Markov chain and then approximating the posterior expectations with sample averages [66]. For sequential cases in which the states are estimated recursively in time as data are available, MCMC can be used for drawing samples from candidate invariant distributions as a step in particle filtering. However, since the posterior distribution evolves over time, MCMC methods are computationally intensive.

In this thesis, we propose to use a Markov chain Monte Carlo move step as a tool for combining multiple sources of information. Our novel approach is constructed by using a multiple hypothesis testing algorithm based on a MCMC method to find a remedy for sample impoverishment problem in particle filtering.

In order to construct the framework for this methodology, we first start with a discussion on Markov chain Monte Carlo. Then, we present the Metropolis-Hastings algorithm, which is the MCMC method we will use in the rest of the thesis. We also review the resample-move algorithm proposed by Gilks and Berzuini [66], which is a sequential implementation of MCMC, before presenting our approach.

3.2.2.2.1. Markov Chain Monte Carlo

Markov chain Monte Carlo is a strategy for generating samples while exploring the state space using a Markov chain mechanism. This mechanism is constructed so that the chain spends more time in the most important regions.

We start with the definition of Markov chain. A Markov chain is a series of random variables $\{X_k\}$ in which the distribution of X_k depends entirely on the value of X_{k-1}, i.e.,

$$p(x_k \mid x_{k-1},\ldots,x_1) = p(x_k \mid x_{k-1}). \tag{3.23}$$

A Markov chain can be specified by the marginal density of the initial state X_0, and the conditional density of X_k given the possible values of X_{k-1}, which is also defined as the transition kernel of the Markov chain as

$$K(x_k \mid x_{k-1}) = p(x_k \mid x_{k-1}). \tag{3.24}$$

If the transition kernel does not depend on time, the Markov chain is homogeneous and it remains invariant for all *k*.

Using the transition kernels, we can find the target density, i.e., the probability of state at time *k+1*

$$p(x_{k+1}) = \int K(x_{k+1} \mid x_k) p(x_k) dx_k . \tag{3.25}$$

The invariant distribution is defined as the distribution over the states of a Markov chain that remains unchanged when once it is reached. In section 2.1, component states are defined as time invariant Markov chains, so that

$$p(c) = \int K(c \mid c_k) p(c_k) dc_k . \tag{3.26}$$

The target density $p(c)$ is invariant with respect to the Markov chain with transition kernel $K(c \mid c_k)$.

For any starting point $C_0 = c_0$, these Markov chains will converge to the invariant density $p(c)$, as long as the transition kernel obeys the following properties:

1. Irreducibility: For any state of the Markov chain, the kernel is constructed such that there is a positive probability of visiting all other states
2. Aperiodicity: The kernel satisfies that the chain should not get trapped in cycles.

A sufficient, but not necessary condition to ensure that the target density $p(c)$ is the desired invariant one is the following reversibility (detailed balance) condition

$$p(c_k) K(c \mid c_k) = p(c) K(c_k \mid c) . \tag{3.27}$$

That is, if a transition occurs from a component state chosen according to the target densities, then the probability of that transition being from component state c_k to c is the same as the probability of it being from the state c to c_k. It is also possible for a distribution to be invariant without detailed balance holding [67].

MCMC methods are based on irreducible and aperiodic Markov chains that have the target distribution as an invariant distribution. One way to design these methods is to ensure that detailed balance is satisfied [68].

It is not merely enough to find a Markov chain that we can sample from an invariant distribution. We also require that the Markov chain be ergodic, which means regardless

of the choice of initial probabilities a target distribution converges to an invariant distribution as $k \to \infty$. Clearly, an ergodic Markov chain can have only one invariant distribution [67].

In MCMC methods, the invariant distribution or density is assumed to be known, but the transition kernel is unknown. In order to generate samples from the invariant distribution, MCMC methods attempt to find a kernel whose n^{th} iteration (for large n) converges to the target distribution given an arbitrary starting point [24].

In the next subsection we present a well known MCMC method, the Metropolis-Hastings algorithm, which we use in our multiple hypothesis testing algorithm.

3.2.2.2.2. The Metropolis–Hastings Algorithm

For high dimensional problems, MCMC simulation is the only known general approach for providing a solution to the Bayesian inference problem within a reasonable time [68]. The Metropolis-Hastings (MH) algorithm is the most popular MCMC method. The MH algorithm was first studied by Metropolis et. al. [69], and later extended for cases when the proposal distribution is not symmetric by Hastings [70].

Assume the conditional proposal density $q(c \mid c_k)$ is easy to simulate from and either explicitly available (up to a multiplicative constant) or symmetric, i.e., $q(c \mid c_k) = q(c_k \mid c)$. The target density $p(c)$ must be available to some extent: a general requirement is that the ratio $p(c)/q(c \mid c_k)$ is known up to a constant [71]. During each iteration of the MH algorithm a candidate sample is drawn from the proposal density $c^{(i)} \sim q(c \mid c_k)$ and accepted with a probability

$$\rho\left(c_k, c^{(i)}\right) = \begin{cases} \min\left[1, \dfrac{p\left(c^{(i)}\right) q\left(c_k \mid c^{(i)}\right)}{p(c_k)\, q\left(c^{(i)} \mid c_k\right)}\right] & p(c_k)\, q\left(c^{(i)} \mid c_k\right) > 0 \\ 1 & o/w \end{cases} \tag{3.28}$$

where $0 < \rho\left(c_k, c^{(i)}\right) < 1$. If the candidate sample is accepted the chain moves to a new state, otherwise the chain is left in its current state.

The MH algorithm is as follows [71]:
Given c_k and for $i = 1,\ldots,N$,

1. Draw a sample from the proposal density, $c^{(i)} \sim q\left(c \mid c_k\right)$.
2. Sample $u \sim U(0,1)$.
3. Compute the acceptance probability $\rho\left(c_k, c^{(i)}\right)$ from Eq. (3.28).
4. If $u < \rho\left(c_k, c^{(i)}\right)$ accept the candidate state $c_{k+1} = c^{(i)}$; otherwise reject it and retain the current state $c_{k+1} = c_k$.

The probability that the Markov chain stays at c_k is given by

$$r\left(c_k\right) = \int q\left(c \mid c_k\right)\left(1 - \rho\left(c_k, c^{(i)}\right)\right)dc\,. \tag{3.29}$$

The transition kernel for the MH algorithm can then be written

$$K_{MH}\left(c_{k+1} \mid c_k\right) = q\left(c_{k+1} \mid c_k\right)\rho\left(c_k, c_{k+1}\right) + \delta\left(c_{k+1} - c_k\right)r\left(c_k\right). \tag{3.30}$$

If $\{C_k\}$ is the Markov chain produced by the MH algorithm, for every conditional density q, the transition kernel satisfies the detailed balance and $p(c)$ is the invariant distribution of the chain [71].

As implied above in the MH algorithm, we only need to know the target distribution up to a constant of proportionality; the normalizing constant of the target distribution is not required. The success or failure of the algorithm depends on the choice of the proposal density. If the proposal is too narrow, only one mode of the target distribution might be visited. On the other hand, if it is too wide, the rejection rate can be very high, resulting in high correlations. If all the modes are visited while the acceptance probability is high,

the chain is said to "mix" well [68].

A practical approach for the construction of a MH algorithm is to consider a local exploration of the neighborhood of the current values of the Markov chain through a random walk. One choice is to simulate $c^{(i)}$ according to

$$c^{(i)} = c_k + \varepsilon^{(i)} \tag{3.31}$$

where $\varepsilon^{(i)}$ is a random perturbation sampled from $q(c - c_k)$ [71].

It is unrealistic to hope for a generic MCMC sampler that would function in every possible setting. The more generic proposals like the random walk MH algorithms are known to fail in large dimension and disconnected supports, because they may take too long to explore the space of interest.

The efficiency of the Metropolis-Hastings algorithm is determined by the ratio of the accepted samples from a proposal density to the total number of samples. Too large or too small variance of the proposal density may result in inefficient sampling. For the random walk MH algorithm, high acceptance rate does not necessarily indicate that the algorithm is moving correctly since it may indicate that the random walk is moving too slowly.

3.2.2.2.3. MCMC Particle Filter

When the system is high dimensional, the performance of the particle filter depends to a large extent on the choice of the proposal distribution. By utilizing MCMC methods in the particle filtering, we can deal with complex non-standard probability densities.

The basic idea is that if the particles are distributed according to the filtering distribution $p(z_k \mid Y_k)$ then applying a Markov chain transition kernel $K(z \mid z_k)$ with invariant

distribution $p(\cdot \mid Y_k)$ such that $\int K(z \mid z_k) p(z_k \mid Y_k) dz_k = p(z \mid Y_k)$ to each particle still results in a set of particles distributed according to the filtering distribution. However, the new particles might have been moved to more "important" areas of the state space. Note that, we can incorporate any of the standard MCMC methods, like Metropolis-Hastings algorithm into the filtering framework, but we no longer require the kernel to be ergodic [68].

One different interpretation of this approach is, one can think of the transition kernel as being used to simulate the dynamics of a modified probabilistic model.

Berzuini and Gilks [72] [66] proposed resample-move algorithm in which they integrated MCMC into particle filtering. An initial set of component states $\left\{c_0^{(i)}\right\}$ is sampled from $p(c_0)$ and is used in the particle filtering algorithm until time step *1*. Then it is resampled and moved in the state space to a new position by using a MCMC method to form another set $\left\{c_1^{(i)}\right\}$. This process continues so that, at time *k+1*, for $k = 1, 2, \ldots$ the current particle set $\left\{c_k^{(i)}\right\}$ is resampled and moved to form $\left\{c_{k+1}^{(i)}\right\}$. Each resampling is an importance weighted resampling, and each resampled particle is moved according to a Markov chain transition kernel.

Having discussed the basics of the MCMC methods and the available algorithms that utilize MCMC in particle filtering, in the next section we construct our new algorithm based on multiple hypothesis testing.

3.3. PARTICLE FILTERING WITH AN MCMC MULTIPLE HYPOTHESIS TESTING STEP

Particle filtering is a powerful tool for state estimation. But as mentioned earlier, the sample impoverishment problem prevents the PF from estimating abrupt changes in the component states. Besides the sample impoverishment problem, for low fidelity systems with high dimensional state space, PF may end up estimating the wrong states. The

reason is that for high dimensional low fidelity models with a limited number of measurements the filtering problem may be ill-posed. One other issue for high dimensional systems is that if the proposal density is not close to the filtering density, then the weights of the particles may be very uneven, that is only few particles with large importance weights will dominate the estimation. Also this problem prevents PF from fully exploring the state space and results in the same effect of the sample impoverishment problem.

In order to resolve these issues, one possible solution is to employ an MCMC method to search the state space of interest. To design an effective algorithm that can work in real time, this scheme should be capable of moving the particles to more important regions without any delay. Since, the best source of data is records kept of the actual systems and equipments being diagnosed, we are proposing the use of a reliability degradation database that can be generated from plant specific data to derive different transition kernels to be tested through an MCMC method.

In order to use a degradation database in construction of these kernels, we first need to analyze the kind of information available.

3.3.1. Reliability Degradation Analysis and Construction of the Degradation Database

The concepts of reliability degradation analysis in nuclear reactors were originally introduced in NUREG/CR-5612, *Degradation Modeling with Application to Aging and Maintenance Effectiveness Evaluations* [73] and were expanded in NUREG/CR-5967, *Development and Application of Degradation Modeling to Define Maintenance Practices* [74]. While NUREG/CR-5612 focused on developing technical methods to evaluate times of degradations and maintenances for time trends and for measures of the efficiency of the maintenance, NUREG/CR-5967 focused on developing Markov models to quantify the probabilities of safety system components being in various degraded states. In NUREG/CR-6415, *Applications of Reliability Degradation Analysis* the connection between these developed models of degradation analysis and applications

were investigated to determine the reliability and risk effects of the maintenances undertaken [75].

In a reliability degradation analysis, by evaluating the records of a component's performance we can identify the occurrences of degradation of that component. One may use records of past operational experience, maintenance reports, manufacturer specifications or expert judgment to construct the database. We would like to note that for degradation analysis, additional evaluation is needed beyond development of a Probabilistic Risk Assessment (PRA) database in which only the potential failures of the components are identified.

The types of data we are interested in are the component degradation reliabilities, corresponding degradation modes and the expected occurrences (frequencies) of these degradation modes.

For example, suppose we would like to estimate n_x system and 3 component states. These components can be residual heat removal (RHR) pumps, service water (SW) pumps and air compressors. At first, we need to have probability density functions for time to degradation in that component. Assuming the time to degradation in a component is distributed according to an exponential distribution, then the probability that the component is degraded at time t is

$$F(t) = 1 - e^{-\lambda t} \tag{3.32}$$

where λ is the rate of degradation.

A representative data set is shown in Table I for this simple case. In the top row, component number, number of modes (nominal and degradation modes) and degradation rate (exponential distribution is assumed for the pdf of time to degradation) for that component are specified. For example, if the first component is the SW pump, then the expected degradation modes can be the erosion of the pump internals causing leakage

Table I. A representative degradation database.

Component Number	Number of Modes	Degradation Rate									
1	3	λ_1									
Minimum Value	Maximum Value	PDF Type	Nominal Mean	Nominal Variance	Nominal Mode Probabilty	Degradation Mode I - Mean	Degradation Mode I - Variance	Degradation Mode I – Probability	Degradation Mode II - Mean	Degradation Mode II - Variance	Degradation Mode II – Probability
c_{1min}	c_{1max}	Gaussian	c_{1mean}	$c_{1var,nom}$	$e^{-\lambda,1t}$	$0.95c_{1mean}$	$c_{1var,d1}$	$(1-e^{-\lambda,1t})/2$	$0.87c_{1mean}$	$c_{1var,d2}$	$(1-e^{-\lambda,1t})/2$
Component Number	Number of Modes	Degradation Rate									
2	3	λ_2									
Minimum Value	Maximum Value	PDF Type	Nominal Mean	Nominal Variance	Nominal Mode Probabilty	Degradation Mode I - Mean	Degradation Mode I - Variance	Degradation Mode I – Probability	Degradation Mode II - Mean	Degradation Mode II - Variance	Degradation Mode II – Probability
c_{2min}	c_{2max}	Gamma	c_{2mean}	$c_{2var,nom}$	$e^{-\lambda,2t}$	$1.05c_{2mean}$	$c_{2var,d1}$	$4(1-e^{-\lambda,2t})/5$	$0.90c_{2mean}$	$c_{2var,d2}$	$(1-e^{-\lambda,2t})/5$
Component Number	Number of Modes	Degradation Rate									
3	2	λ_3									
Minimum Value	Maximum Value	PDF Type	Nominal Mean	Nominal Variance	Nominal Mode Probabilty	Degradation Mode I - Mean	Degradation Mode I - Variance	Degradation Mode I – Probability			
c_{3min}	c_{3max}	Gaussian	c_{3mean}	$c_{3var,nom}$	$e^{-\lambda,3t}$	$0.60c_{3mean}$	$c_{3var,d1}$	$(1-e^{-\lambda,3t})$			

past the impeller to the suction side of the pump or a small hole in the coupling cooling water line. In order to decide if the component is in the nominal or in a degraded state, we define component characteristics. A component characteristic represents the operability of the physical component. For the SW pump, the component characteristic can be the mass flow rate.

The hard constraints for that component value are entered in the third row as minimum and maximum admissible values for that component (minimum and maximum mass flow rate for the SW pump). Then the type of probability distribution functions (Gaussian, gamma, uniform, etc.) for the nominal and degraded modes along with the parameters of that distribution are recorded. For a Gaussian the parameters are location and scale, for gamma they are shape and scale. The gamma process is also considered because it is a natural model for degradation processes in which deterioration is supposed to take place gradually over time in a sequence of tiny increments [76]. Assuming a Gaussian pdf is chosen, the mean and variance of the nominal distribution is specified. For all modes, then the probability that the component is in that mode at time *t* is needed to complete the database. For the nominal case, since we assumed that time to degradation in a component is distributed according to exponential distribution, the reliability at time *t* is

$$R(t) = e^{-\lambda t} \tag{3.33}$$

For the degradation modes, it is indeed the expected occurrence of the modes, which can be calculated using the normalized expected frequencies at time *t*.

3.3.2. Degradation Estimation Using Multiple Hypothesis Testing with MCMC

As mentioned in reviewing the Metropolis-Hastings algorithm, there is no generic scheme to apply to all of the problems. Adding a reliability degradation database introduces real plant information into this scheme in order to assist the filter to explore the important state space regions of interest and by doing so opens up the state space for

the particle filter to be able to converge to the true states even if they are not explicitly introduced by the database.

As stated in our nonlinear system model, the component state $c \in \mathbb{R}^{n_c}$ is assumed to undergo random, discrete transitions and stays constant between these transitions for nominal conditions

$$c_{k-1} = c_{k-2} + w_{k-1}^{c}. \tag{3.34}$$

Degradation changes the nominal trajectory of the component as

$$c_k = c_{k-1} + \Delta c_k + w_k^{c}. \tag{3.35}$$

Since we do not know the amount of degradation, Δc_k, we cannot switch the nominal model to the degraded model in the particle filtering algorithm in order to update the prior transition density. In most cases the particle filtering has been in operation for a long time before the detection of the degradation and may suffer from a sample impoverishment problem, which prevents it to explore the state space effectively. We propose to use past real plant operational data that have been quantified in the reliability degradation database to generate proposal densities (candidate transition kernels) for improving the search for the state space through an MCMC technique. These densities are characterizing various degradation modes for all components in the database. In the database, the conditional density that the component is in a degraded state given that it was in its nominal state

$$q\left(\left(\Delta c_k\right)_{j,d} = c_k - c_{k-1}\right); j = 1,\ldots,n_c; d = 1,\ldots,n_d(j) \tag{3.36}$$

is stored. $\left(\Delta c_k\right)_{j,d}$ is the distribution of the change from nominal state c_{k-1} to degraded state c_k for component *j* and degradation mode *d* and $n_d(j)$ is the total number of possible degradation modes for component *j*. The probability of finding the component *j* in the nominal state at time *k* is given by its reliability, $\left(R_k\right)_j$. The occurrence probability

of degradation mode d for component j at time k is $(\omega_k)_{j,d}$, and the sum of the occurrence probabilities of all of the degradation modes $d = 1,\ldots,n_d(j)$ at time k satisfies $\left(1-(R_k)_j\right) = \sum_{d=1}^{n_d(j)} (\omega_k)_{j,d}$ and are also available in the database.

The true invariant target density is the filtering density $p(z_k \mid Y_k)$. By using the degradation database, we can construct the following proposal density for the component state

$$q(c_k \mid c_{k-1}) = \sum_{j=1}^{n_c} \alpha_j \left[(R_k)_j \, q\left((w_k)_j = c_k - c_{k-1}\right) + \sum_{d=1}^{n_d(j)} (\omega_k)_{j,d} \, q\left((\Delta c_k)_{j,d} = c_k - c_{k-1}\right) \right] \quad (3.37)$$

where α_j represents the likelihood of component j being degraded at the detection time of the degradation. If the time to degradation is distributed according to an exponential distribution, then it is simply the ratio of the degradation rate of component j to the total degradation rates, $\alpha_j = \frac{\lambda_j}{\sum_l \lambda_l}$. However, after the detection time, α_j will be treated as a variable in the adaptation scheme described in Subsection 3.3.2.1. It will be made proportional to the acceptance ratio of the particles from the degradation modes of component j.

The proposal distribution for the component state $q(c_k \mid c_{k-1})$ given in Equation (3.37) is built on characteristics of the degraded components and corresponding modes extracted from the reliability degradation database. We calculate the proposal distribution for the augmented state as in Equation (3.6)

$$q(z_k \mid z_{k-1}) = p(x_k \mid x_{k-1}, c_k) q(c_k \mid x_{k-1}, c_{k-1}). \quad (3.38)$$

This proposal density increases the variance of the filtering density. For high dimensional systems, exploring the state space for all combinations of the degradations may take a

long time. Therefore, it is useful to draw samples from one mode at a time, keeping all the other ones fixed. The proposal density described above is also multimodal. If the modes are separated by regions of very low probabilities, it may become difficult to jump from one region to another. A multiple hypothesis testing algorithm, described below, will resolve both of these issues.

Moreover, in degradation monitoring our aim is not only to estimate the magnitude of the degradation in a component, but also try to isolate the cause of the degradation, namely identifying the degradation mode. If one uses the Kalman filter or its derivatives to have an MMSE or MAP estimate of the component state, just by checking the distance between e.g., the means of the estimate and the degradation modes, and deciding on which mode is in effect based on this information can lead to an incorrect decision on the degraded mode. The problem is that whenever there is degradation in a component caused by a specific mode, the component state does not change the same exact amount. We use a pdf to represent this behavior. Then, in order to isolate the correct degradation mode, we need to match our estimated density with the one from the mode and decide based on the overlapping regions. One other way of doing this is by creating a multiple hypothesis testing algorithm based on MCMC, which takes care of matching these densities intrinsically and quantifies the probability of having a specific degradation mode in effect by analyzing the number of particles accepted from different hypotheses.

Assume we have one component with two degradation modes, which are equally likely to occur at time step *k*. Then Equation (3.37) can be rewritten ($\alpha = 1$ for one component)

$$q\left(c_k \mid c_{k-1}\right) = \left(R_k\right)_1 q\left(\left(w_k\right)_1 = c_k - c_{k-1}\right) + \frac{\left(1-\left(R_k\right)_1\right)}{2} q\left(\left(\Delta c_k\right)_{1,1} = c_k - c_{k-1}\right) + \frac{\left(1-\left(R_k\right)_1\right)}{2} q\left(\left(\Delta c_k\right)_{1,2} = c_k - c_{k-1}\right). \tag{3.39}$$

A representative pdf for the nominal component state at time *k*, given the component state at time *k-1,* is estimated through the particle filtering algorithm and expected to be highly peaked because of the sample impoverishment problem is shown in Figure 13(a).

The proposal pdf constructed by assuming all modes are Gaussian using Equation (3.39) for the component state at time *k*, given the nominal component state at time *k-1* is illustrated in Figure 13(b).

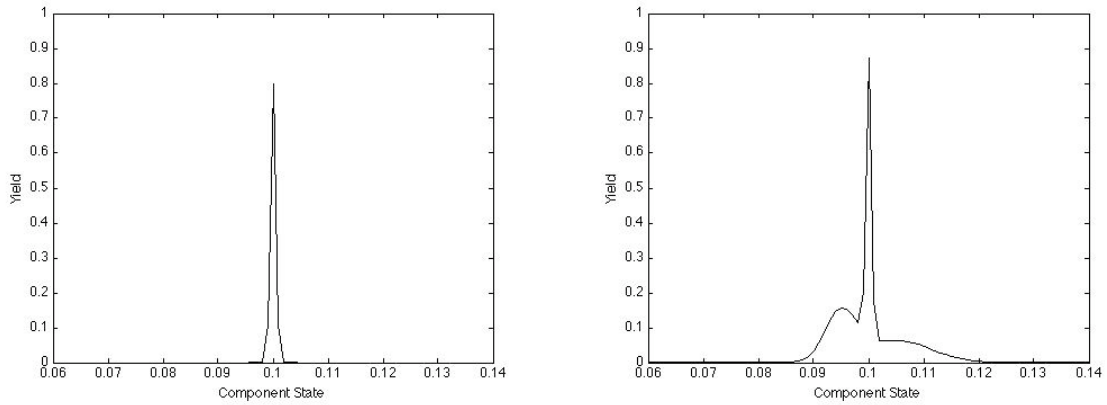

(a) The pdf for filter estimate at time *k*. (b) The proposal pdf at time *k*.

Figure 13. The conditional probability density for the filter estimate and the proposal.

As seen in Figure 13(b), the proposal distribution is multimodal, which may suffer from the problem mentioned earlier. We also lose some information about degradation modes because of the overlapping regions. We propose to use a multiple hypothesis testing algorithm by which we treat the support of each degradation mode separately as shown in Figure 14.

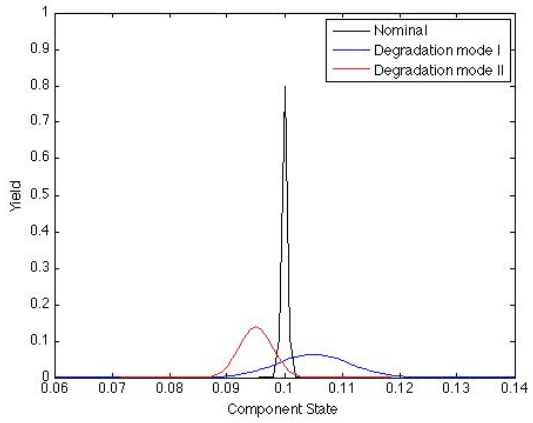

Figure 14. The pdfs for the nominal and degraded modes of a component.

Multiple hypotheses are built on different proposal densities that explore the state space in the direction of single, binary, etc degradation modes. We construct the hypotheses according to the components and respective degradation modes then calculate the proposal density for the augmented state using Equation (3.38). The no degradation hypothesis is constructed as

$$H_0 : c_k^{(i)} \sim q\left(\left(w_k\right)_j = c_k - c_{k-1}\right); j = 1,\ldots,n_c . \tag{3.40}$$

The hypotheses for single degradations are generated by assuming one of the components is degraded, but the rest are not. If we have $n_d(j)$ degradation modes for each component j, then the total number of hypotheses for single degradations is

$$n_{\text{single}} = \sum_{j=1}^{n_c} n_d(j).$$

Then, for $h = 1,\ldots,n_{\text{single}}$ and $j = 1,\ldots,n_c$, the single degradation hypotheses are constructed as

$$H_h : \begin{array}{l} c_k^{(i)} \sim q\left(\left(\Delta c_k\right)_{j,d} = c_k - c_{k-1}\right); d = 1,\ldots,n_d(j) \\ c_k^{(i)} \sim q\left(\left(w_k\right)_l = c_k - c_{k-1}\right); l \neq j; l = 1,\ldots,n_c \end{array} \tag{3.41}$$

For n_c components, the total number of possible binary degradations is

$$n_{\text{binary}} = \sum_{l=1, l\neq j}^{n_c} \sum_{j=1}^{n_c} n_d(j) \times n_d(l).$$

For $h = 1,\ldots,n_{\text{binary}}$ and $j = 1,\ldots,n_c, l = 1,\ldots,n_c$, $l \neq j$ the binary degradation hypotheses are constructed as

$$
\begin{aligned}
& c_k^{(i)} \sim q\left(\left(\Delta c_k\right)_{j,d_1} = c_k - c_{k-1}\right); d_1 = 1,\ldots,n_d(j) \\
H_{jl}: \quad & c_k^{(i)} \sim q\left(\left(\Delta c_k\right)_{l,d_2} = c_k - c_{k-1}\right); d_2 = 1,\ldots,n_d(l) \\
& c_k^{(i)} \sim q\left(\left(w_k\right)_p = c_k - c_{k-1}\right); p \neq l \neq j; p = 1,\ldots,n_c.
\end{aligned} \tag{3.42}
$$

Hypotheses based on triple and more degradations can be constructed in the same way. The number of hypotheses increases as the dimension of the component states and number of possible degradation modes increase. In PF, the number of particles should be large enough to provide the necessary support for all of the hypotheses. In Section 3.3.3, we propose a degradation isolation algorithm in order to obtain a feasible set of degraded components as a solution to this problem.

The following MH acceptance probability [29] is used in our multiple hypothesis testing algorithm

$$
\rho\left(\hat{z}_k^-, z_k'\right) = \min\left\{1, \frac{p\left(y_k \mid z_k'\right) q\left(z_k' \mid \hat{z}_{k-1}^{(i)}\right)}{p\left(y_k \mid \hat{z}_k^-\right) p\left(\hat{z}_k^- \mid \hat{z}_{k-1}^{(i)}\right)}\right\}. \tag{3.43}
$$

where $\hat{z}_{k-1}^{(i)} \sim p\left(z_{k-1} \mid Y_{k-1}\right)$ denotes the a posteriori estimate of the augmented state by the particle filter at time *k-1*, $\hat{z}_k^-$ is the a priori estimate of the augmented state by the particle filter given $\hat{z}_{k-1}^{(i)}$, $z_k'^{(i)} \sim q\left(z_k' \mid \hat{z}_{k-1}^{(i)}\right)$ is the proposed state based on single or multicomponent degradation hypotheses. The first fraction in Eq. (3.43) is the ratio of the measurement probability conditioned on the proposed particle to the measurement probability conditioned on the a priori particle estimated through PF. The second fraction is the ratio of the probability of the proposed particle to the probability of the a priori particle estimated through PF, both conditioned on the a posteriori particle at the previous time. The acceptance probability increases as the probability of the new particle increases and the a priori particle estimated through PF is therefore changed to the proposed one if it has a low probability of being selected.

If the number of particles generated for the particle filtering is N, we draw a total of N samples from the proposal distributions of all of the hypotheses. The number of particles to be sampled from hypothesis *h* is

$$N_h = N \times \alpha_j \times \beta \tag{3.44}$$

where α_j the likelihood that component *j* being degraded at the detection time of the degradation, $\beta = \left(R_k\right)_j$ for no degradation hypothesis of component *j*, or $\beta = \left(\omega_k\right)_{j,d}$ for single degradation hypothesis of component *j* and degradation mode *d*, or $\beta = \left(\omega_k\right)_{j_1,d_1} \times \left(\omega_k\right)_{j_2,d_2}$ for binary degradation hypothesis of component j_1 and degradation mode d_1 and component j_2 and degradation mode d_2, etc.

Let Z'_k denote the set of all the particles generated by all hypotheses at time *k,* $Z'_k = \left\{z'^{(i)}_k\right\}_{i=1}^{N}$ and let $A_{k,h}$ be the subset of Z'_k that consists of the particles accepted from hypothesis *h* by the MH algorithm at time *k*, $A_{k,h} = \left\{z'^{(i)}_k ; u^{(i)} < \rho\left(\hat{z}^-_k, z'^{(i)}_k\right)\right\}_{i=1}^{N_h}$ where $u^{(i)} \sim U(0,1)$ and $\rho\left(\hat{z}^-_k, z'^{(i)}_k\right)$ is the acceptance probability. We define the relative likelihood of hypothesis H_h as the ratio of the number of particles accepted from hypothesis *h* to the total number of particles accepted

$$p\left(H_h \mid \rho\right) = \frac{\sum_{i=1}^{N_h} 1_{A_{k,h}}\left(z'^{(i)}_k\right)}{\sum_{h=1}^{n_{hyp}} \sum_{i=1}^{N_h} 1_{A_{k,h}}\left(z'^{(i)}_k\right)} \tag{3.45}$$

where $1_{A_{k,h}}\left(z'^{(i)}_k\right) = \begin{cases} 1 & z'^{(i)}_k \in A_{k,h} \\ 0 & z'^{(i)}_k \notin A_{k,h} \end{cases}$ is an indicator function.

Our multiple hypothesis testing algorithm is as follows:
Given the degradation is detected at time k', for $k = k', k'+1, k'+2, \ldots$

1. Construct n_{hyp} hypotheses $H_0, H_1, \ldots$ representing no degradation, single degradations, binary degradations, etc. by extracting the proposal densities $q_0, q_1, \ldots$ from the reliability degradation database.
2. Sample $\hat{z}_{k-1}^{(i)} \sim p\left(z_{k-1} \mid Y_{k-1}\right)$ for $i = 1, \ldots, N$.
3. Sample $\left(\hat{z}_k^-\right)^{(i)} \sim p\left(z_k \mid \hat{z}_{k-1}^{(i)}\right)$ for $i = 1, \ldots, N$.
4. For $h = 1, 2, \ldots, n_{hyp}$
    a. Compute the number of particles to be sampled from each hypothesis from Eq. (3.44).
    b. Sample $z_k'^{(i)} \sim q_h\left(z_k' \mid \hat{z}_{k-1}^{(i)}\right) = p\left(x_k' \mid \hat{x}_{k-1}^{(i)}, c_k\right) q_h\left(c_k \mid \hat{c}_{k-1}^{(i)}\right)$ for $i = 1, \ldots, N_h$.
    c. Compute the acceptance probability

$$\rho\left(\hat{z}_k^-, z_k'\right) = \min\left\{1, \frac{p\left(y_k \mid z_k'\right) q_h\left(z_k' \mid \hat{z}_{k-1}^{(i)}\right)}{p\left(y_k \mid \hat{z}_k^-\right) p\left(\hat{z}_k^- \mid \hat{z}_{k-1}^{(i)}\right)}\right\}.$$

    d. If $u < \rho\left(\hat{z}_k^-, z_k'\right)$ accept the candidate state z_k'; otherwise reject it and retain the current state $\hat{z}_k^-$.
    e. Compute the relative likelihood of hypothesis *h*, $p\left(H_h \mid \rho\right)$, which is the ratio of the number of particles accepted from hypothesis *h* to the total number of particles accepted from Eq. (3.45)

This algorithm, in which we utilized the MH algorithm in a multiple hypothesis testing setting moves the particles to the important regions of the state space and consequently provides better estimates than PF alone. By monitoring the likelihood of the hypotheses computed, it is also possible to find the right degradation mode without any additional effort.

The transition kernel for the MH algorithm is obtained as

$$K\left(z_k^- \mid \hat{z}_{k-1}^{(i)}\right) = \sum_h q_h\left(z_k^- \mid \hat{z}_{k-1}^{(i)}\right) \rho\left(\hat{z}_k^-, z_k^-\right) + \delta\left(z_k^- - \hat{z}_k^-\right) r\left(\hat{z}_k^-\right). \tag{3.46}$$

This transition kernel causes the particles to visit the state space of all probable degradation modes.

In the next section, we discuss how this hypothesis testing algorithm may be used adaptively to find the feasible set of degraded components and modes.

3.3.2.1. Adaptive MCMC Hypothesis Testing Algorithm

As mentioned in the section 3.2.2.2.2, the efficiency of the MCMC methods is determined by the ratio of the accepted samples to the total number of samples.

As the number of components and the number of degradation modes increase the computational burden of the MCMC hypothesis testing algorithm increases. One way to handle this is to eliminate those hypotheses for which the samples drawn from the corresponding degradation's proposal density are not accepted or have a very low acceptance ratio and to draw more samples from the proposal density of a hypothesis if more particles are accepted from that hypothesis. This adaptation scheme works like a resampling algorithm, which organizes the state space to be explored in the support of the proposal densities from which more particles are accepted.

The algorithm for the adaptation scheme is as follows
Given the degradation is detected at time k', for $k = k'$

1. Follow the steps of the multiple hypothesis testing algorithm

For $k = k'+1, k'+2, \ldots$

2. Replace step 4.a by $N_h = N \times p\left(H_h \mid \rho\right)$ and follow the same algorithm

If the number of particles in each hypothesis is not enough to represent the support of the proposal density that they built on, or if some of the hypotheses mask the effect of the other ones, then it may take some time for the PF itself to start exploring the right directions in the state space. We call this the burn-in period of the MCMC hypothesis testing algorithm. The adaptive part of the algorithm in this form may suffer during this

burn-in period. Therefore, given the degradation is detected at time k', we run the first step of the adaptation algorithm for $k = k', k'+1, \ldots, k'+t_b$ where t_b is the burn-in period that is determined by training. Then we continue with step 2.

For the possibility of having two or more degradations occurring at different times, we never eliminate a hypothesis totally. Even if there are no particles accepted from hypothesis *h, i.e.,* $p(H_h \mid \rho) = 0$, we still keep sampling from the proposal density of that hypothesis according to a predetermined threshold for samples.

3.3.3. Degradation Detection and Isolation

The principle of degradation detection is always based on the comparison between actual and redundant information. In the case of hardware redundancy, the redundant information is generated by several sensors measuring the same physical quantity. Another way of generating redundancy is via the mathematical description of the process. The model reflects the behavior of the process in the nominal state and the process signals are compared with this reference information. If the model contains time-dependent differential equations where the history of the measurement information is used to solve them, it is called temporal analytical redundancy. If the process can be described by algebraic or transcendental equations, only actual measurement values are needed for the fault detection, which is called non-temporal analytical redundancy [77].

Assuming analytical redundancy exists, in order to detect degradation we should see the influence of the degradation upon the analytical redundancy. That is, a degradation with a certain mode is detectable if at least one of the static and/or temporal relationships among measurements and/or inputs becomes incorrect after the degradation occurs [78].

Two challenges in the detection problem are the complexity and the nonlinearity of the process models. Most of the detection models are developed for the cases when linear

models are available or nonlinear models can be linearized around an operating point or nonlinear models can be decomposed into static nonlinearities and linear dynamics [8].

As mentioned in Chapter 1, parameter/state estimation methods, dedicated observers, parity equations, and change detection and symptom generation methods are examples of fault detection and isolation methods. In the case of abrupt changes, state estimations and parity equations may react faster than parameter estimation. That is due to the fact that parameter estimation is intended for the estimation of constant values and removing the influence of disturbances with time. Introducing time-varying parameters by including a dynamic state space model for them as in our joint estimation framework helps to overcome this problem on cost of disturbance rejection [2].

In this dissertation we focused on using particle filtering for the detection and isolation of the degradations.

3.3.3.1. Degradation Detection with Particle Filtering

Change detection using particle filtering has received considerable attention recently. Li and Kadirkamanathan [79] used a particle filtering based likelihood ratio approach for fault diagnosis. Before the degradation, the component is in nominal state, i.e., $c = c_{nom}$. After the degradation, assuming the amount of degradation is known, the component state is $c = c_{\deg}$. The detection problem given all the observations up to time *n*, consists of testing between two hypotheses which can be written as

$$H_0 : k > n$$
$$H_1 : k \le n$$

where *k* is the unknown degradation time. Hypothesis H_0 is the null hypothesis stating no degradation is detected before time *n*. Hypothesis H_1 is constructed based on the degradation occurred before time *n*. Replacing the unknown degradation time *k* by its maximum likelihood estimate (MLE) under H_1, i.e.,

$$\hat{k}_n = \arg\max_{1\le k\le n} p\left(Y_n \mid c_{nom}, c_{\deg}, k\right) = \arg\max_{1\le k\le n} S_k^n \tag{3.47}$$

with

$$\begin{aligned} p\left(Y_n \mid c_{nom}, c_{\deg}, k\right) &= \prod_{j=0}^{n} p\left(y_j, Y_{j-1} \mid c_{nom}, c_{\deg}, k\right) \\ &= \prod_{j=0}^{k-1} p\left(y_j, Y_{j-1} \mid c_{nom}\right) \prod_{j=k}^{n} p\left(y_j, Y_{j-1} \mid c_{\deg}\right) \end{aligned} \tag{3.48}$$

where $p\left(y_j, Y_{j-1} \mid c_{nom}, c_{\deg}, k\right)$ denotes the predictive density of y_j given Y_{j-1} when one has $c = c_{nom}$ for the time interval $\{0,1,\ldots,k-1\}$ and $c = c_{\deg}$ afterwards.

The likelihood ratio (LR) is

$$S_k^n \triangleq \sum_{j=k}^{n} \ln\left(\frac{p\left(y_j, Y_{j-1} \mid c_{\deg}\right)}{p\left(y_j, Y_{j-1} \mid c_{nom}\right)}\right) \tag{3.49}$$

The change detector can be obtained

$$g_n \triangleq S_{\hat{k}_n}^n = \max_{1\le k\le n} S_k^n \underset{H_0}{\overset{H_1}{\gtrless}} \lambda \tag{3.50}$$

where g_n is the decision function and λ is the threshold. That is, decide H_1 whenever g_n exceeds λ and H_0 otherwise. The change alarm is set at the time given by

$$t_{alarm} = \min\left\{n : g_n > \lambda\right\} = \min\left\{n : \max_{1\le k\le n} S_k^n > \lambda\right\} \tag{3.51}$$

If the degraded model, namely $c_{\deg}$ is not known as in our case, then Eq. (3.49) is a function of two independent unknown parameters, the change time and the degraded state. In this case, it should be written as

$$S_k^n = S_k^n\left(c_{\deg}\right) = \sum_{j=k}^{n} \ln\left(\frac{p\left(y_j, Y_{j-1} \mid c_{\deg}\right)}{p\left(y_j, Y_{j-1} \mid c_{nom}\right)}\right) \tag{3.52}$$

One solution is to replace $c_{\deg}$ by its MLE, which results in the generalized likelihood ratio (GLR) algorithm. Thus the decision function of the GLR change detector, which involves the double maximization, is given by

$$g_n = \max_{1 \le k \le n} \sup_{c_{\deg}} S_k^n\left(c_{\deg}\right). \tag{3.53}$$

The detection rule is the same as in Eq. (3.51). It is difficult to make any precise theoretical statement on the optimal properties of such a test in the nonlinear non-Gaussian framework [80].

If the degraded model is known, the particle filtering implementation of this LR approach requires computing Eq. (3.49) . This can be done using particle methods. However, to compute the LR for a given *k* one needs two particle filters (change at time *k* and no change). This means that to compute g_n one requires *n+2* particle filters: one for $c = c_{nom}$ between *0* and *n* and *n+1* filters where $c = c_{nom}$ for $j < k$ and $c = c_{\deg}$ for $j \ge k$. When the degraded model is not known and $c_{\deg}$ belongs to a finite set of cardinality *M*, one has to use *Mn+1* particle filters. When $c_{\deg}$ is a continuous set, one would need to use the Eq. (3.53) [80]. For high dimensional systems where the multi-component degradations are possible, as in our work, this method is computationally very intensive and the algorithm becomes very complex.

3.3.3.2. Degradation Detection and Isolation Using Multiple Hypothesis Testing with MCMC

In this dissertation, we focus on the detection of degradations via parameter/state estimation in which degradations occur within the components of a system. The component characteristics follow the model in Eq. (3.1). The system states and

measurements evolve through the nonlinear models Eqs. (3.1) and (3.2). We also assume analytical redundancy exists and degradations are detectable.

A multiple hypothesis testing algorithm designed as a dedicated bank of observers has been used in this area for a long time [81], [56], [82]. The methodology we proposed for the estimation of the degradations in a multi-component system via a multiple hypothesis-testing algorithm in section 3.3.2 can be modified to be used as an efficient degradation detection scheme. Even though this algorithm is capable of detecting the degradation, for the sake of generating an algorithm that can work in real time with a limited number of particles, we introduce this step specifically designed for the detection of the degradation/s and for isolation of the prospective components that can lead to degradation/s.

The difference between this modified algorithm and the original one is that in this detection scheme we only have two degradation modes, which are created in order to set a threshold for the detection of degradation in each component. These degradation modes need not be a real representation of any expected modes. Each mode represents a change in the nominal characteristics. By drawing samples from these prospective pdfs and using these with the nominal estimated particles coming from the filter in the MH algorithm at each time step, we can determine which particles are more consistent with the real measurements. Even though the MH Algorithm is being used to find the invariant distribution, neither are we seeking to find this distribution nor are we exploring the state space to find which moves are better. The idea is to generate a scheme to detect a change from nominal and isolate the candidate components that may cause this change in a high dimensional system.

Assume we have two components. Before the degradation, both components are in their nominal states, c_{nom}. After the degradation, we assume that the component states $c_{\deg}$ are still constant but uncertain. As we reviewed in section 3.3.3.1, Li and Kadirkamanathan [79] set up the detection problem based on testing the two hypotheses given all the observations up to time t_n

$$H_{t0} : t_k > t_n$$
$$H_{t1} : t_k \le t_n \tag{3.54}$$

where t_k is the unknown change time and subscript t indicates that this test is for detection time.

Assuming the change in the component states is detectable, after the degradation the likelihood function at time *k*, $p(y_k \mid z_k) = p(y_k \mid c_{\deg}, x_k)$ should be different than the likelihood function at time *k-1*, $p(y_{k-1} \mid z_{k-1}) = p(y_{k-1} \mid c_{nom}, x_{k-1})$. Here $c_{\deg}$ does not mean that both components are degraded, it just represents that each component state is uncertain, i.e., may be degraded or not.

As mentioned earlier, we do not know the degraded model. Also, we may not use the particle filter to identify the degraded model because of the sample impoverishment problem. In order to detect the deviation in the measurements caused by component degradation, we propose to use our multiple hypothesis testing algorithm with MCMC in particle filtering by setting artificial degradation modes to construct the database rather than using a reliability degradation database based on real plant operating characteristics. For one component degradation, we propose two proposal pdfs. Each of these pdfs is constructed by setting a positive or negative shift in the distribution of the component state. Uniform distribution is a good choice to represent these pdfs, because we do not want overlapping proposal densities for the sake of detection.

As we did in Section 3.3.2 we construct the hypotheses according to the components and respective degradation modes, then calculate the proposal density for the augmented state using Eq. (3.38). Since we are not trying to estimate the amount of degradations and we only want to detect and isolate the degradations in this algorithm, we only construct the null hypothesis and hypotheses based on single degradation. This makes the detection scheme computationally inexpensive. We use the same hypothesis construction scheme presented in Eqs. (3.40) and (3.41) as

$$H_0 : c_k^{(i)} \sim q\left(\left(w_k\right)_j = c_k - c_{k-1}\right); j = 1,\ldots,n_c,$$

and for $h = 1,\ldots,n_{\text{single}}$ and $j = 1,\ldots,n_c$,

$$H_h : \begin{matrix} c_k^{(i)} \sim q\left(\left(\Delta c_k\right)_{j,d} = c_k - c_{k-1}\right); d = 1,\ldots,n_d(j) \\ c_k^{(i)} \sim q\left(\left(w_k\right)_l = c_k - c_{k-1}\right); l \neq j; l = 1,\ldots,n_c. \end{matrix}$$

In this method, we use the relative likelihoods of the hypotheses to decide if there is degradation or not. Since we do not know the degraded model, we systematically use the MH algorithm for each hypothesis to doubly maximize

$$\max_{1\le k\le n} \sup_{c_{\text{deg}}} S_k^n\left(c_{\text{deg}}\right). \tag{3.55}$$

Note that, we do not try to explore the state space to find the degraded state that maximizes the test statistic globally. Instead, we are interested in finding a local maximum of the test statistic with the given artificial degradation modes of that component to detect the deviation from the nominal state.

We use two different tests for change detection. Both of them are based on different characteristics of the relative likelihoods of the hypotheses. Assume we are in the process of estimating the nominal states. We start using our modified multiple hypothesis testing algorithm with artificial modes. We monitor the maximum number of particles accepted from each hypothesis except the nominal one, which has the current maximum number of particles accepted. Degradation in a component moves the component state in the direction of a specific degradation mode. Since the proposal densities of the artificial modes do not have the support of the target distribution, we indeed expect a sample impoverishment problem that causes the particles to collapse on one of the boundaries of the uniform distribution. Geometrically, this will increase the number of particles accepted for the hypotheses that are close to the target distribution. Even if a single degradation is simulated, there could be more than one hypothesis that has high

acceptance ratios because of the noisy measurement. If the measurement is smoothed then the number of potential hypotheses will decrease (see Chapter 4).

By using the information of maximum number of particles accepted we construct two tests. The first one is based on directly monitoring the relative likelihoods of the hypotheses

$$S_k^n\left(c_{\deg}\right) = \max_h p\left(H_h \mid \rho\right). \tag{3.56}$$

The change detector can be obtained from

$$g_n = S_{\hat{k}_n}^n = \max_{1\le k\le n} S_k^n \underset{H_{t0}}{\overset{H_{t1}}{\gtrless}} \lambda \tag{3.57}$$

where g_n is the decision function and λ is the threshold. That is, decide H_{t1} whenever g_n exceeds λ and H_{t0} otherwise. The change alarm is set at the time given by

$$t_{alarm} = \min\left\{n : g_n > \lambda\right\} = \min\left\{n : \max_{1\le k\le n} S_k^n > \lambda\right\} \tag{3.58}$$

Roberts et. al. [83], recommend the use of distributions with an acceptance ratio close to 0.25 for models of high dimension and equal to 0.5 for models of dimension 1 or 2. This heuristic rule is based on the asymptotic behavior of an efficiency criterion equal to the ratio of the variance of the estimator based on an i.i.d. sample and variance of the estimator. Therefore, for high dimensional systems we chose $\lambda = 0.25$ as the threshold.

The second test is based on the change in variance of the maximum number of particles accepted. The change detector is

$$g_n = S_{\hat{k}_n}^n = \left(S_k^n - m_k^n\right) \underset{H_0}{\overset{H_1}{\gtrless}} \lambda \tag{3.59}$$

where

$$S_k^n\left(c_{\deg}\right) = \operatorname{var}\left(\max_h p\left(H_h \mid \rho\right)\right) \tag{3.60}$$

and

$$m_k^n\left(c_{\deg}\right) = \min_{1\le p\le n} S_p^n. \tag{3.61}$$

The change alarm is set at the time given by

$$t_{alarm} = \min\left\{n : g_n > \lambda\right\} = \min\left\{n : \max_{1\le k\le n} S_k^n > m_k^n + \lambda\right\} \tag{3.62}$$

If the influence of the degradation on the measurement is significant, the first test can be used to determine the degradation time. If the influence of the degradation on the measurement is not significant, it is better to monitor the variance of the maximum number of accepted particles to decide if a degradation has occurred or not. In Chapter 4, we present how we use both tests effectively.

In order to isolate the candidate components that can be degraded, after detection of the degradation we first gather the relative likelihoods of the hypotheses constructed for the same component, e.g., hypothesis 1 is constructed based on the proposal density of component 1 degradation mode 1, and hypothesis 2 is constructed based on the proposal density of component 1 degradation mode 2, so that $p\left(c_1 \mid \rho\right) = p\left(H_1 \mid \rho\right) + p\left(H_2 \mid \rho\right)$. We monitor the change in $p\left(c_j \mid \rho\right)$ for each component *j*. We define

$$S_j^{n_c} = p\left(c_j \mid \rho\right) \tag{3.63}$$

and the mean of the relative likelihood of component *j* before the degradation as

$$m_{k,j}^{n,n_c}\left(c_j\right) = \mathrm{E}\left[S_j^{n_c}\left(t\right)\right] \tag{3.64}$$

where $1 \le t \le k$ and k is the time that degradation is detected. So the isolation detector is

$$g_j = S_{\hat{j}}^{n_c} = \left(S_j^{n_c} - m_{k,j}^{n,n_c} \right) \underset{H_0}{\overset{H_1}{\gtrless}} \lambda . \tag{3.65}$$

The isolated component set is given by

$$c = \left\{ c_j ; g_j > \lambda \right\}. \tag{3.66}$$

The characteristics of these prospective pdfs affect the efficiency of the algorithm. If the total number of particles is small and the variances of the pdfs are too large then the MH algorithm can reject a lot of particles. Therefore, especially for high dimensional systems, the characteristics of these pdfs need to be determined after detailed analysis for the detection of different multi-component degradations.

Having chosen an acceptance ratio, the characteristics of the prospective pdfs can be calibrated individually for high dimensional systems by taking into account the detectability of the degradations. In practice, the use of a MH algorithm must be preceded by a calibration step, which determines an acceptable range for the simulation of distributions.

One of the major advantages of this step is to isolate the components that can be degraded and disengage the rest of them in the estimation part for faster computation with limited number of particles.

CHAPTER 4

DEMONSTRATIVE APPLICATION: BWR BALANCE OF PLANT

In the preceding chapters we presented the theoretical basis of estimation theory, and the problem and possible solutions to the inability of a filter to estimate an abrupt change, which in this dissertation corresponds to the estimation of degradation in the components of a nonlinear system. For the extensions of the nonlinear Kalman filtering, we generated two algorithms. The first algorithm, which utilizes the EKF, is based on generating multiple hypotheses by perturbing the error covariance of the modeling noise in order to match the difference on the residual covariance before and after the degradation. The second algorithm is constructed on the UKF and is based on combining an additional data source, which is the reliability degradation database, with the UKF in a multiobjective optimization problem. In Section 3.3 we proposed a solution to the sample impoverishment problem of PF. We generate multiple hypotheses based on different degradation modes of components in a system. The necessary data to construct these hypotheses, such as the probability that a degradation mode can occur at a specific time, the pdf of degraded state given the nominal state, etc., are extracted from a reliability degradation database. We test these hypotheses in a MCMC move step and this algorithm allows the PF to explore the state space in the direction of degradation.

In this chapter, we demonstrate how our novel particle filtering algorithm based on multiple hypotheses testing with an MCMC move step works in a general degradation monitoring framework. In the next section, we present the system model in which we implement our algorithm, and then in subsequent sections we present results of our PF algorithm in detecting and diagnosing various degradations in this system.

4.1. SYSTEM MODEL

We consider a low order nonlinear model developed for the balance of plant (BOP) of Big Rock Point boiling water reactor (BWR) [60]. The system model is explained in detail in Appendix C. The schematic diagram for the balance of plant is shown in Figure 15. The system accepts saturated steam at 6.89 MPa from a main steam line to produce a station output of 50 MW(e). In the process, a small portion of feed steam is bled to the reheater through a reheat steam valve, while the remainder of the steam passes through a main steam valve and into the steam chest of the high pressure (HP) turbine. The steam undergoes a slight expansion in the steam chest before expanding across the HP turbine. Wet steam is bled from the end of the HP turbine to supply the HP feedwater heater (FWH) while the remainder is passed through a moisture separator and reheater before entering the low pressure (LP) turbine as saturated steam. Condensed steam from the moisture separator and reheater is then fed into the HP FWH where it combines with the bleed flow, tapped from the HP turbine, and flows into the LP FWH. Additional LP FWH stock is tapped at several locations along the expanse of the LP turbine, thus resulting in only 50% of the total bleed steam contributing to power production in the LP turbine. The combined bleed flows and condensed reheater flow are then extracted from the shell side of the LP FWH and diverted to a water treatment system. A constant enthalpy make-up flow is provided from the condenser and is pumped through both FWHs and returned to the reactor [48].

A time-lag representation is used to describe the dynamics of the turbines, FWHs, and reheater, while Callender's empirical relationship [84] is used as an equation of state for saturated steam. The FWHs are represented with a simplified model that assumes the heat transfer is directly proportional to the shell-side flow and inversely proportional to the tube-side flow. The reheater is represented as a point for the purpose of modeling heat transfer. The intermediate and LP turbines are lumped together and modeled as one LP turbine while the flow-pressure drop relationship for both HP and LP turbines is effectively represented by a simple correlational model. Efficiencies are assumed independent of operating level for both HP and LP turbines. The condenser and pump

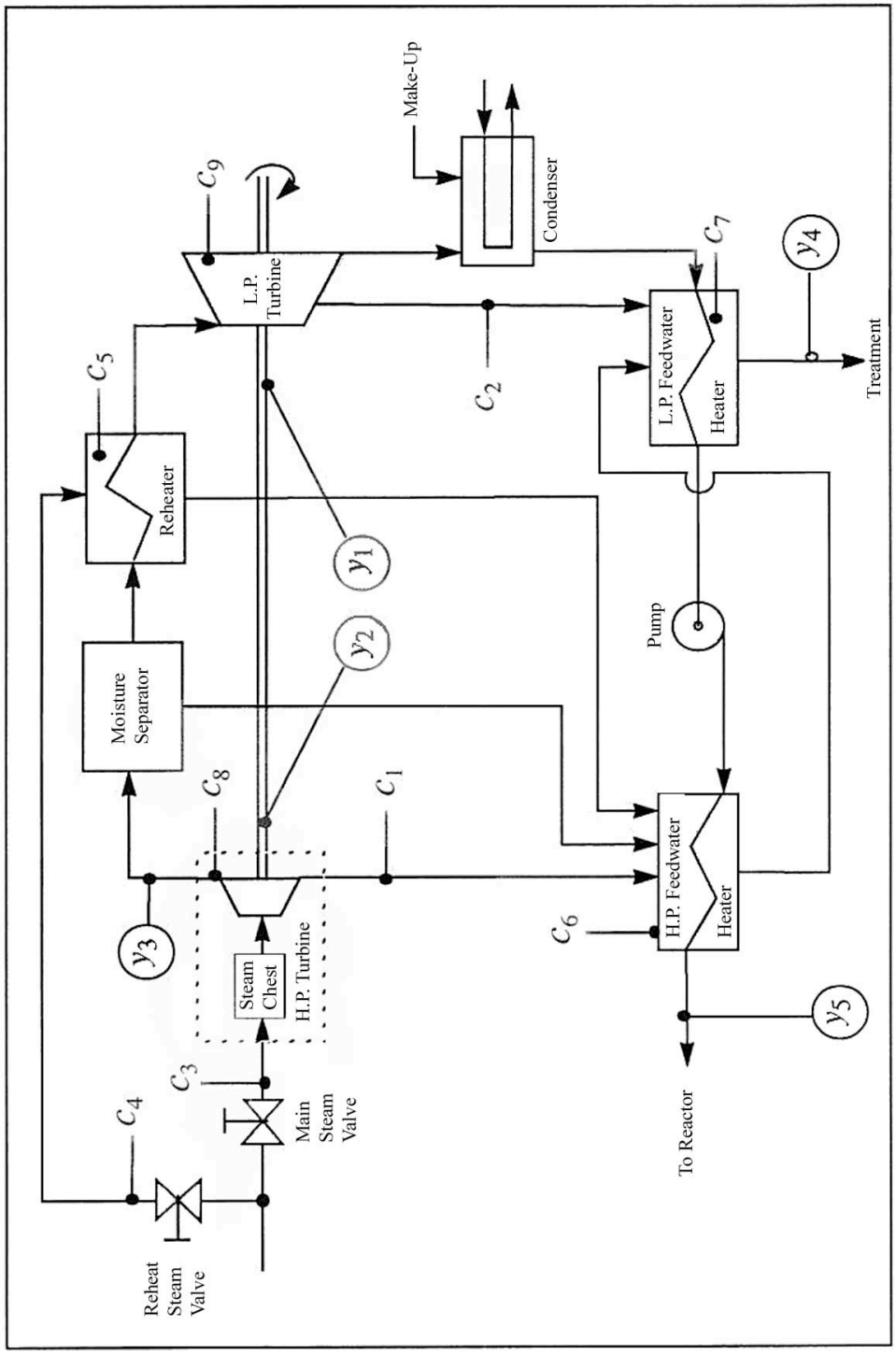

Figure 15. Schematic diagram for the balance of plant.

dynamics are not explicitly modeled; rather a constant feedwater flow rate of 77.3 kg/s at a constant enthalpy of 151.8 J/kg from the condenser and a constant pump head are assumed. Control is also not explicitly represented. The overall system model for the BOP is based on the analysis of Shankar [60].

4.1.1. Component and System States

The BOP is represented via 11 system states $\{x_1, x_2, \ldots, x_{11}\}$ as described in Table II. The differential equations describing this system are developed based on the work of Shankar [60] and presented in Appendix C. The model parameters representing the Big Rock Point BWR are obtained from Aumeier [85]. Nine component characteristics $\{c_1^v, c_2^v, \ldots, c_9^v\}$ are chosen for this demonstration, each of which is described in Table III and indicated in Figure 15. The set of component characteristics was chosen so that each characteristic represents a single component state, i.e., $c = c^v$.

Table II. System state variables.

Variable	Description	Nominal Value
x_1	Saturated steam enthalpy at steam chest (HP turbine feed) (kJ/kg)	2766.8
x_2	Saturated steam density at steam chest (HP turbine feed) (kg/m^3)	36.487
x_3	Wet steam flowrate out of HP turbine (kg/s)	63.240
x_4	Saturated steam density out of reheater (kg/m^3)	5.895
x_5	Saturated steam enthalpy out of reheater (kJ/kg)	2965.2
x_6	Reheat steam flow to HP FWH (kg/s)	6.662
x_7	Heat transfer rate in reheater (MW)	9.558
x_8	Steam flowrate out of LP turbine (kg/s)	40.980
x_9	Feedwater enthalpy into HP FWH (kJ/kg)	507.0
x_{10}	Feedwater enthalpy out of HP FWH (kJ/kg)	742.9
x_{11}	Reheat steam flowrate from HP FWH to LP FWH (kg/s)	22.639

Table III. Component state variables.

Variable	Component	Description	Nominal Value
c_1	HP bleed taps and associated piping	HP steam bleed (%)	8.80
c_2	LP bleed taps and associated piping	LP steam bleed (%)	23.31
c_3	Main steam valve	Effective flow area (m^2)	5.24×10^{-2}
c_4	Reheat steam valve	Effective flow area (m^2)	6.67×10^{-4}
c_5	Reheater	Heat Transfer Parameter (kJ/kgK)	44.29
c_6	HP FWH	Heat Transfer Parameter (kJ/kgK)	760.6
c_7	LP FWH	Heat Transfer Parameter (kJ/kgK)	804.7
c_8	HP turbine	Turbine efficiency (%)	86.0
c_9	LP turbine	Turbine efficiency (%)	83.0

4.1.2. Observations and Detectability

As shown in Figure 15, sensors are placed to obtain 5 different measurements and working with a sampling frequency of 1 Hz. In our simulations, we treated the sensor noise by adding 1% white Gaussian noise on the measurements. The observation variables are listed in Table IV.

Table IV. System observation variables.

Variable	Description	Nominal Value
y_1	Torque on LP turbine shaft (kJ)	93.55
y_2	Torque on HP turbine shaft (kJ)	44.98
y_3	HP turbine exhaust pressure (MPa)	1.391
y_4	Feedwater flowrate out of LP FWH (kg/s)	35.03
y_5	Feedwater temperature out of HP FWH (^oC)	175.3

Detectability of degradation is a function of the dynamics of the degradation. Therefore, as we mentioned in Section 3.3.3 it is harder to detect degradations of low magnitudes

especially in a noisy environment. In order to determine that the degradations in the component states are detectable through the observations for this BOP model, we performed a sensitivity analysis. We modeled degradations as a 5% change in the component states and plot the absolute change in the measurements (without sensor noise) as functions of time given in Figures 16 - 24. Note that, this analysis is mainly performed for single component degradations. For simultaneous multicomponent degradations, this analysis is not enough to decide if those degradations are detectable or not. The reason is that some multicomponent degradations may produce similar measurements that are particularly hard to distinguish when there is measurement noise. Therefore, for degradation monitoring of a real plant, more detailed analysis is required for detectability of simultaneous multi-component degradations.

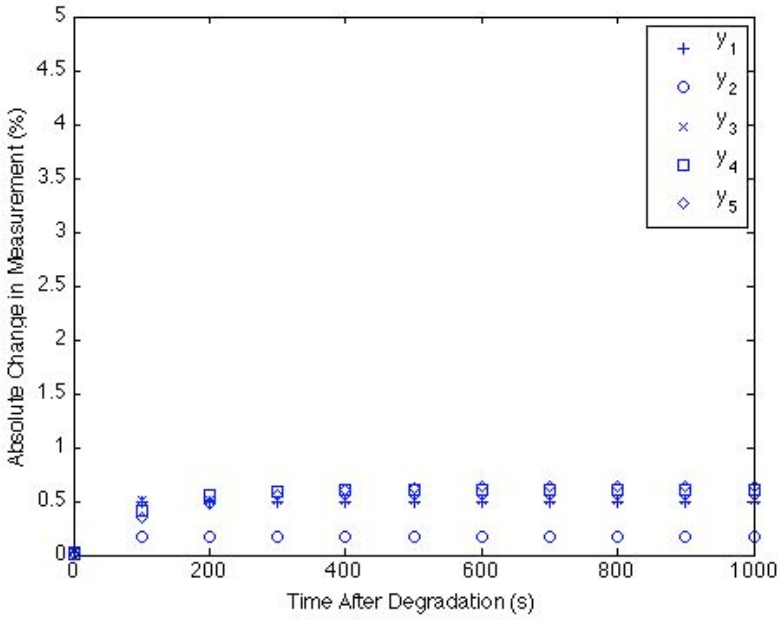

Figure 16. The absolute change in the measurements after degradation in component 1 is introduced at $t = 0$ s.

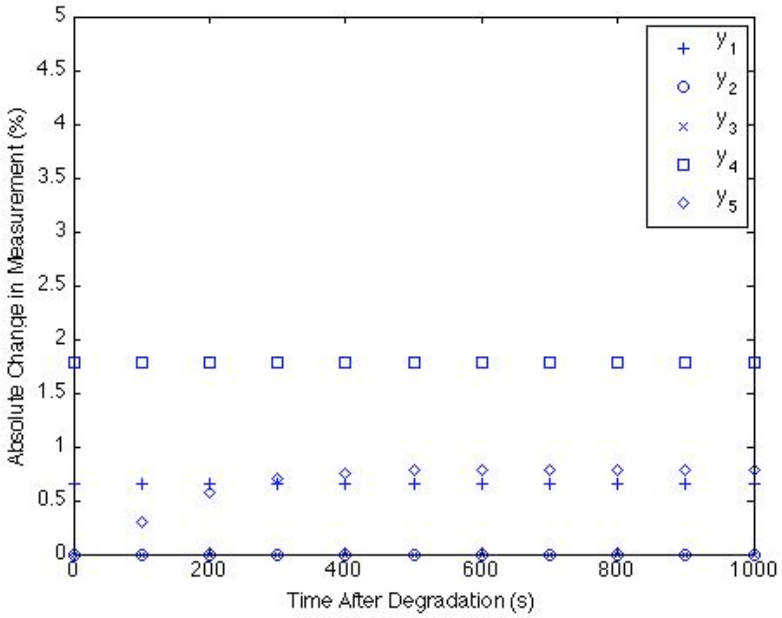

Figure 17. The absolute change in the measurements after degradation in component 2 is introduced at $t = 0$ s.

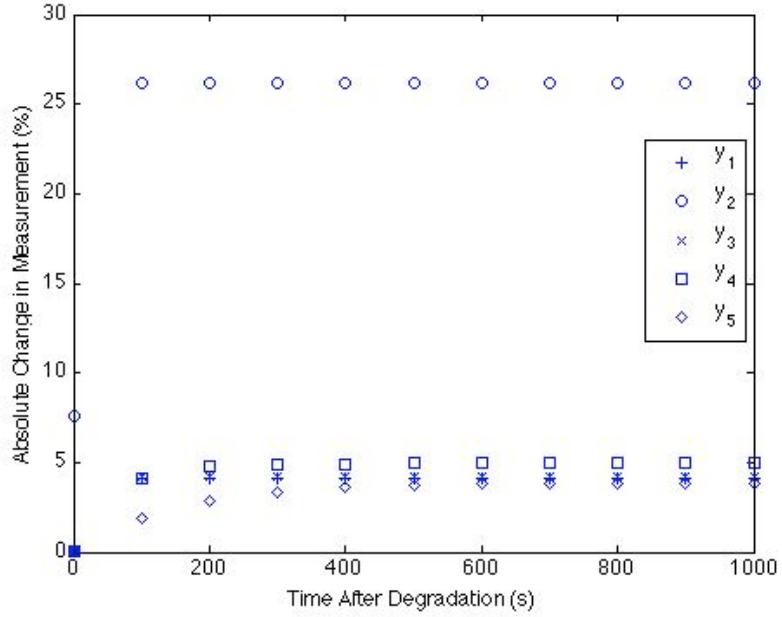

Figure 18. The absolute change in the measurements after degradation in component 3 is introduced at $t = 0$ s.

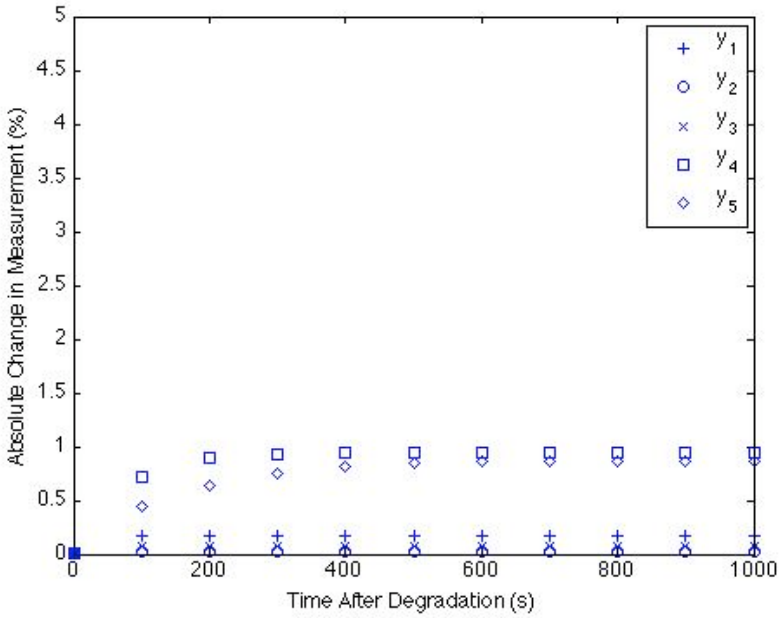

Figure 19. The absolute change in the measurements after degradation in component 4 is introduced at $t = 0$ s.

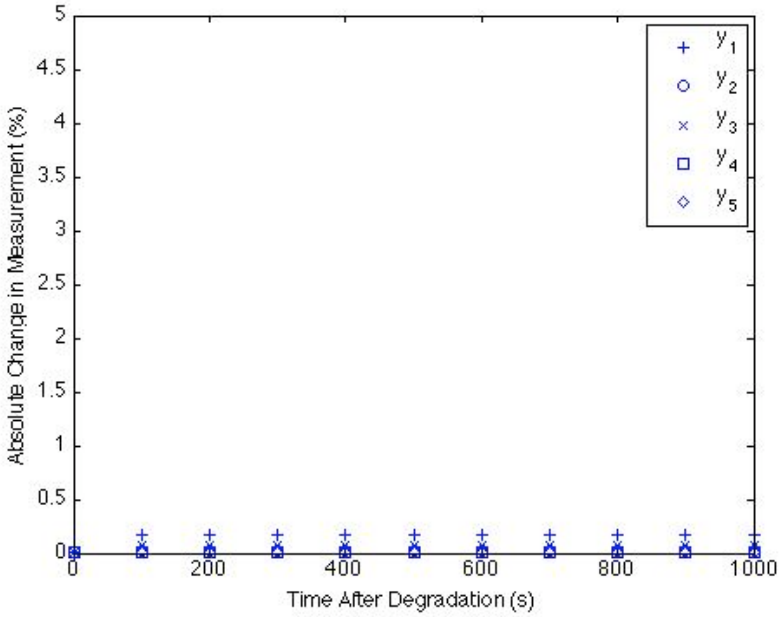

Figure 20. The absolute change in the measurements after degradation in component 5 is introduced at $t = 0$ s.

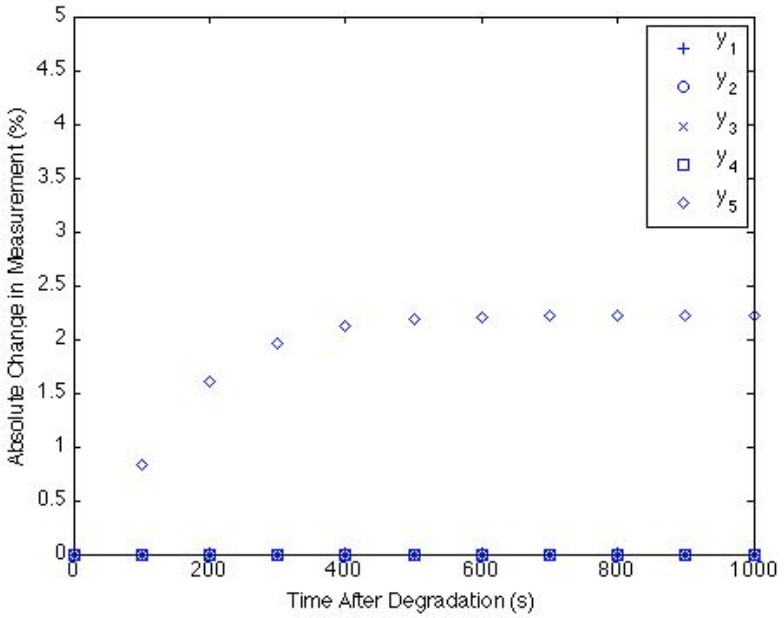

Figure 21. The absolute change in the measurements after degradation in component 6 is introduced at $t = 0$ s.

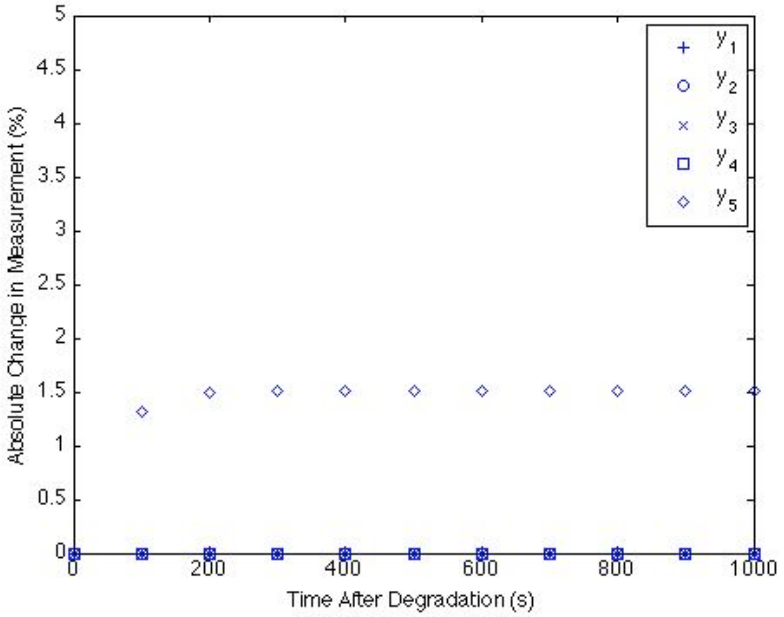

Figure 22. The absolute change in the measurements after degradation in component 7 is introduced at $t = 0$ s.

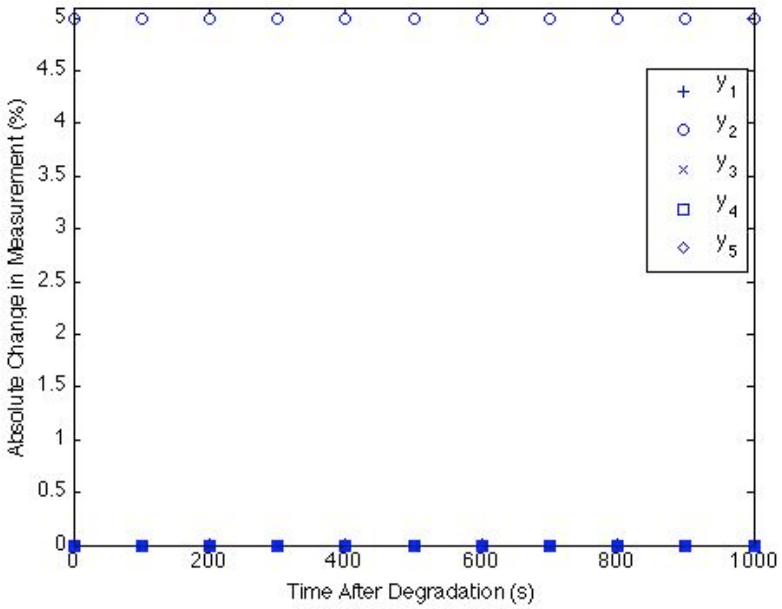

Figure 23. The absolute change in the measurements after degradation in component 8 is introduced at $t = 0$ s.

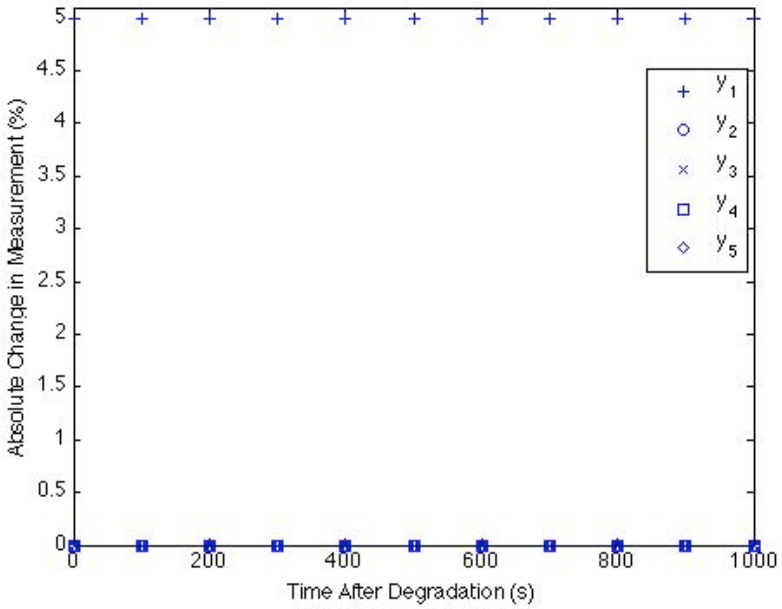

Figure 24. The absolute change in the measurements after degradation in component 9 is introduced at $t = 0$ s.

As observed in this analysis, component degradations that are introduced as abrupt changes in their states do not all affect the measurements in the same way. Some of the measurements react to these changes immediately, while the responses of others are slowly varying. This can be a characteristic of the degradation dynamics or the sensor may be placed far from the component so that the effect of the component shows a delay on the measurement. This is often a problem of sensor placement, but in many cases we cannot replace the sensors because of the limitations of the environment. In these circumstances, we must know that even though analytical redundancy exists, we cannot detect the degradations immediately.

This preliminary analysis on the detectability of the component degradations shows that the impact of degradations in components 2, 3, 8 and 9 on some of the measurements are notable and instant, which makes degradations in these components relatively easy to detect. Degradations in components 1 and 4 do not have significant effects on the measurements, and when the measurement noise is large, it will be difficult to detect these degradations. The effects of degradations in components 6 and 7 on the measurements are slowly varying and because of that it may take a while to detect these degradations. The effect of degradation in component 5 on the measurements is very small because there is not any sensor placed around the reheater to detect any degradation in the heat transfer characteristics of the reheater. So, it is almost impossible to detect it; we really need to place another sensor in the system to detect this degradation.

In the next section, we present how we constructed the reliability degradation database for both the estimation and detection of degradations.

4.2. RELIABILITY DEGRADATION DATABASE

For this BOP system, we constructed a representative reliability database to demonstrate the basic concepts and the capabilities of the algorithms we propose. This degradation database is constructed for demonstrational purposes only and it cannot be used for application to any real system.

All of the component states are represented in this database. We assume that each component has two degradation modes. We also set the same degradation rate for all components. This makes the monitoring problem more challenging for the components that degrade more frequently than the others in the real operational life. Considering the time to degradation is distributed according to an exponential distribution, the probability of having component *j* degraded at time t_k is $\alpha_j = 1 - e^{-\lambda t_k}$. By assuming the degradation rate as $\lambda = 0.0002$ (1/h), we expect in 6 months all of the components can degrade with a probability of 0.6. For demonstration purposes, we believe that any of these components can degrade equally likely and consequently in our multiple hypothesis testing algorithm we start with an equal number of samples drawn for the hypotheses constructed for each component.

We set the hard constraints for each component state by considering the physical range of values that it can take. For example, for the component states 8 and 9, which are LP and HP turbine efficiencies, we set the range of values as $(0,1]$. If in the sampling step, we draw a sample beyond these limits, we continue sampling until we obtain a sample in this range.

The conditional pdfs $q(c_k \mid c_{k-1})$ representing the nominal and the degraded modes are chosen as Gaussians. The mean and the variance of each pdf are specified in the database. We also set the probability that a component is in a particular mode (nominal or degraded) at time *t*, which we defined previously as the occurrence probability of that mode. This occurrence probability may change with time. For the nominal mode of a component, this is the reliability of the component, which is the probability that the component is not degraded. Again, considering the time to degradation is distributed according to exponential distribution, for the nominal mode this is $e^{-\lambda t_k}$. For the degradation mode *d* and component *j,* we set these occurrence probabilities according to the expected frequencies at time t_k $(\omega_k)_{j,d}$ and normalize these probabilities for each component, e.g., if up to time t_k on average, 4 components degraded with mode 1, and 2 components degraded with mode 2, then the total probability of degradation is $(1 - e^{-\lambda t_k})$

and the occurrence probability of each mode is $(\omega_k)_{j,1} = \frac{2}{3}\left(1 - e^{-\lambda t_k}\right)$ and $(\omega_k)_{j,2} = \frac{1}{3}\left(1 - e^{-\lambda t_k}\right)$.

A representative data set is given in Appendix D for the estimation problem.

4.3. A PRELIMINARY ANALYSIS ON PARTICLE FILTERING

In this section, we analyze the performance of the particle filter without any modifications by using our BOP model. Throughout this section we use the SIR algorithm described in Subsection 2.4.4.6. We start this analysis by estimation of the nominal component states for different setups. At first, we analyze the effect of the modeling error on the PF estimates for this high dimensional system. We run the particle filter with 1000 particles for both 1% and 0.5% modeling noise. The estimated component state corresponding to the main steam valve flow area is plotted in Figure 25.

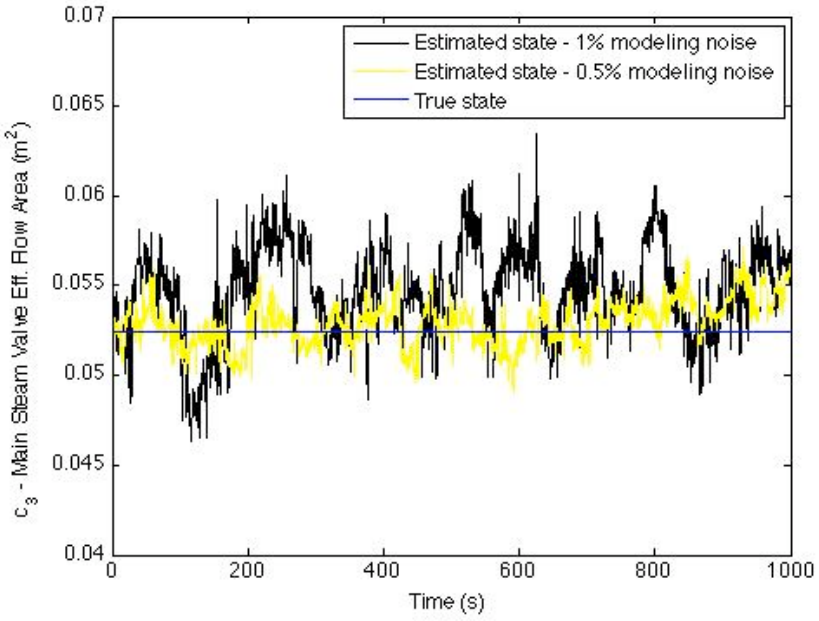

Figure 25. The estimated main steam valve flow area for 1% and 0.5% modeling noise by using the PF only.

For this high dimensional system adding additional modeling noise into the state parameters deteriorates the component state estimates. This results in PF being non robust for high modeling noises and prevents us from applying techniques like roughening where we add additional modeling noise to assist the filter in exploring the state space.

We also analyzed the effect of the number of particles on the component state estimates for 1% modeling noise. For this purpose we run the PF for 100 and 1000 particles. The component state estimates corresponding to the main steam valve flow area for these cases are given in Figure 26.

As we stated in Section 2.4.4.1, increasing the number of particles in the PF helps the filter in obtaining better estimates, but this also increases the computational burden. For this case increasing the number of particles by a factor of 10 increases the computational time approximately by a factor of 10.

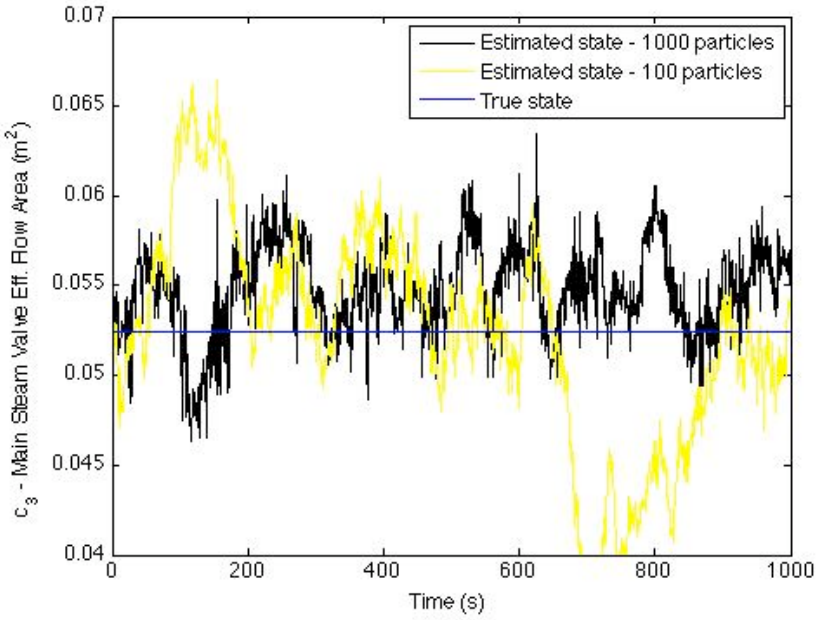

Figure 26. The estimated main steam valve flow area for 100 and 1000 particles by using the PF only.

Finally, we analyzed the performance of the PF in the case of a degradation. We assumed degradation in LP bleed taps or associated piping caused a 5% decrease in the LP steam bleed at t = 1000 s. We run the PF for 2000 seconds for 10000 particles. The estimates of component state 2 are plotted in Figure 27.

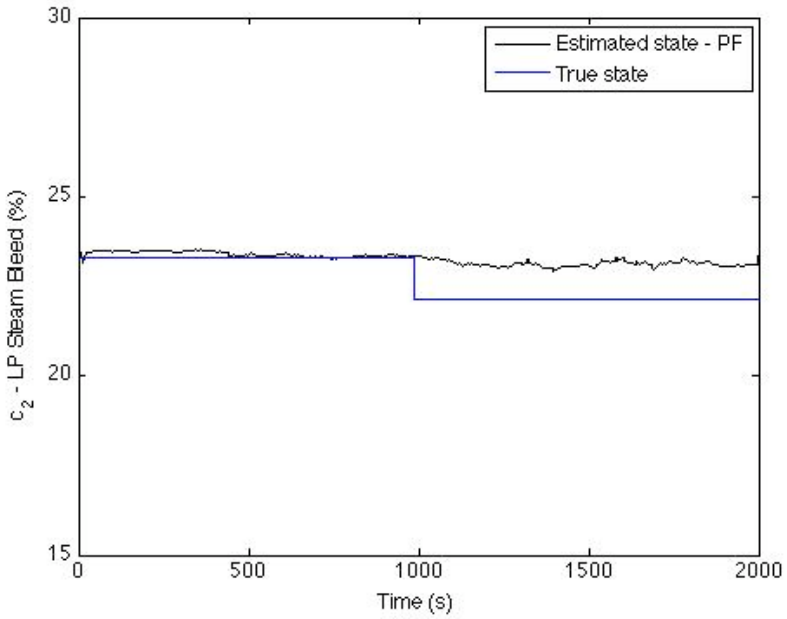

Figure 27. The estimates of component state 2 for 10000 particles by using the PF only.

As mentioned in Chapter 3, even though the number of particles in the filter is increased because of the sample impoverishment problem, PF cannot respond to an abrupt change in the states.

In the next section, we analyze the performance of our new algorithm described in Section 3.3, for both degradation detection and isolation, and degradation estimation.

4.4. DEGRADATION DETECTION AND ISOLATION

As we discussed in Section 3.3.3, for the degradation detection problem we construct another database with artificial modes. Artificial modes are designed to represent slight

deviations from the nominal states in order to detect the degradations. The idea is, when the test statistics given in Eq. 3.57 or Eq. 3.59 computed by using one of the hypotheses constructed with the proposal density of one of these artificial modes exceeds some threshold, then we reject the null hypothesis given in Eq. 3.54 in favor of the alternative one stating that there is degradation.

The database constructed to detect the degradations in this system model is given in Appendix D. As suggested before, we chose the pdfs representing the modes distributed according to uniform distribution. The nominal mode is constructed for component *j* as

$$q\left(c_{j,k} = c_{j,nom} \mid c_{j,k-1} = c_{j,nom}\right) = U\left(0.995 \times \overline{c}_{j,nom}, 1.005 \times \overline{c}_{j,nom}\right)$$

where $\overline{c}_{nom}$ is the mean of the nominal distribution. The two proposal pdfs are constructed for the degradation modes as

$$q\left(c_{j,k} = = c_{\deg} \mid c_{j,k-1} = c_{nom}\right) = U\left(0.995 \times \left((1-r) \times \overline{c}_{j,nom}\right), 1.005 \times \left((1-r) \times \overline{c}_{j,nom}\right)\right)$$

$$q\left(c_{j,k} = = c_{\deg} \mid c_{j,k-1} = c_{nom}\right) = U\left(0.995 \times \left((1+r) \times \overline{c}_{j,nom}\right), 1.005 \times \left((1+r) \times \overline{c}_{j,nom}\right)\right)$$

where r is the threshold for degradation detection representing the deviation from the nominal mean. The selection of r may affect the isolation of the degraded components. As shown in Figure 28, picking r too large may opt for the nominal hypothesis even though the component is degraded. Also extra caution should be taken in the selection of r, because some components may have larger effect on the measurements than the other ones. So, picking the same r for all of the components may mask the detectability of some of the components. From that point of view, r also can be used to balance the component effects on the measurement. A detailed analysis should be performed before implementing this scheme in a real plant to determine the best choices for the threshold.

In this application after a preliminary analysis, we chose $r = 2\%$ for component states 2, 3, 4 and 5 and $r = 10\%$ for component states 1, 6, 7, 8 and 9. The support of the uniform

distribution is arranged to detect a minimum change of 5% in the component states. The database we constructed for degradation detection is given in Appendix D.

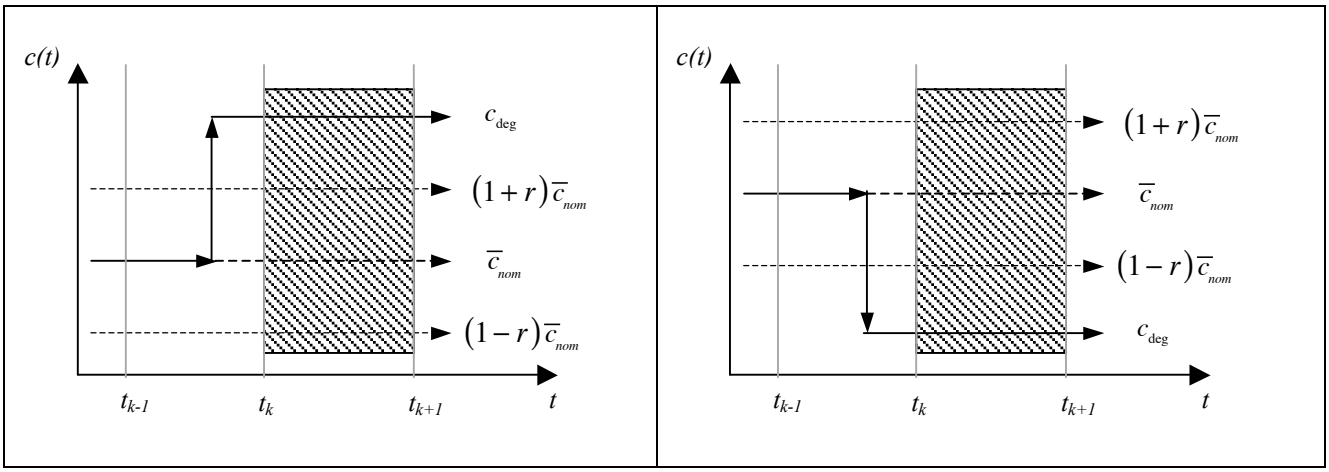

Figure 28. True nominal and uncertain degraded component states, and expected values of the component states for the two hypotheses.

As mentioned before, there is no adaptation step in terms of multiplying or eliminating the particles drawn from these pdfs. Starting with the same initial conditions, all of the hypotheses are being tested by the MH algorithm first to find the best set of particles among the modes that has the ability to reproduce the measurements, then the best set of particles coming through the database is being compared with the particles from the particle filter to help the filter to perform better for the nominal estimation and to detect the component degradations.

We first set the thresholds for the test statistics to be used in the multiple hypothesis testing algorithm. For the first test in which the test statistic is the maximum acceptance ratio of the particles for each hypothesis, as we discussed in Subsection 3.3.3.2 we chose a threshold of 0.5. For the second test for degradation detection in which the test statistic is the maximum change in the variance of the acceptance ratio of the particles for each hypothesis, we chose a threshold of 0.005. For the third test in which the test statistic is the change in the relative likelihood of the component after the detection of the degradation we chose a threshold of 0.01.

Based on our preliminary analysis, we observed that incorrect hypotheses might have higher relative likelihoods than the correct ones. The main reason is that if the measurement noise is high at an instant of time and the impact of degradation in a component is not notable on the measurements, then particles drawn from the incorrect hypotheses may reproduce the measurements and get accepted. This can be eliminated by smoothing the measurements with a moving average technique, which results in better isolation of the components that are degraded, but it might reduce the performance in promptly detecting the true degradation time. This is a necessary trade-off.

In order to improve the degradation isolation capability of our algorithm, we smoothed the noisy measurements through a moving average filter only for the first part of the algorithm by replacing the measurement at time step k with the average of neighboring data points within a span

$$(y_s)_k = \frac{1}{M+1} \sum_{j=-M}^{0} (y_s)_{k+j}$$

where $M+1$ is the span and $s \in \mathbb{R}^{n_y}$. In the second part of the algorithm where we are updating the particles coming from the particle filtering with the ones coming from the hypotheses, we used regular noisy measurements.

We tested our proposed algorithm in detection and isolation of single, binary and triple component degradations.

4.4.1. Single Component Degradations

We chose two cases to demonstrate single component degradations. In the first one, we consider degradation in the main steam valve (component 3). We simulated the degradation as a 5% step increase in the effective flow area of the main steam valve at t = 1000 s. We run our detection and isolation algorithm for 2000 seconds. The computed test statistics for degradation detection are plotted in Figure 29.

By observing both of the tests statistics, we reject the null hypothesis in favor of the alternative one constructed on the onset of degradation. In this case, we chose the first test (Figure 29(a)), which is statistically significant and detects the degradation earlier at t = 1010 s than the second test. We also plotted the test statistic for degradation isolation in Figure 30.

In Figure 30, we only plotted the components whose test statistics are higher than the threshold. We observe that the test statistics of hypotheses constructed with the degradation modes of components 3 and 9 are significantly high after the detection time 1010 seconds. Therefore, we only need to consider components 3 and 9 when we wish to estimate the amount of degradation. We not only isolated the correct degraded component successfully in this set of components, but also reduced the number of hypotheses to be constructed in the degradation estimation part dramatically.

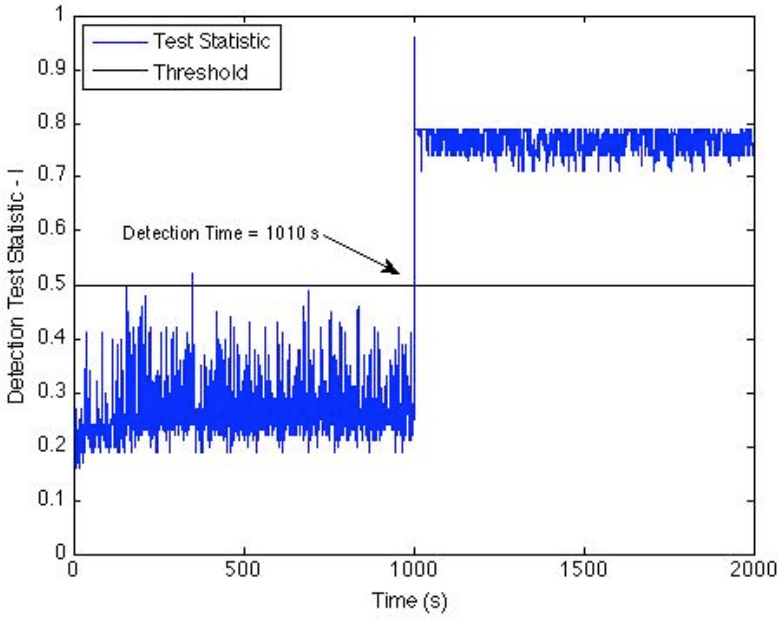

(a) The maximum relative likelihoods of the hypotheses.

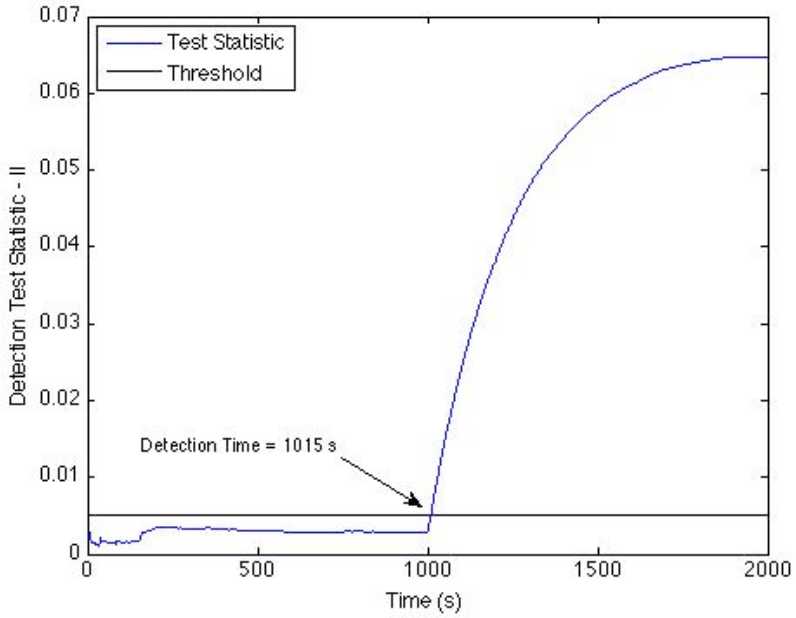

(b) The change in the variance of the maximum relative likelihoods of the hypotheses.

Figure 29. The test statistics for degradation detection in the main steam valve.

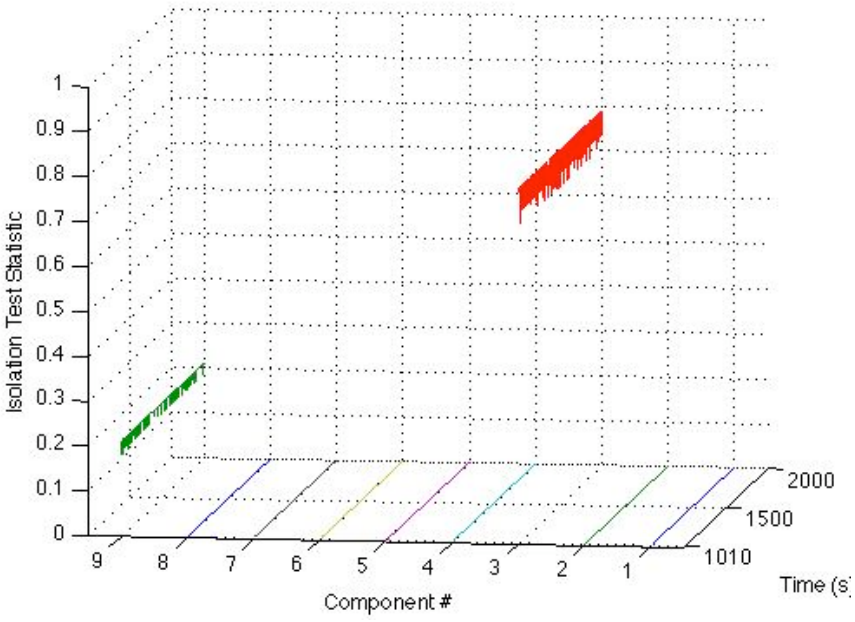

Figure 30. The test statistics for degradation isolation in the main steam valve.

In the second case we consider degradation in the LP bleed taps and associated piping (component 2). This time we consider an incipient degradation, which develops slowly in time starting at t = 1000 s and ends 200 seconds later, reaching to a total of 5% decrease in the LP steam bleed. The computed test statistics for the degradation detection of this incipient degradation are plotted in Figure 31.

By observing both of the tests statistics, we chose the second test (Figure 31(b)), which is statistically more significant and detects the degradation at t = 1055 s. In this slowly developing degradation at the time of the detection, the degradation has perturbed the component state by 1.25%. This shows how sensitive is our detection scheme even for small degradations. We also plotted the test statistic for degradation isolation in Figure 32.

From the degradation isolation statistic, we observe that the hypotheses constructed with the degradation modes of components 1, 2 and 8 are statistically significant. Even for the slowly varying degradations, our detection and isolation algorithm performs quite well.

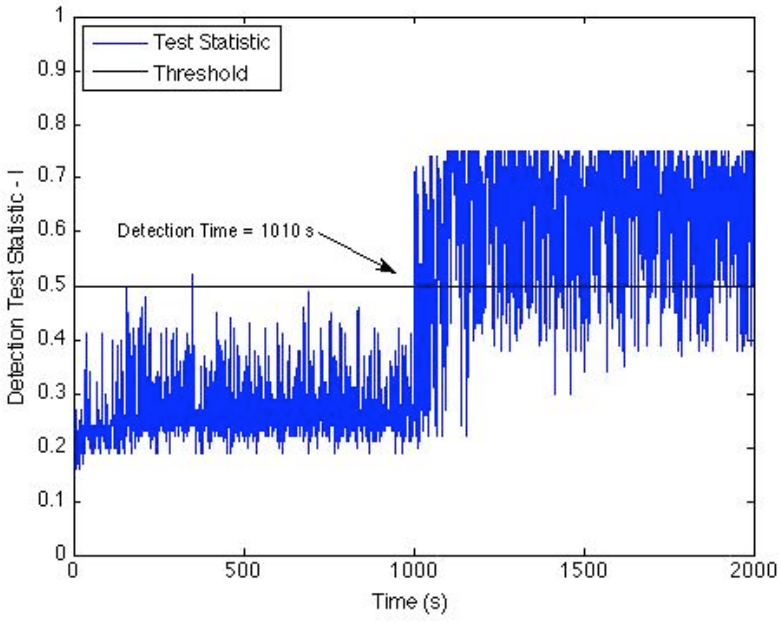

(a) The maximum relative likelihoods of the hypotheses.

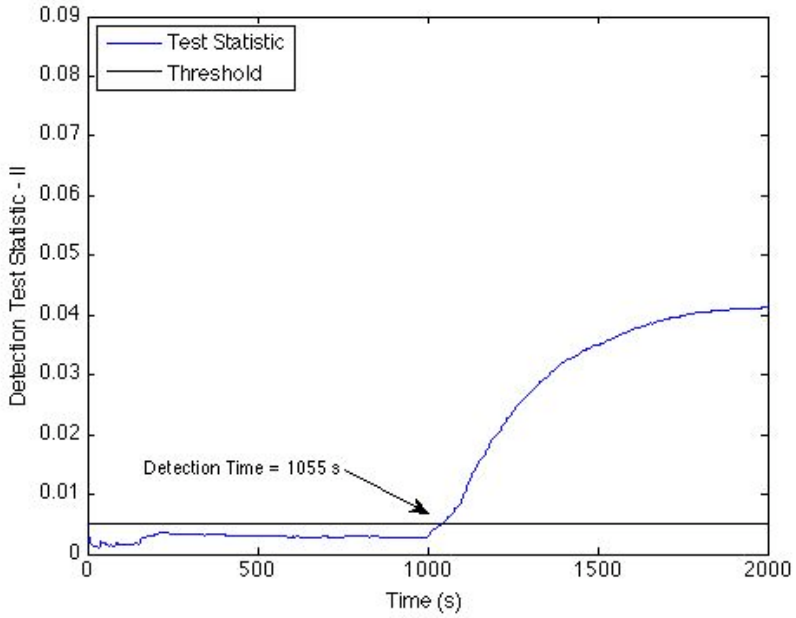

(b) The change in the variance of the maximum relative likelihoods of the hypotheses.

Figure 31. The test statistics for detection of a slowly varying degradation in the LP bleed taps and piping.

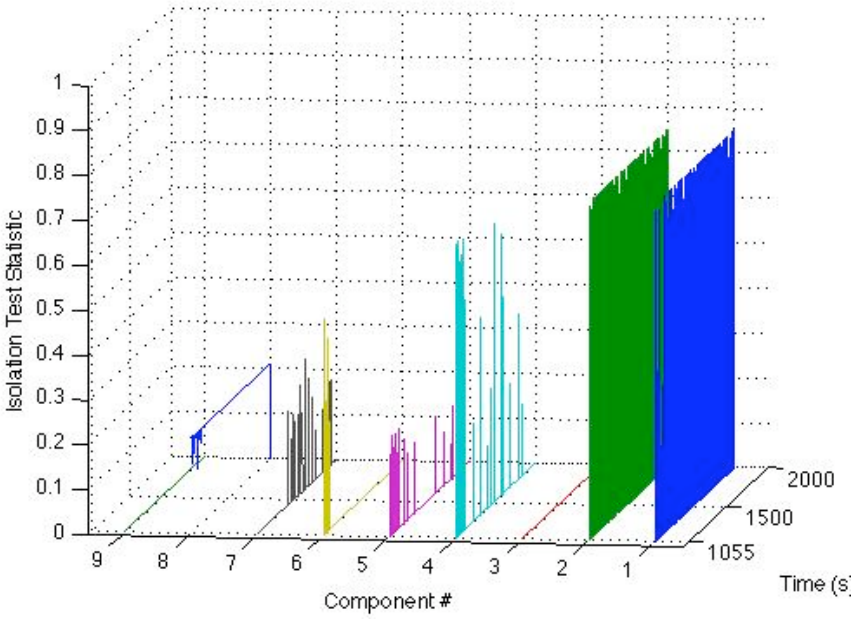

Figure 32. The test statistics for degradation isolation in the LP bleed taps and piping.

4.4.2. Binary Component Degradations

One of the biggest challenges is to detect and estimate simultaneous multiple degradations. The problem is, if different degradations occur at the same time, one may mitigate the effect of the other on the measurements and the detection algorithm may not be able to respond to these changes, especially if the change disappears within the noisy measurements. From this point of view, the detection algorithm should be very sensitive even to the slight changes and have the ability to be trained for hard to follow transitions.

In this subsection, we use our algorithm to detect multiple degradations occurring simultaneously at one instant in time. Degradations occurring one at a time can be modeled as single degradations even if one degradation triggers another one. This is due to the delay that is a function of the change in the environment or component characteristics.

We demonstrate the performance of our algorithms with two different binary component degradations. In the first case, we consider simultaneous degradations in components 3 and 8, which are the main steam valve and HP turbine. We simulated the degradations as a 5% step increase in the effective flow area of the main steam valve and a 5% step decrease in the HP turbine efficiency at t = 1000 s. We run our detection and isolation algorithm for 2000 seconds. The computed test statistics for degradation detection are plotted in Figure 33.

By observing both of the tests statistics, we set the detection time to 1015 seconds. We also plotted the test statistic for degradation isolation in Figure 34.

From the degradation isolation statistic, we observe that the hypotheses constructed with the degradation modes of components 3 and 8 are statistically significant and our isolation algorithm correctly determines the components for this binary degradation case. As shown in Figure 30, the degradation in component 3 isolated the potential degraded

components as component 3 and 9. By introducing this binary degradation, our algorithm eliminates component 9 and detects the effect of component 8, successfully.

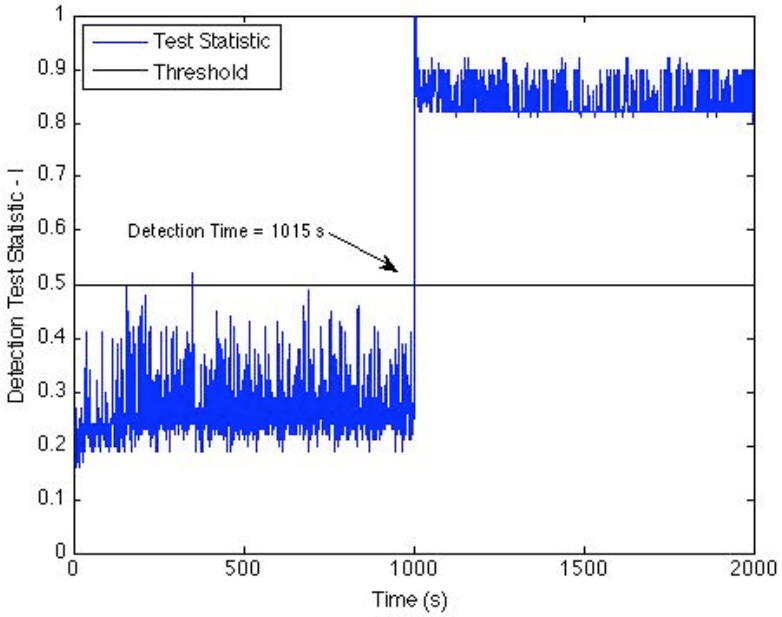

(a) The maximum relative likelihoods of the hypotheses.

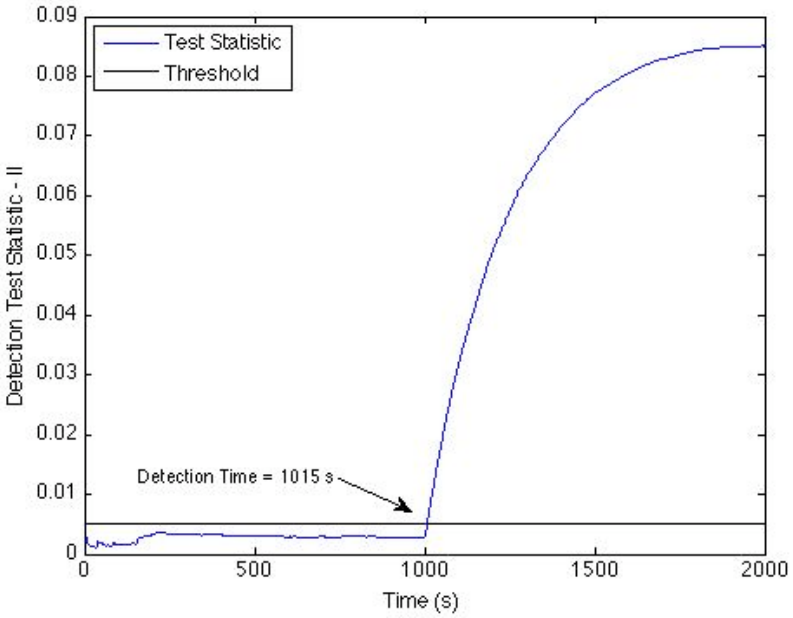

(b) The change in the variance of the maximum relative likelihoods of the hypotheses.

Figure 33. The test statistics for detection of simultaneous binary degradations in the main steam valve and HP turbine.

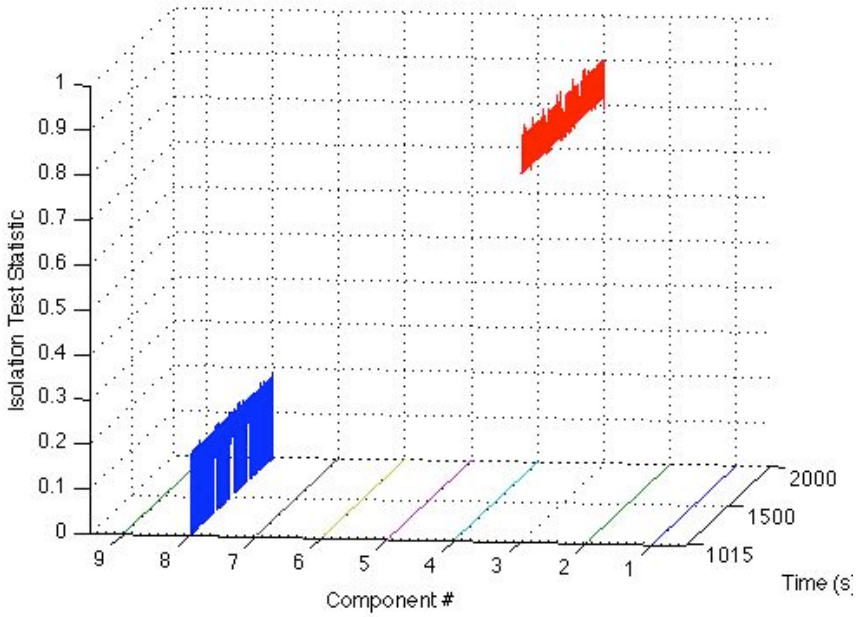

Figure 34. The test statistics for isolation of simultaneous binary degradations in the main steam valve and HP turbine.

In the second case, we consider simultaneous degradations in components 2 and 4, which are the LP bleed taps and piping, and reheat steam valve. We simulated the degradations as a 5% step decrease in the LP steam bleed and a 10% step increase in the effective flow area of the reheat steam valve occurring at t = 1000 s. We run our detection and isolation algorithm for 2000 seconds. The computed test statistics for degradation detection are plotted in Figure 35.

By observing both of the tests statistics, we set the detection time to 1025 seconds. We also plotted the test statistic for degradation isolation in Figure 36.

For this binary component degradation case, the isolation test statistics for components 2, 3, 4, 5, 7 and 8 are statistically significant. At the onset of degradation, components 1 and 6 also have significant statistics but then the consistency of their test statistics diminishes. Our algorithm isolates a set of components in which the correct degraded components are present. The reason for isolating a large set is mainly because of the detectabilities of each component. As mentioned in Section 4.1.2, some of the components may produce

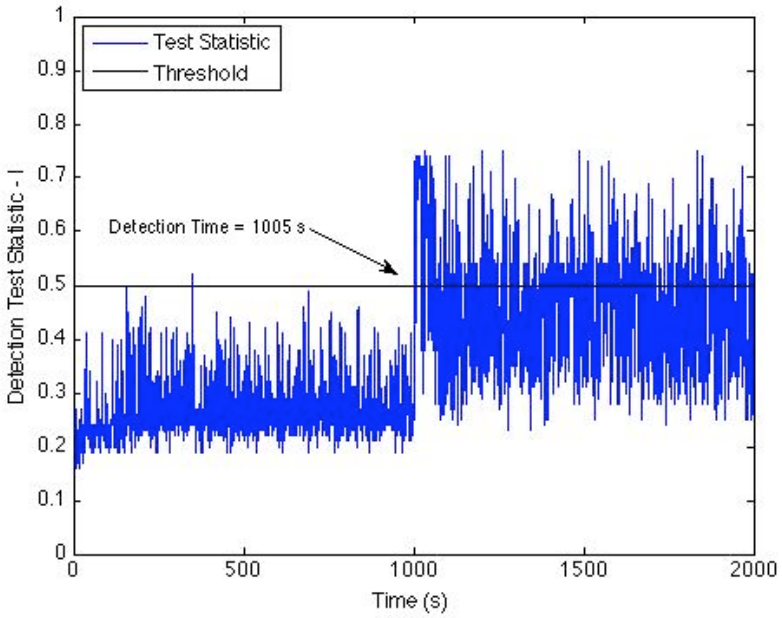

(a) The maximum relative likelihoods of the hypotheses.

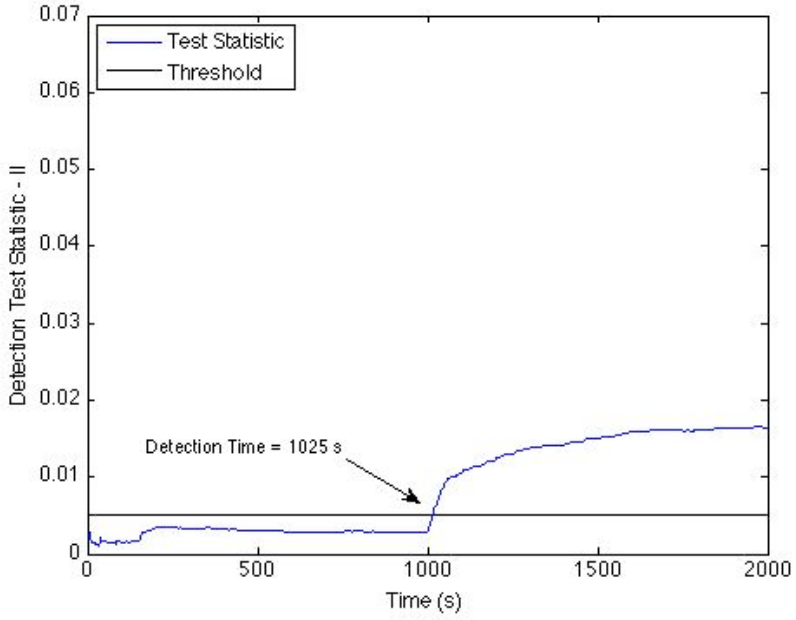

(b) The change in the variance of the maximum relative likelihoods of the hypotheses.

Figure 35. The test statistics for detection of simultaneous binary degradations in the reheat steam valve and LP bleed taps and piping.

the same impact on the measurements and if these impacts are not significant, e.g., large, then it is harder to isolate the components. In these cases, one should carry out all

candidate components derived from these hypotheses to our adaptive estimation algorithm to modify the reliability degradation database.

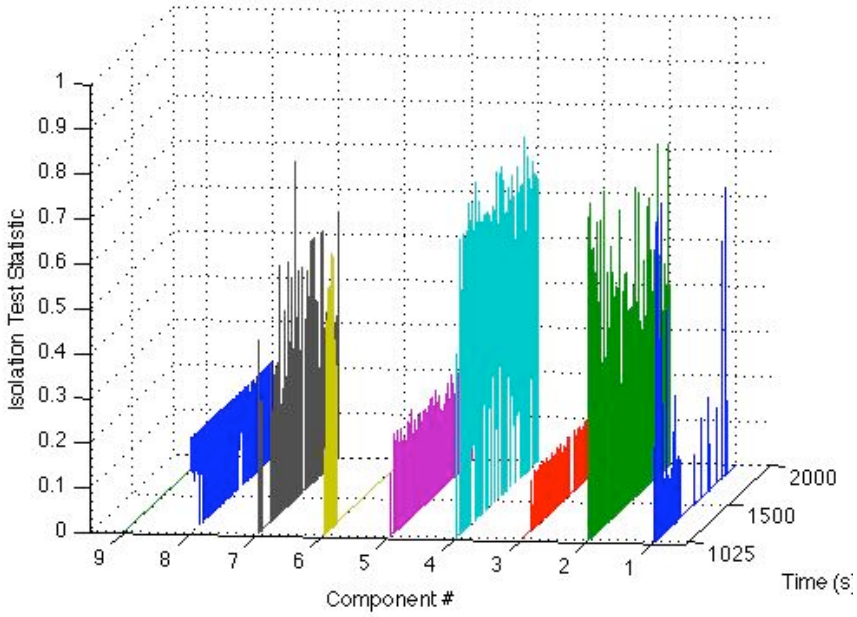

Figure 36. The test statistics for isolation of simultaneous binary degradations in the reheat steam valve and LP bleed taps and piping.

4.4.3. Triple Component Degradations

As discussed in the preceding sections, as the number of simultaneous component degradations increase, it may get harder to detect the degradations and isolate the components because of the ill-posedness of the problem. Therefore more observations are needed for these cases. In this section we test our algorithm in detection and isolation of simultaneous triple component degradations.

We consider simultaneous degradations in components 1, 2 and 4, which are the HP bleed taps and piping, LP bleed tap and piping and reheat steam valve. We simulated the degradations as a 5% step decrease in the HP steam bleed, a 5% step decrease in the LP steam bleed and a 10% step increase in the effective flow area of the reheat steam valve

occurring at t = 1000 s. We run our detection and isolation algorithm for 2000 seconds. The computed test statistics for degradation detection are plotted in Figure 37.

By observing both of the tests statistics, we set the detection time to 1025 seconds and plotted the test statistic for degradation isolation in Figure 38.

The isolation test statistics show that components 1, 2, 3, 4, 5 and 8 are statistically significant. Adding component 1 into the binary degraded components of the previous case (Figure 36) gives rise to its test statistics as expected and at the same time component 7 was eliminated from the set of isolated components. The reason is that adding degradation of component 1 changed all the observations except feedwater temperature, which is the only measurement, that component 7 can be detected.

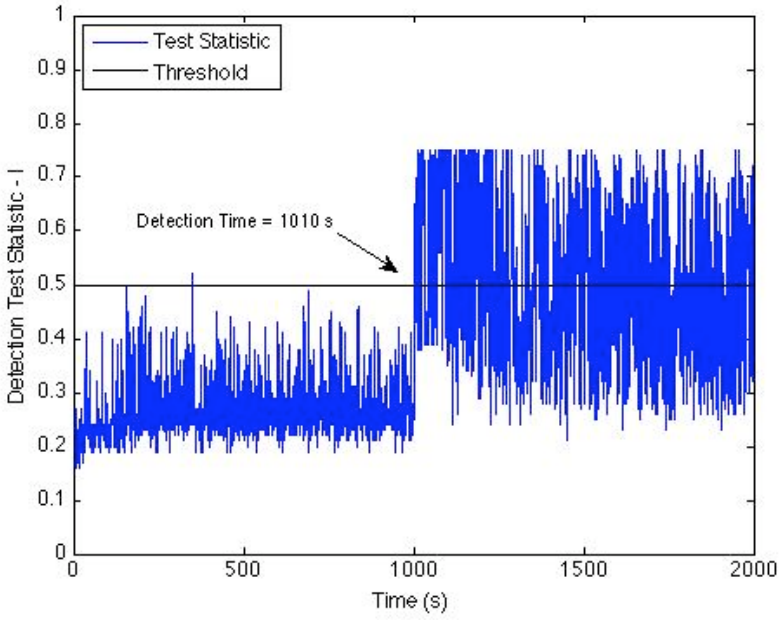

(a) The maximum relative likelihoods of the hypotheses.

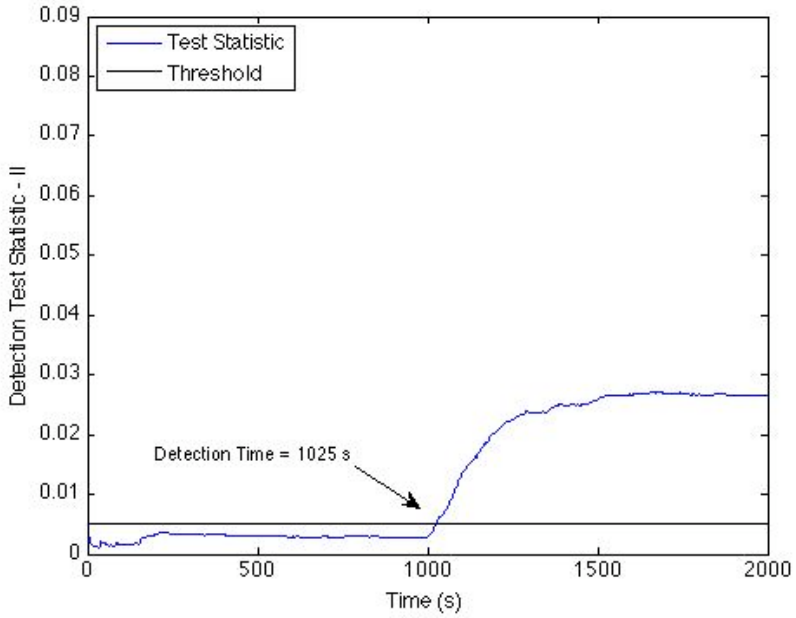

(b) The change in the variance of the maximum relative likelihoods of the hypotheses.

Figure 37. The test statistics for detection of simultaneous binary degradations in the reheat steam valve, LP bleed taps and piping and HP bleed taps and piping.

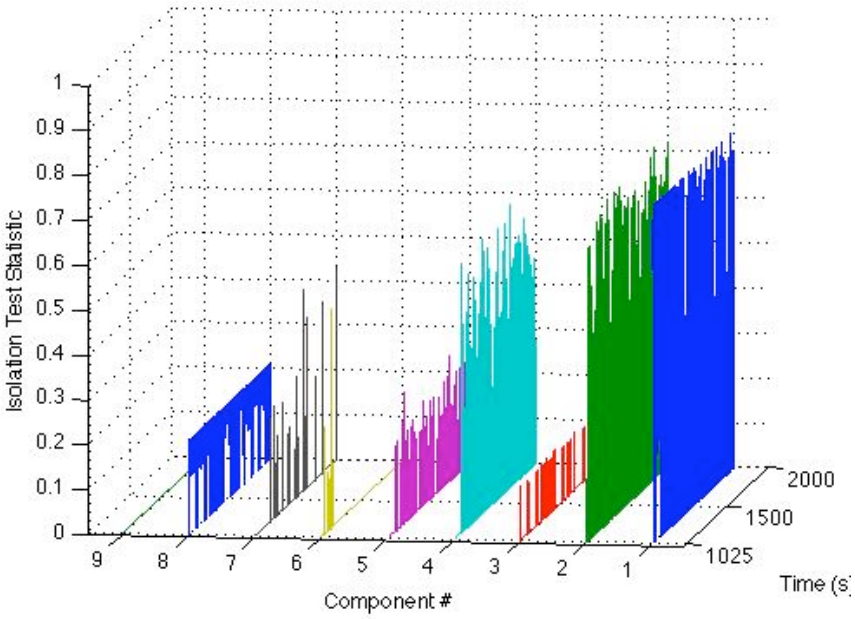

Figure 38. The test statistics for isolation of simultaneous binary degradations in the reheat steam valve, LP bleed taps and piping and HP bleed taps and piping.

These results show that our algorithm performs well in detecting and isolating the degradations introduced by single, binary and triple components if analytical redundancy exists and if the degradations in the components are detectable.

4.5. DEGRADATION ESTIMATION

In this section, we test our degradation estimation algorithm for selected single, binary and triple component degradations. We use the reliability database given in Appendix D in this scheme where for each component we consider 2 degradation modes. We started testing the algorithm with single component degradation.

4.5.1. Single Component Degradation

In Section 4.4.1, we considered degradation in the main steam valve (component 3) and tested our degradation detection and isolation algorithm for this case. We simulated the degradation as a 5% step increase in the effective flow area of the main steam valve at t = 1000 s.

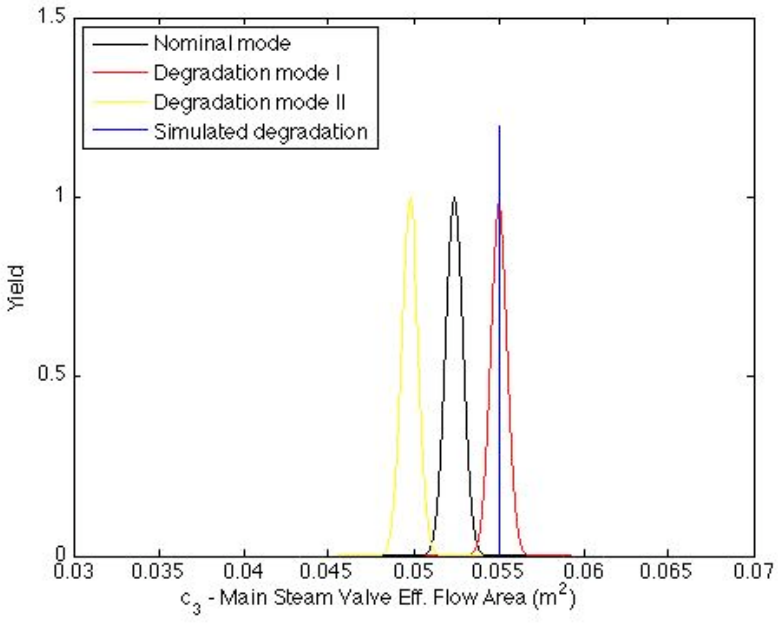

Figure 39. The pdfs for nominal and degradation modes stored in the database, and the simulated degradation of component 3.

This change corresponds to the mean of one of the degradation modes of component 3, that is stored in the reliability degradation database for estimation given in Appendix D, as illustrated in Figure 39.

As shown in the preceding section, after running our algorithms we detected the degradation at 1010 seconds, just 10 seconds after it actually occurred, and we isolated components 3 and 9 as the probable degraded ones. In our new estimation algorithm, we therefore focus on only these two components and construct our proposal densities by using the degradation modes of components 3 and 9 and the nominal modes of the rest of the components. We run our estimation algorithm for 1990 seconds after the detection time. The estimated means of component states 3 and 9 are plotted in Figure 40.

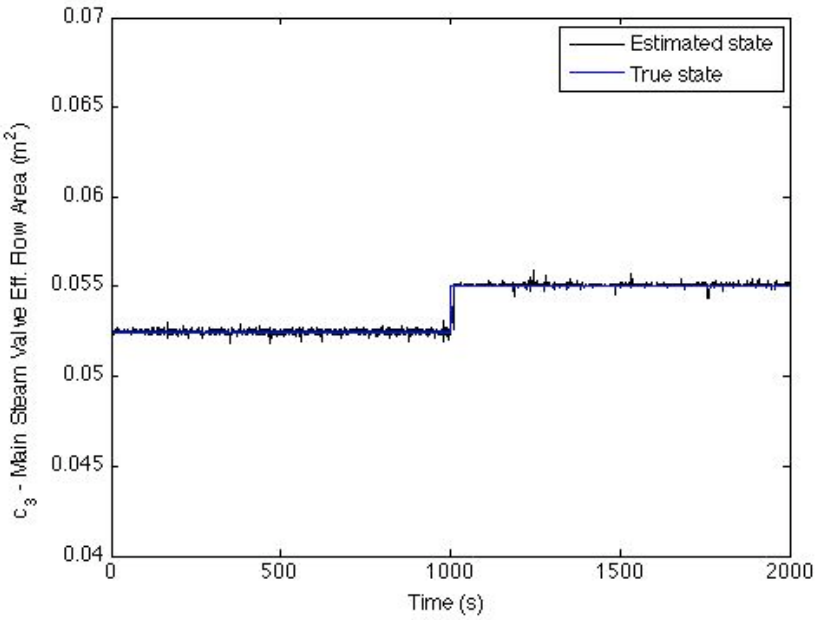

(a) The true and estimated effective flow area for the main steam valve.

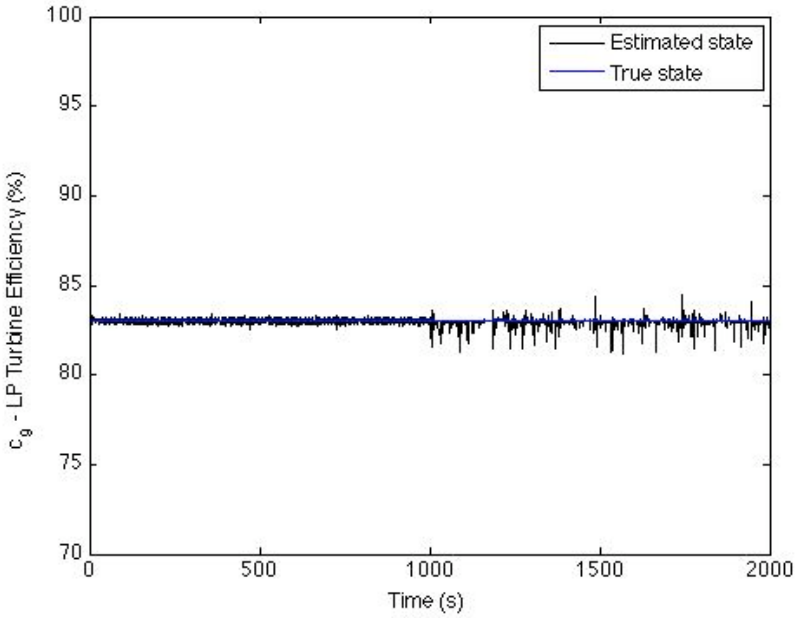

(b) The true and estimated LP turbine efficiency.

Figure 40. The estimated means of the isolated component states 3 and 9.

As stated in 3.3.2.1, the occurrence probabilities of component *j* and degradation mode *d*, $(\omega)_{j,d}$ in the database are used only at the time of the detection. After that they are set as variables proportional to the relative likelihoods of the hypotheses in the adaptation scheme. Monitoring these probabilities help us to distinguish the correct degradation mode among all the modes. In Figure 41, the evolution of occurrence probabilities of the degradation modes of component 3 is given.

Degradation mode I, which corresponds to the correct degradation mode, consistently generates the highest number of particles that are accepted through the MH algorithm. We also expect some particles generated by the nominal mode to be accepted because of the overlapping support regions. Due to modeling and measurement noise particles generated by the proposal densities of degradation mode 2 is also observed to be accepted, but the acceptance ratio is very low.

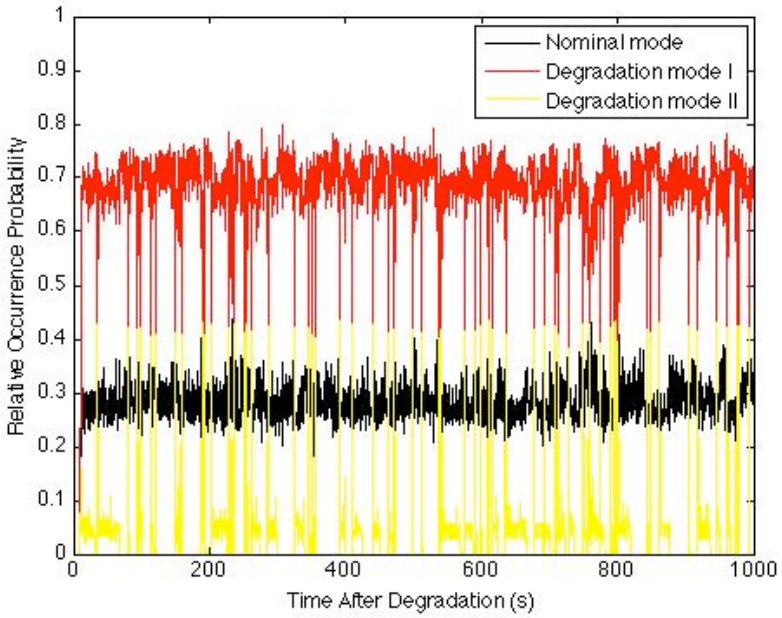

Figure 41. The evolution of occurrence probabilities of the degradation modes of component 3.

As seen in Figure 40(a) and (b), our algorithm estimates the true degradation for component 3 along with no degradation in component 9, promptly. In this estimate we used a database that has the correct degradation mode. This is indeed the main idea behind introducing a reliability degradation database in our calculations; helping the filter explore the most probable regions of interest and quickly converge to the true component state. But sometimes components degrade randomly or there is not any degradation reported on this new degradation mode, so that the database might not contain any information about some new degradation.

In order to explore the effect of not having the simulated degradation mode in the database or having the simulated degradation mode lying in the very low probability regions of the other modes in the database, we prepared two different databases. For both cases, we simulated the degradation as a 5% step increase in the effective flow area of the main steam valve at t = 1000 s. The first database is constructed by changing the characteristics of one of the degradation modes of component 3 in the original database.

This mode is moved such that the simulated degradation is located between the nominal mode and this mode as illustrated in Figure 42.

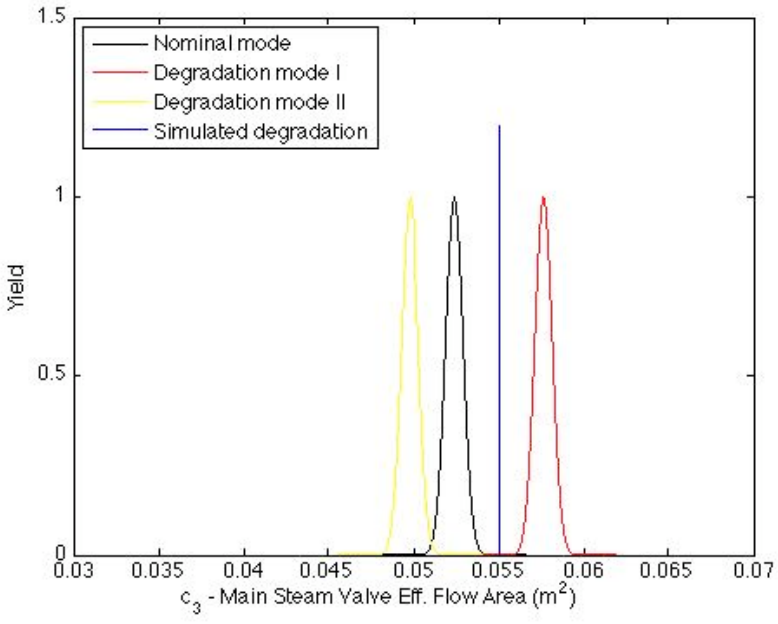

Figure 42. The pdfs of the nominal and degradation modes stored in the updated database 1, and the simulated degradation of component 3.

This change in the characteristics of one of the degradation modes in the database leaves the simulated degradation in a very low probability region. We ran our estimation algorithm with this updated database and plotted the estimated means of component state 3 in Figure 43. Note that we did not plot the component state 9 estimates, because the change in its estimates is not noticeable for this database update.

Even though the correct degradation is located in a very low probability region, our algorithm successfully estimates the amount of degradation. This shows the strength of combining a particle filter with a database. Both of them are working together to get the best estimate. The evolution of occurrence probabilities of the degradation modes of component 3 is given in Figure 44.

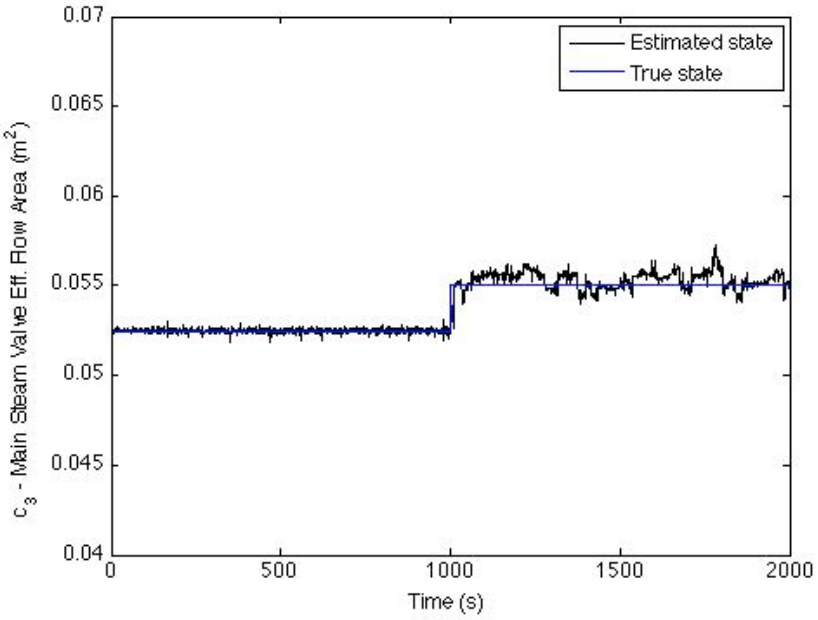

Figure 43. The estimated means of component state 3 by using the updated database 1.

For this case, it is hard to decide which mode is in effect, because the simulated degradation is located between the means of the nominal and one of the degradation modes. By considering the particle filter itself suffers from the sample impoverishment problem, we believe that its estimates of component 3 are based on the nominal state and the variance of the estimates are smaller than the variance of the nominal mode in the database. Consequently, this will increase the number of particles accepted from the degradation database, because some of the particles generated from the nominal mode of the database are no better in reproducing the measurements than the particles coming from the particle filter. Therefore in Figure 44, we observe that the occurrence probability of degradation mode I is higher than that of the nominal mode, and our algorithm correctly determines the right degradation mode.

The second database is constructed by moving one of the degradation modes such that the simulated degradation is not set in the direction of the expected degradations as illustrated in Figure 45.

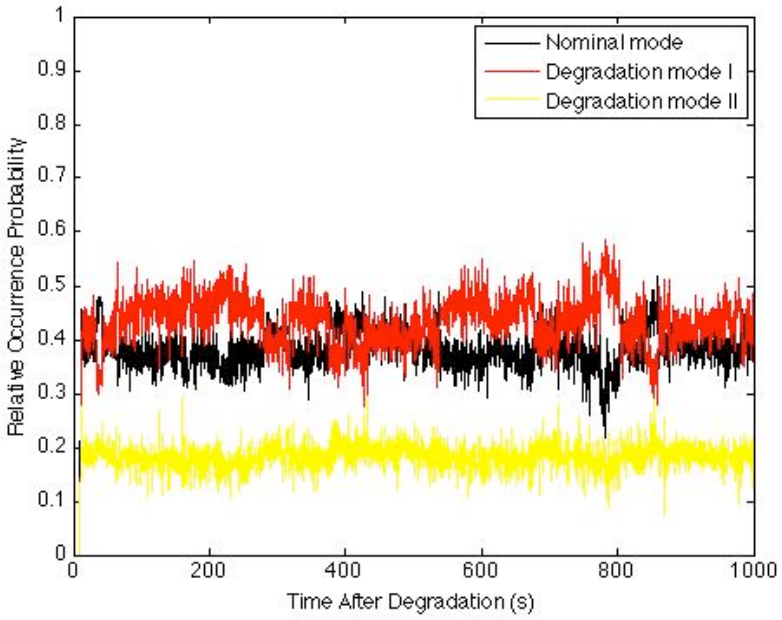

Figure 44. The evolution of occurrence probabilities of the degradation modes of component 3 for the updated database 1.

This change in the characteristics of one of the degradation modes in the database leaves the simulated degradation again in a very low probability region. We ran our estimation algorithm with this updated database and plotted the estimated means of component state 3 in Figure 46.

This case is a very good example showing that even if the degradation modes are not able to represent the true degradations, our algorithm still correctly estimates the amount of degradation. This is due to the inclusion of a nominal mode in the database. The sample impoverishment problem in the particle filtering minimizes the variance of the nominal state estimates. Since the nominal mode with a Gaussian pdf we introduced in the database has a larger variance, this helps the filter to explore the state space better than the particle filtering. As a remark, in general exploring the state space with only one mode that has a very large variance increases computational burden as in the grid based filter, because the efficiency mainly depends on the number of particles generated.

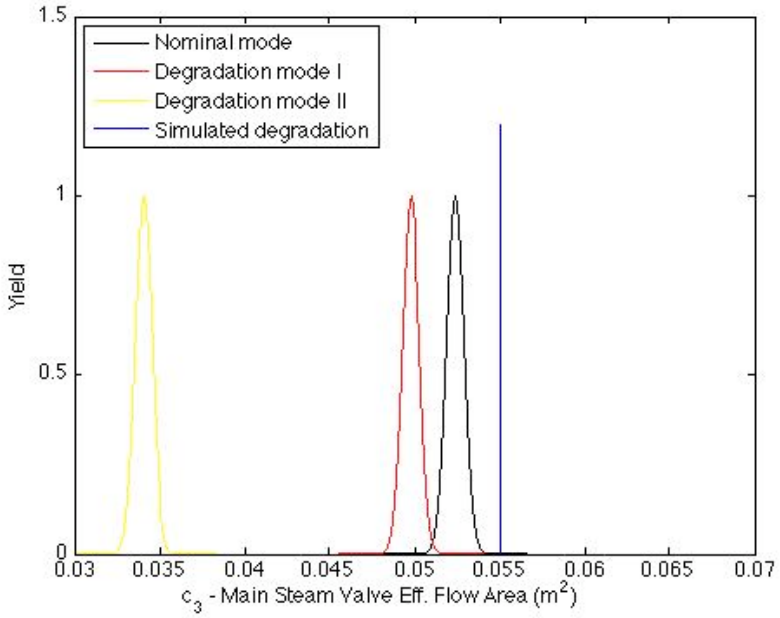

Figure 45. The pdfs of the nominal and degradation modes stored in the updated database 2, and the simulated degradation of component 3.

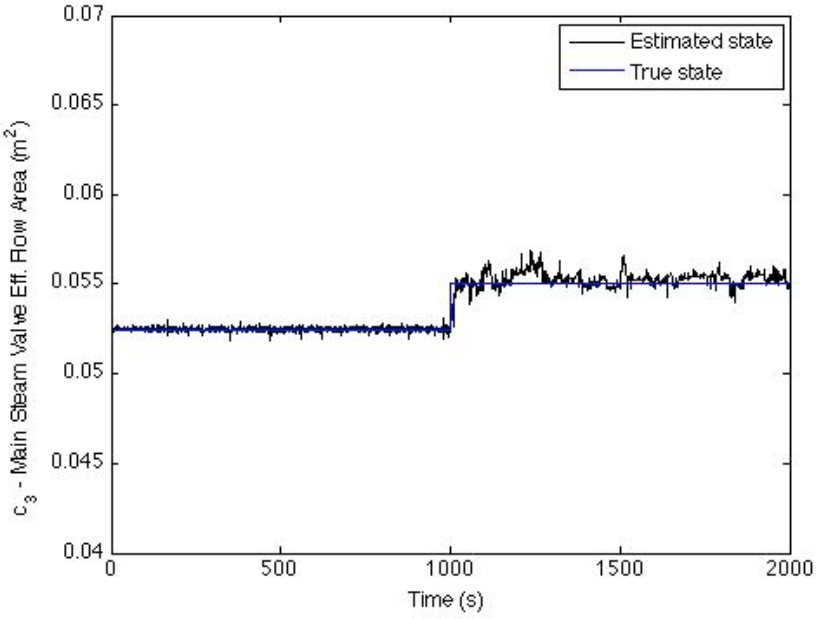

Figure 46. The estimated means of component state 3 by using the updated database 2.

Introducing the degradation modes both reduces the computational time dramatically because of the ability to work with a smaller sample size and helps to identify the correct degradation modes.

By monitoring the occurrence probabilities of the modes, as expected we found that the nominal mode has the highest number of particles accepted. In these cases, since there is not any degradation mode in the direction of the degradation, we cannot use the scheme for identifying the degradation mode. After the estimation of this degradation, one should know that this degradation has not been reported before and should be analyzed further in the real process.

4.5.2. Binary Component Degradations

In Section 4.4.2, we considered simultaneous degradations in components 3 and 8, which are the main steam valve and HP turbine. We simulated the degradations as a 5% step increase in the effective flow area of the main steam valve and a 5% step decrease in the HP turbine efficiency and by observing the tests statistics for degradation detection we decided that the degradation is detected at 1015 seconds, just 15 seconds after the degradation occurs. We also run our degradation isolation algorithm and by monitoring the test statistics we observed that the correct hypotheses, which are constructed with the degradation modes of components 3 and 8, are statistically significant. We run our estimation algorithm for 1985 seconds after the detection time. The estimated means of component states 3 and 8 are plotted in Figure 47.

In this simultaneous binary component degradation case, our algorithm successfully estimates the true degradations of components 3 and 8. The database for estimation given in Appendix D, which contains the true degradation modes, is used in this test case.

In order to distinguish the correct degradations for both of the components, we monitored the occurrence probabilities. In Figure 48 the degradation modes of components 3 and 8 are given.

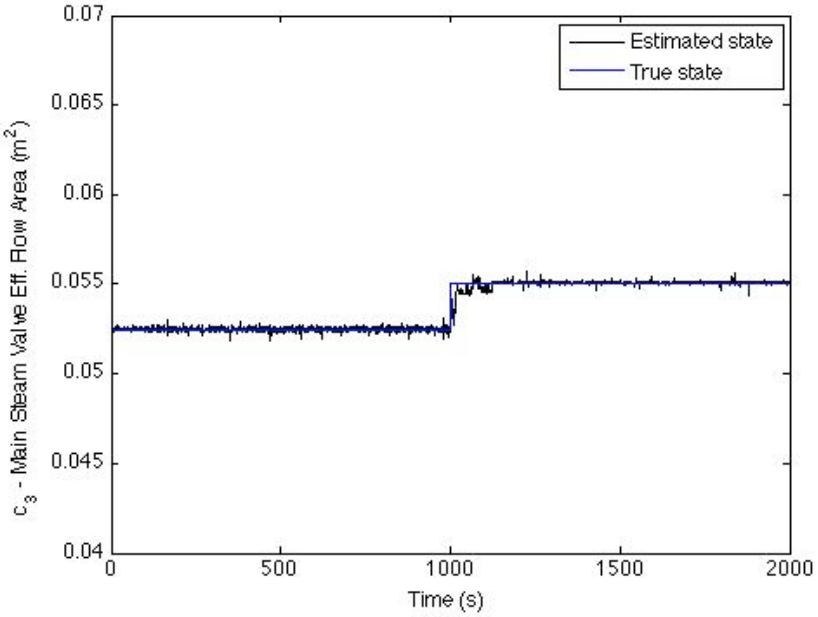

(a) The true and estimated effective flow area for the main steam valve.

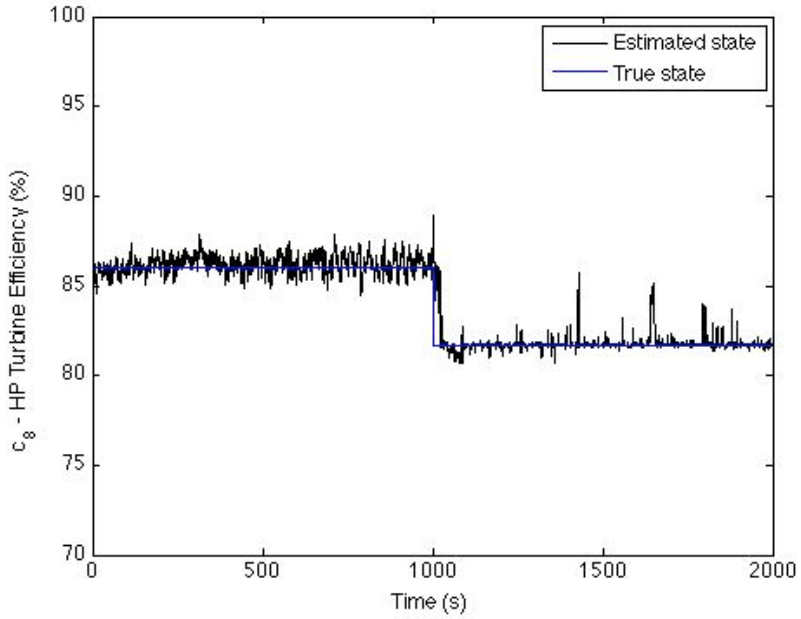

(b) The true and estimated HP turbine efficiency.

Figure 47. The estimated means of the isolated component states 3 and 8.

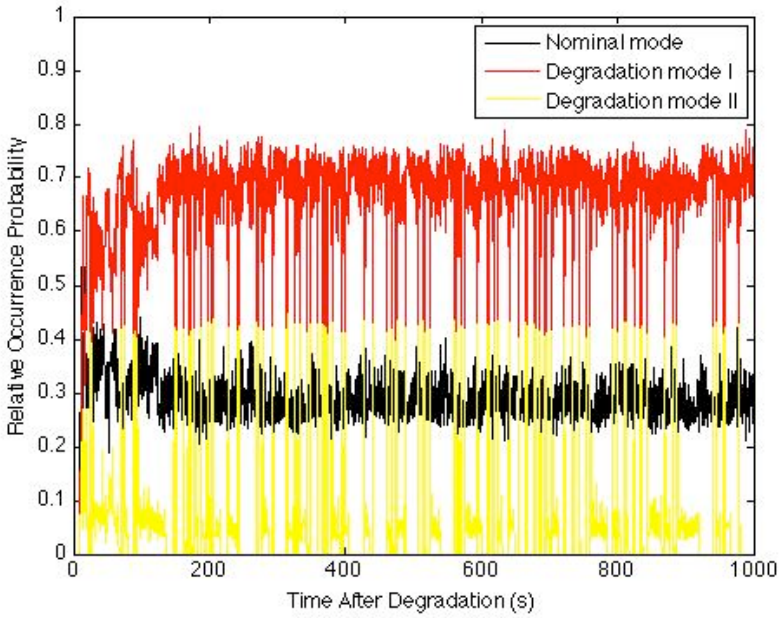

(a) Computed occurrence probabilities of the degradation modes of component 3.

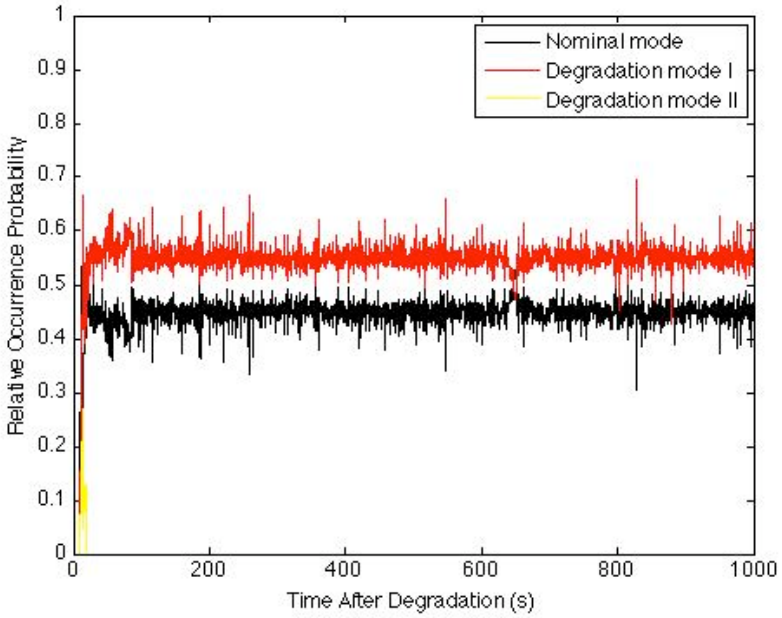

(b) Computed occurrence probabilities of the degradation modes of component 8.

Figure 48. The evolution of occurrence probabilities of the degradation modes of components 3 and 8.

In both component degradations, mode I is the correct degradation mode and consistently generates the highest number of particles that are accepted through the MH algorithm. As mentioned before, for component 3 some particles generated by the nominal mode also get accepted because of the overlapping support regions. Due to the modeling and measurement noises, particles generated by the proposal densities of degradation mode II are also observed to be accepted, but the acceptance ratio is very low. For component 8, the distinction between the modes is more notable and after some time the degradation mode II does not contribute to the number of particles accepted. This is mainly due to the sensitivity of the measurements for this change in the component state 8. In this binary case our degradation estimation algorithm not only estimates the correct amount of degradations but also identifies the correct degradation modes.

4.5.3. Triple Component Degradations

For simultaneous triple degradations we use the same case from Section 4.4.3. We assumed simultaneous degradations in components 1, 2 and 4, which are the HP bleed taps and piping, LP bleed tap and piping and reheat steam valve. We simulated the degradations as a 5% step decrease in the HP steam bleed, a 5% step decrease in the LP steam bleed and a 10% step increase in the effective flow area of the reheat steam valve occurring at t = 1000 s. By observing the test statistics of our degradation detection algorithm, we concluded that the degradation occurred at 1025 seconds, 25 seconds after the degradation occurs. Also, our degradation isolation algorithm showed that components 1, 2, 3, 4, 5 and 8 are statistically significant.

We set up our degradation estimation algorithm based on the hypotheses of components 1, 2, 3, 4, 5 and 8 and set the rest of the component states to their nominal values. We run our estimation algorithm for 1975 seconds after the detection time. The estimated means of component states 1, 2, 3, 4, 5 and 8 are plotted in Figure 49.

As seen in Figure 49(a), (b) and (d), our algorithm is able to estimate the change in the component states. Even though the estimated component states are noisy, the trends of

the estimates are indicating the correct amount of degradation. Also, our algorithm identifies that the components 3,5 and 8 are not degraded as shown in Figure 49(c), (e) and (f).

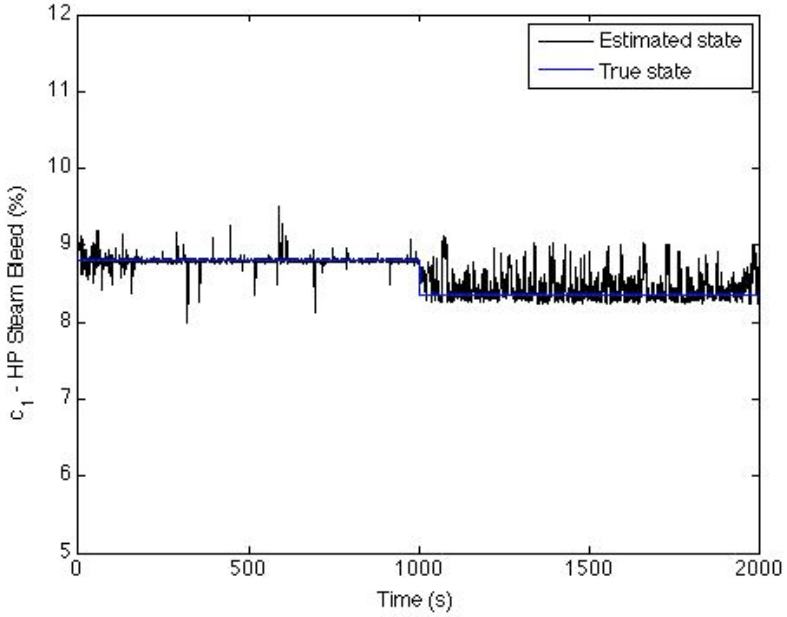

(a) The true and estimated HP steam bleed.

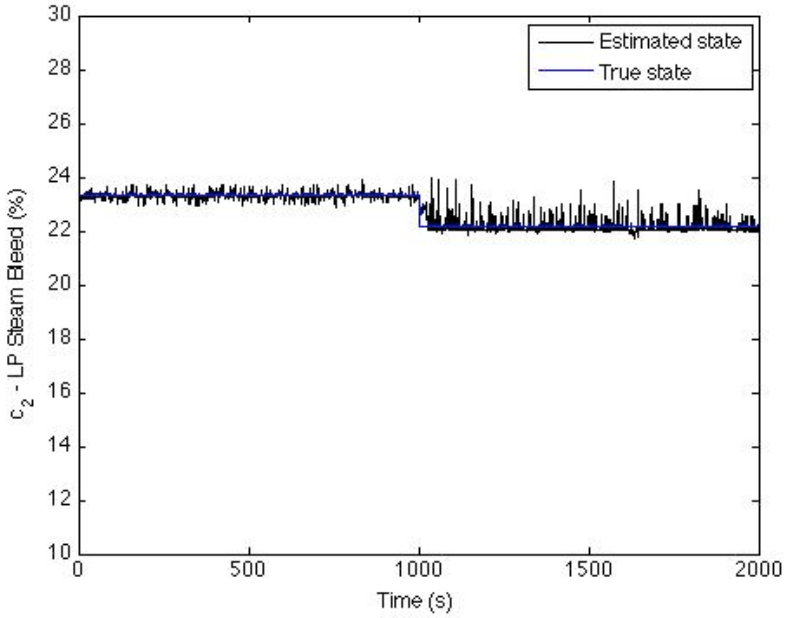

(b) The true and estimated LP steam bleed.

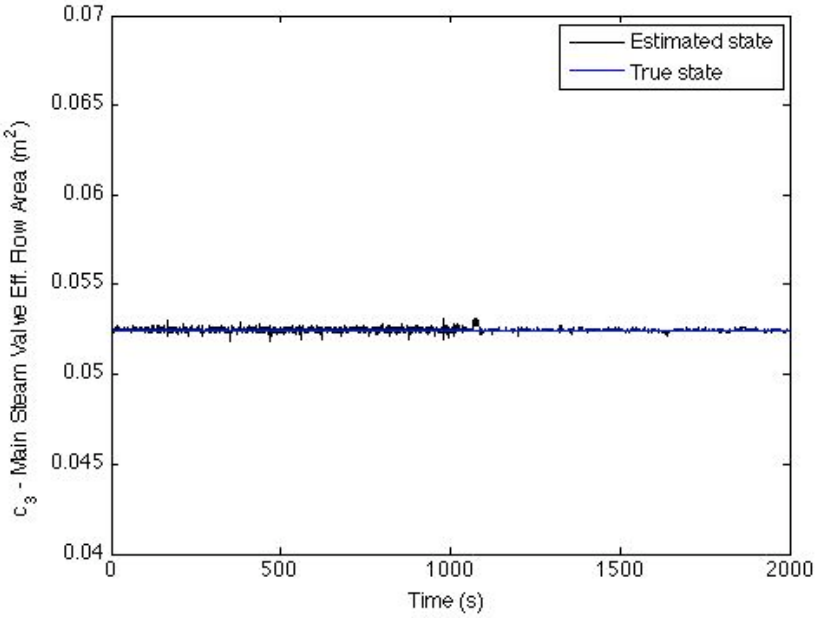

(c) The true and estimated effective flow area for the main steam valve.

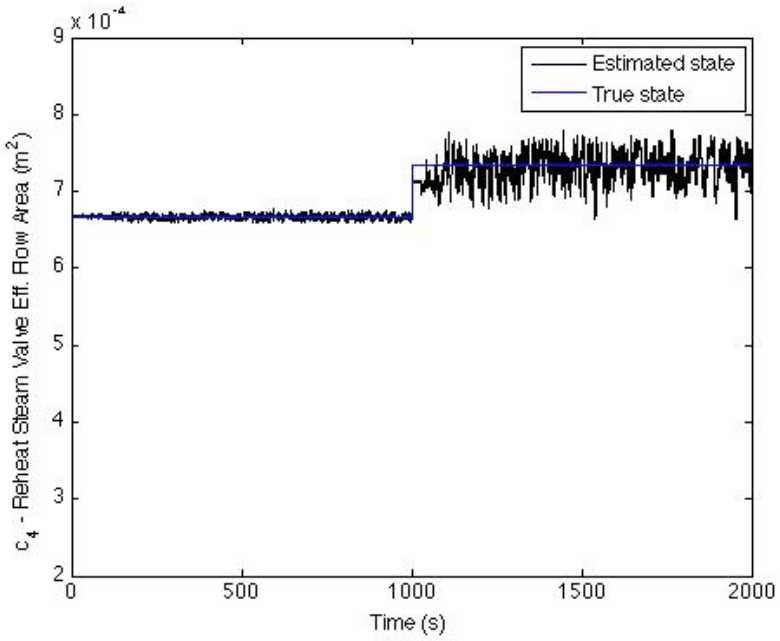

(d) The true and estimated effective flow area for the reheat steam valve.

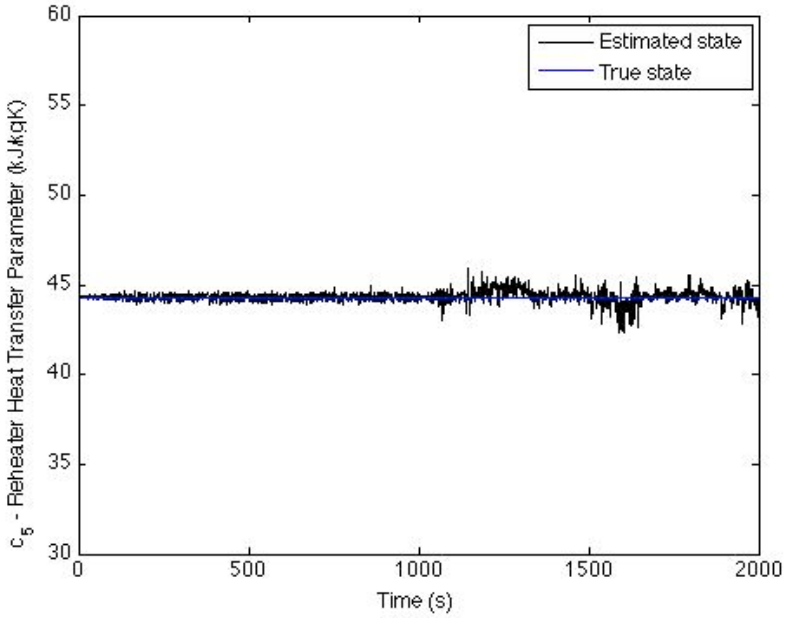

(e) The true and estimated heat transfer parameter of reheater.

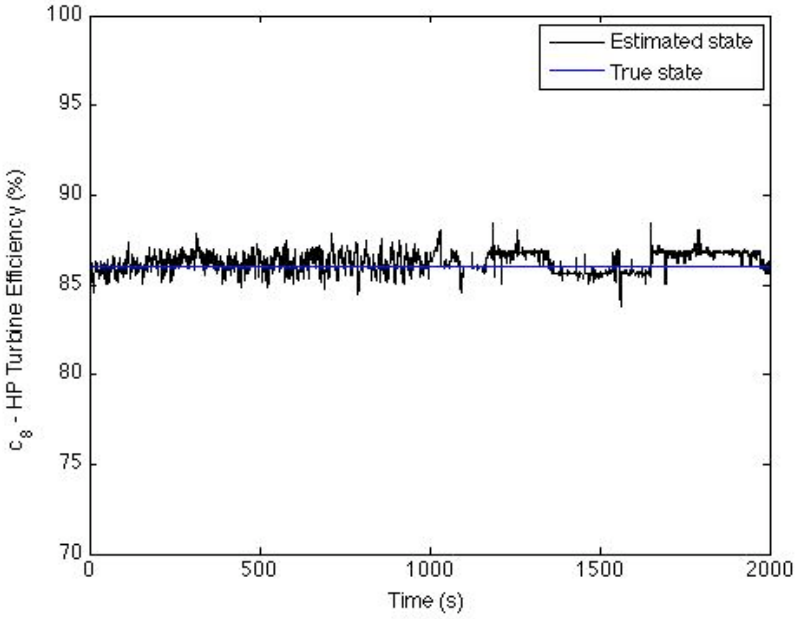

(f) The true and estimated HP turbine efficiency.

Figure 49. The estimated means of the isolated component states 1, 2, 3, 4, 5 and 8.

We also monitored the relative occurrence probabilities of each degradation mode for components 1,2 and 4. The evolution of the occurrence probabilities is given in Figure 50.

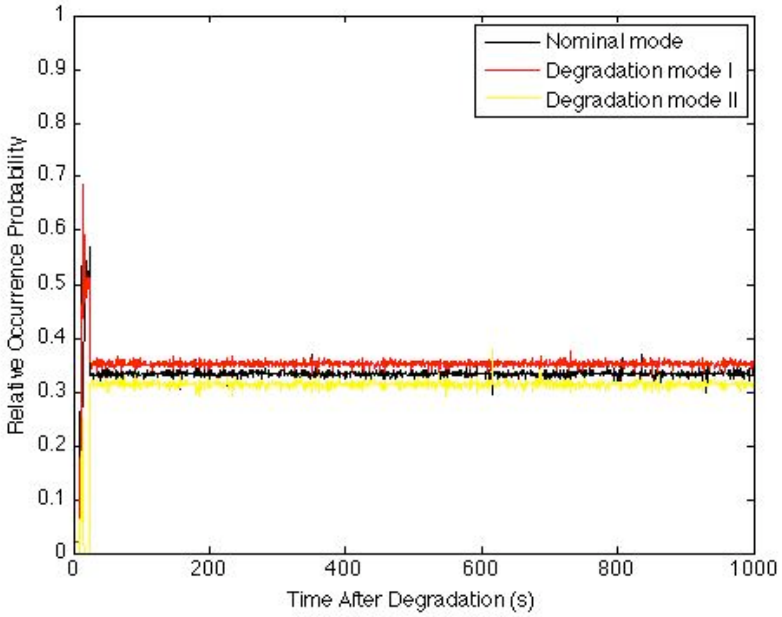

(a) Computed occurrence probabilities of the degradation modes of component 1.

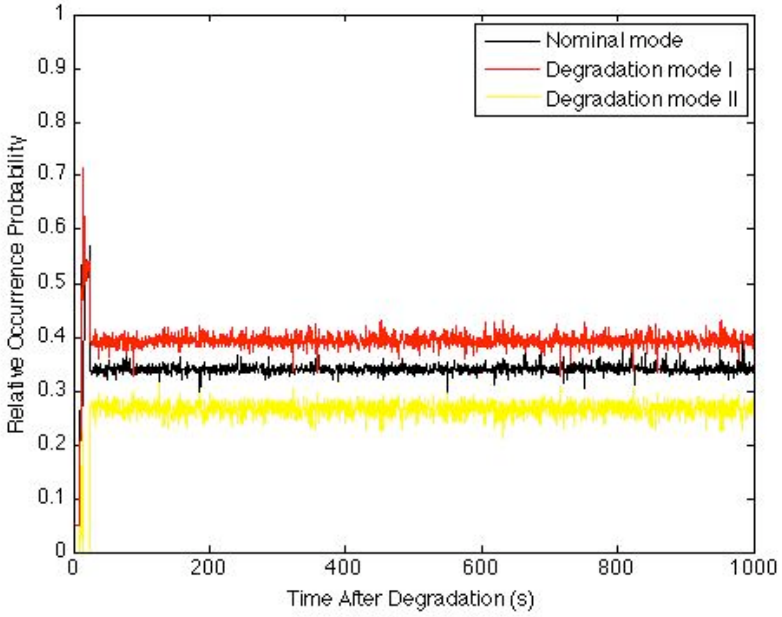

(b) Computed occurrence probabilities of the degradation modes of component 2.

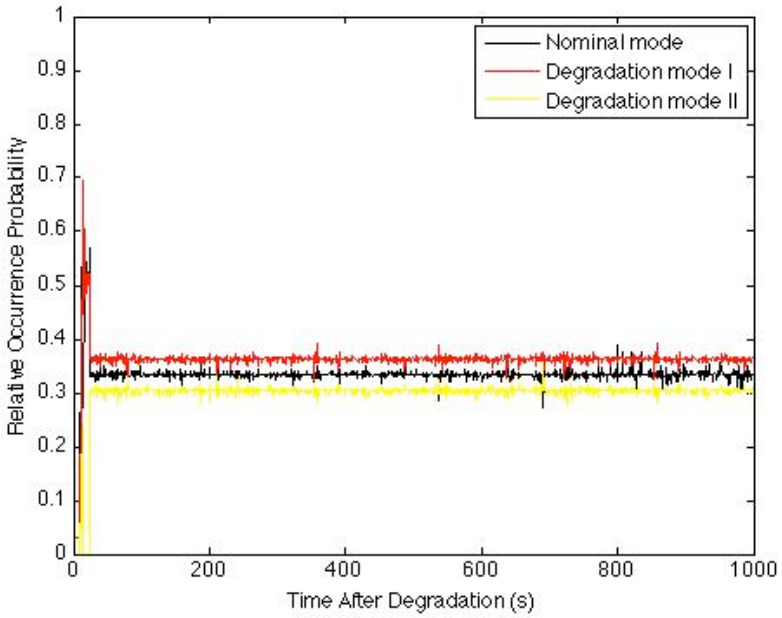

(c) Computed occurrence probabilities of the degradation modes of component 4.

Figure 50. The evolution of occurrence probabilities of the degradation modes of components 1, 2 and 4.

For all of the component degradations, mode I is the correct degradation mode and it generates the highest number of particles that are accepted through the MH algorithm. Besides the overlapping of the support regions of pdfs for different degradation modes and noises in the system, we differentiated one more effect, which is the sample size. For small sample sizes, it may be hard for a sampling algorithm to generate particles that cover the support of the real pdf. This may result in closer occurrence probabilities for each mode and makes it hard to distinguish the real degradation mode. Increasing the sample size helps to solve this problem.

It is hard to identify small component degradations, because their effects on the observations may not be noticeable. It is also hard to monitor simultaneous multiple degradations because the counter effects of the degradations in multiple components may mask each other's effect. As shown in this chapter, our degradation monitoring algorithm is able to detect, isolate and estimate both single and simultaneous multiple degradations.

CHAPTER 5
CONCLUSIONS

In this dissertation we constructed a degradation monitoring framework in which we used a novel multiple hypothesis testing algorithm based on the Metropolis Hastings method by incorporating a reliability degradation database. This algorithm was proposed to address the inability of a filter to respond to an abrupt change, ill-posedness of a filter for high dimensional systems and the poor performance of a filter for low fidelity models.

In Chapter 1, the necessity of having a degradation monitoring system in a nuclear power plant was outlined and the challenges for developing a robust and efficient degradation monitoring system capable of detecting and identifying multiple component degradations were discussed. We set our objectives as:

- To construct a unified framework for degradation monitoring based on sequential probabilistic inference for high dimensional and nonlinear systems
- To utilize a reliability degradation database within sequential probabilistic inference to:
    - Improve estimation of nominal states for low fidelity system models
    - Design a robust degradation detection and isolation scheme
    - Develop techniques to improve the performance of a filter when it cannot follow an abrupt change due to obliviousness or sample impoverishment
- To develop practical algorithms that work online, in particular by developing a method that can work with relatively few particle

- To test these algorithms for monitoring simultaneous multicomponent degradations.

With this set of objectives, in Chapter 2 we reviewed the available techniques in order to construct a unified degradation monitoring framework. We concentrated on model-based methods, which utilize the process measurements with the model of the monitored plant. We utilized nonlinear filtering techniques based on state/parameter estimation to develop a framework based on sequential probabilistic inference, which is the problem of estimating the hidden variables of a system in an optimal and consistent fashion given noisy or incomplete observations. We employed a hidden Markov model structure where the states are unobservable and derived the recursive Bayesian estimation formulation in order to estimate the marginalized posterior density of the states given the measurement history. We reviewed various approximate methods to find a tractable solution for the sequential probabilistic inference problem in high dimensional nonlinear systems. We addressed the problem of treating nonlinearity in transforming a probability density function and derived the nonlinear extensions of Kalman filtering and particle filtering, and discussed their approximations for dealing with the nonlinearities in the system model. We presented an application of degradation monitoring in which we detected and diagnosed fouling in steam generators of the IRIS reactor using unscented Kalman filtering.

In Chapter 3, we addressed an important problem with the nonlinear filtering techniques, which is the inability of a filter to respond to an abrupt change. This prevents their use as "black boxes" for any application. This problem is known as the oblivious filter problem in nonlinear extensions of Kalman filtering, and the sample impoverishment problem in particle filtering. We proposed an algorithm based on covariance matching in extended Kalman filtering and applied this algorithm for the diagnosis of degradations of multiple components. We tested our algorithm with a balance of plant model of a boiling water reactor. We also proposed another algorithm to combine an unscented Kalman filtering algorithm with a reliability degradation database by solving a multiobjective optimization

problem. We presented an application of this scheme in degradation monitoring of a fast reactor.

By addressing the approximations of the nonlinear extensions of Kalman filtering and the proposed algorithms, we focused on particle filtering. We discussed the sample impoverishment problem in particle filtering and its negative effect on detection and diagnosis of component degradations. After reviewing different techniques to address this problem, we proposed a novel technique based on multiple hypothesis testing. This technique helped the filter explore the state space more effectively in order to estimate the degradations in the system by introducing another data source, which is a reliability degradation database. The Metropolis Hastings algorithm was utilized in the selection of the "important" regions of the state space to be explored based on the consistency of the real and the expected measurements. We also extended this algorithm for detection and isolation of the degradations to complete the construction of the degradation monitoring framework.

In Chapter 4, we tested our new algorithm with a balance of plant model of a boiling water reactor. We applied both the degradation detection and isolation algorithm, and the degradation estimation algorithm to test problems with single degradations and simultaneous binary and triple degradations in this nuclear power plant system to evaluate the performance of these algorithms. For example, we studied a binary degradation where degradations in the main steam valve and high pressure turbine are assumed to take place at the same time. By monitoring the test statistics (Eqs. (3.57) and (3.59)) of our degradation detection algorithm, we detected the degradation just 15 seconds after it actually occurred, as shown in Figure 33. Our degradation isolation algorithm (Eqs. (3.63) – (3.66)) identified two components, which are indeed the real degraded components, and so reduced the number of probable component degradations dramatically. By using 2 components with 1 nominal and 2 degradation modes each, we constructed 4 hypotheses based on single component degradations (Eq. (3.41)) and 4 hypotheses based on binary component degradations (Eq. (3.42)). In our degradation estimation algorithm after drawing particles from the proposal densities of each

hypothesis, we used the MH algorithm (Eq. (3.43)) to test these particles with those estimated through a particle filtering algorithm based on their capability of reproducing the measurements. This scheme helped us determine the marginalized posterior density that represents the true evolution of the states by which we calculated the expectations of the estimates as shown in Figure 47. By monitoring the relative likelihoods of each hypothesis based on their contributions to the marginalized posterior density (Eq. (3.45)) as presented in Figure 48, we also identified the correct degradation modes that caused this binary degradation.

The performance of the new algorithm was shown to be quite satisfactory for detecting, isolating and estimating abrupt and incipient degradations, and single and simultaneous multi-component degradations. In addition, this algorithm successfully isolates the correct degradation mode by which the component degrades.

In summary,

- We developed techniques to modify filtering algorithms in order to utilize additional data sources in detection and estimation of degradations
- We constructed a degradation monitoring framework in which we use a novel multiple hypothesis testing algorithm based on the Metropolis Hastings method while utilizing a reliability degradation database:
    - To solve the sample impoverishment problem in the particle filtering
    - To improve the performance of particle filtering for small sample size and for low fidelity models
    - To construct a degradation detection and isolation algorithm
    - To construct a degradation estimation algorithm:
        - To estimate the magnitude of the degradations
        - To isolate degradation modes.

The algorithms presented were shown to be very effective for monitoring of multiple component degradations. However, there remain several areas that could be given additional attention:

- **Real time computing:** Based on our results for the balance of plant model, processing 1 second takes approximately 25 seconds on a single 3MHz cpu with 1GB RAM. This is almost the same for both the degradation detection and isolation, and degradation estimation algorithms. In order to obtain real time computing, we need to decrease the computing time at least by a factor of 25. The following approaches should be studied for the real time implementation of the algorithm.
    - Parallelization: Similar to other Monte Carlo methods, particle filtering algorithms are parallelizable. In the adaptation part of our algorithm, we gather the information of accepted particles in order to calculate the new distribution of particles. Therefore, the effect of the adaptation part on parallelization should be studied. If we assume a 100% parallelization, then we need 25 cpus for 1000 particles and 250 cpus for 10000 particles to run our algorithm for this application in real time. These are certainly achievable numbers as part of a nuclear power plant degradation system.
    - Using deterministic sampling techniques: As we reviewed in Section 2.4.3, we can find a set of points to approximate certain moments of a pdf. For standard and unimodal pdfs, one may use deterministic sampling to reduce the sample size, with a corresponding reduction of the computing time.
- **Introducing environmental effects to improve the performance of the technique:** The adaptation scheme that we proposed in Subsection 3.3.2.1 also can be used to introduce environmental effects into the hypothesis testing algorithm. If we believe that a change in the environmental variables, which we can detect by a measurement or an estimate of a system state through our algorithm, triggers degradation, then we can update our adaptation algorithm according to this effect. Suppose that a particular change in a system state triggers

the degradation of a specific component e.g., decreased steam quality may increase the likelihood of reduced bleed flow due to plugging of the taps. After estimating the change in the system state through the algorithm, one may update the relative likelihood of that hypothesis with a correction factor that represents the cascade effect.

- **Introduction of degradation monitoring in probabilistic risk assessment (PRA):** The static safety profile of a nuclear power plant based on failures in a system can be derived from a probabilistic risk assessment application. By updating the base PRA of a plant to reflect the changes in the parameters and the environment introduced by the degradations in the components, the instantaneous and average risk can be quantified in real time. In addition, by employing prognostics models for the degradations, risk predictions in the future can be carried out. Living PRA and risk monitoring techniques are based on determining the risk associated with the expected unavailability of systems and components. Degradations in the system can affect both the PRA model structure and model parameters. By using our algorithm to estimate the degradations in the components, with some modifications within the living PRA or risk monitoring techniques, a more informative safety profile of the plant can be obtained in real time.
- **Lack or quality of a reliability degradation database:** The performance of the proposed algorithms depends on the quality of the component reliability data. It is important to emphasize that the data extracted from past operational experience have value only to the extent that the conditions under which the data were generated remain applicable. Therefore having a plant specific reliability database is essential. If no reliability data exists, then the only choice is to generate probability density functions of degradation modes based on a grid representation.
- **Application of this technique to different areas:** The idea of introducing a data source into particle filtering may help in solving problems in other disciplines. One possible application is in music analysis and transcription. For single instruments playing one note at a time, music transcription is an easy task. But,

for the cases of many notes playing simultaneously, it is hard to detect which instruments are playing, what their pitches are, etc. By using a harmonic modeling approach and constructing a database to represent the characteristics of the instruments, one may use our proposed technique in music transcription.

Although there remains additional challenges as stated above, we met our objectives in this dissertation.

APPENDICES

APPENDIX A
PROPERTIES OF THE GAUSSIAN DISTRIBUTION

Definition: If $X \in \mathbb{R}^{n_x}$ is a random vector and has multivariate Gaussian distribution with mean $\bar{x}$ and the covariance P, the probability density function is

$$N(x;\bar{x},P) = \frac{1}{\sqrt{(2\pi)^{n_x}|P|}} \exp\left(-\frac{1}{2}(x-\bar{x})^T P^{-1}(x-\bar{x})\right). \tag{A.1}$$

Lemma A.1: (Joint density of Gaussian variables) If random vectors $X \in \mathbb{R}^{n_x}$ and $Y \in \mathbb{R}^{n_y}$ have the Gaussian pdfs

$$(X = x) \sim N(x;\bar{x},P) \tag{A.2}$$

$$(Y = y \mid X = x) \sim N(y;Hx,R) \tag{A.3}$$

then, the joint density of X and Y and the marginal distribution of Y are [27]

$$(X = x, Y = y) \sim N\left(\begin{bmatrix} \bar{x} \\ H\bar{x} \end{bmatrix}, \begin{bmatrix} P & PH^T \\ HP & HPH^T + R \end{bmatrix}\right) \tag{A.4}$$

$$(Y = y) \sim N(H\bar{x}, HPH^T + R) \tag{A.5}$$

Lemma A.2: (Conditional density of Gaussian variables) If random vectors $Z_1 \in \mathbb{R}^{n_{z1}}$ and $Z_2 \in \mathbb{R}^{n_{z2}}$ have the joint pdf,

$$\left(Z_1 = z_1, Z_2 = z_2\right) \sim N\left(\begin{bmatrix} a \\ b \end{bmatrix}, \begin{bmatrix} A & C \\ C^T & B \end{bmatrix}\right) \tag{A.6}$$

then the marginal and conditional densities of Z_1 and Z_2 are [27]

$$\left(Z_1 = z_1\right) \sim N\left(z_1; a, A\right) \tag{A.7}$$

$$\left(Z_2 = z_2\right) \sim N\left(z_2; b, B\right) \tag{A.8}$$

$$\left(Z_1 = z_1 \mid Z_2 = z_2\right) \sim N\left(z_1; a + CB^{-1}\left(z_2 - b\right), A - CB^{-1}C^T\right) \tag{A.9}$$

$$\left(Z_2 = z_2 \mid Z_1 = z_1\right) \sim N\left(z_2; b + C^T A^{-1}\left(z_1 - a\right), B - C^T A^{-1}C\right) \tag{A.10}$$

Lemma A.3: (Matrix inverse). If $A = B^{-1} + CD^{-1}C^T$, then the inverse of matrix A is [27]

$$A^{-1} = B - BC\left(D + C^T BC\right)^{-1} C^T B. \tag{A.11}$$

APPENDIX B

DERIVATION OF THE KALMAN FILTER IN THE BAYESIAN FRAMEWORK

We followed the work of Sarkka [27] and Chen [24] in this derivation. In order to obtain the marginal distribution of x_k, $p(x_k \mid Y_{k-1})$, we first calculate the joint distribution of x_k and x_{k-1} given the measurement history up to time *k-1*, $p(x_k, x_{k-1} \mid Y_{k-1})$ by using Lemma A.1

$$\begin{aligned} p(x_k, x_{k-1} \mid Y_{k-1}) &= p(x_k \mid x_{k-1}) p(x_{k-1} \mid Y_{k-1}) \\ &= N(x_k; F_{k,k-1}\hat{x}_{k-1}, Q_k) N(x_{k-1}; \hat{x}_{k-1}, P_{k-1}) \\ &= N\left(\begin{bmatrix} x_{k-1} \\ x_k \end{bmatrix}; \begin{bmatrix} \hat{x}_{k-1} \\ F_{k,k-1}\hat{x}_{k-1} \end{bmatrix} \begin{bmatrix} P_{k-1} & P_{k-1}F_{k,k-1}^T \\ F_{k,k-1}P_{k-1} & F_{k,k-1}P_{k-1}F_{k,k-1}^T + Q_k \end{bmatrix} \right). \end{aligned} \tag{B.1}$$

The marginal distribution of x_k is obtained using Lemma A.2

$$p(x_k \mid Y_{k-1}) = N(x_k; \hat{x}_k^-, P_k^-) \tag{B.2}$$

where $\hat{x}_k^- = F_{k,k-1}\hat{x}_{k-1}$ and $P_k^- = F_{k,k-1}P_{k-1}F_{k,k-1}^T + Q_k$.

Next, we wish to calculate $\hat{x}_k$ and P_k using Eq. (2.10). We write

$$p(x_k \mid Y_k) = \frac{N(y_k; H_k x_k, R_k) N(x_k; \hat{x}_k^-, P_k^-)}{p(y_k \mid Y_{k-1})}. \tag{B.3}$$

Since multiplication of two Gaussians is again a Gaussian and the denominator is a normalizing constant, we can write

$$p(x_k \mid Y_k) \propto A \exp\left(-\frac{1}{2}(y_k - H_k x_k)^T R^{-1}(y_k - H_k x_k) - \frac{1}{2}(x_k - \hat{x}_k^-)^T (P_k^-)^{-1}(x_k - \hat{x}_k^-) \right). \quad \text{(B.4)}$$

where A is a constant. For Gaussian posterior densities, the mode and median estimates coincide with the mean. Then, for example the MAP estimate of the state is

$$\left. \frac{\partial \log p(x_k \mid Y_k)}{\partial x_k} \right|_{x_k = \hat{x}_k} = 0. \quad \text{(B.5)}$$

Applying Eq. (B.5) in Eq. (B.4) yields

$$\hat{x}_k = \left(H_k^T R^{-1} H_k + (P_k^-)^{-1} \right)^{-1} \left(P_k^- \hat{x}_k^- + H_k^T R^{-1} y_k \right). \quad \text{(B.6)}$$

By using Lemma A.3 it is simplified as

$$\hat{x}_k = \hat{x}_k^- + K_k \left(y_k - H_k \hat{x}_k^- \right) \quad \text{(B.7)}$$

where K_k is the Kalman gain defined as

$$K_k = P_k^- H_k^T \left(H_k P_k^- H_k^T + R_k \right)^{-1}. \quad \text{(B.8)}$$

By using Eq. (B.7) and Eq. (2.20), the covariance of the estimate error at time *k,* $P_k = \mathrm{E}\left[(x_k - \hat{x}_k)(x_k - \hat{x}_k)^T \right]$ can be written

$$P_k = P_k^- - K_k S_k K_k^T \quad \text{(B.9)}$$

where $S_k = H_k P_k^- H_k^T + R_k$ is the covariance of the innovation $\xi_k = \left(y_k - H_k \hat{x}_k^- \right)$.

APPENDIX C
SIMULATION MODEL OF THE BALANCE OF PLANT

The simulation model of balance of plant (BOP) is based on the Aumeier's compilation [85] of Shankar's work [60]. The following assumptions are made in this model:

- The relationship between enthalpy, specific volume and pressure (i.e., the equation of state) for the superheated steam follows Callender's empirical relationship [84] for all non-constant pressure processes.
- The flow-pressure drop relation for the high pressure (HP) and low pressure (LP) turbine follows $w = K\sqrt{\Delta(P\upsilon)}$ where $\Delta(P\upsilon)$ is the change in the product of pressure and specific volume from the turbine inlet to the turbine exit and K is a constant.
- Turbine dynamics are represented via simplified time-lag models.
- Turbine efficiencies are assumed constant for all power levels.
- HP turbine bleed flow is tapped after steam expansion and thus the entire flow through the turbine contributes to power production. LP turbine bleed flow is tapped at various points in the steam expansion process resulting in only 50% of bled steam contributing to power production.
- Heat exchange in the reheater is assumed to be perfect and the dynamics of mass balance and energy balance are lumped at a point.
- Heat transfer in HP and LP feedwater heaters (FWH) is directly proportional to the shell side and inversely proportional to the tube side flow.

- Condenser and feedwater pumps are not explicitly modeled. Condenser supplies constant enthalpy feedwater stream. Pump produces constant head.
- Valve coefficients are constant
- System accepts saturated steam at a constant pressure of 6.895 MPa.

With these assumptions the system equations representing the BOP may be derived using the appropriate conservation laws and state relationships.

1. Steam Chest Model

Steam enters the steam chest from the main steam line (via main steam admission valve) where it undergoes a slight expansion before expanding across the HP turbine. We begin with the following equations for conservation of mass and energy:

$$V_c \frac{d}{dt}\rho_c = w_1 - w_2 \tag{D.1}$$

$$V_c \frac{d}{dt}\left(\rho_c h_c\right) = w_1 h_s - w_2 h_c + V_c \frac{dP_c}{dt} \tag{D.2}$$

where

V_c = volume of steam chest (m^3),

ρ_c = density of steam in steam chest (kg/m^3),

P_c = pressure of steam chest (MPa),

w_1 = steam flow rate entering steam chest from main steam admission valve (kg/s),

w_2 = steam flow rate into HP turbine (kg/s),

h_c = enthalpy of steam in steam chest (J/kg),

h_s = enthalpy of steam entering steam chest (J/kg).

If one assumes the density ρ_c is approximately constant, Eq. (D.2) may be written as

$$V_c \rho_c \frac{d}{dt} h_c = w_1 h_s - w_2 h_c + V_c \frac{dP_c}{dt} \tag{D.3}$$

A simplified form of Callender's equation:

$$P_c = \rho_c \left(k_1 h_c - k_2 \right) \tag{D.4}$$

can be differentiated, and if one makes the assumption that $\frac{d}{dt}\rho_c \neq 0$, the result can be inserted into Eq. (D.3) to yield

$$\left(1 - k_1\right)\frac{d}{dt}h_c = \frac{w_1 h_s - w_2 h_c}{V_c \rho_c} + \frac{P_c}{\rho_c^2}\frac{d\rho_c}{dt} \tag{D.5}$$

where k_1 and k_2 are constants from Callender's empirical equation determined for a given nominal operating point.

Shankar's inconsistency in the treatment of $\frac{d}{dt}\rho_c$ introduces little error since for the small, relatively fast transients, this term is typically small. An empirical relationship is used to model the HP turbine and is written as:

$$w_2 = A_{k2}\sqrt{P_c \rho_c - P_r \rho_2} \tag{D.6}$$

where

A_{k2} = constant descriptive of steam expansion in steam chest,

P_r = pressure at HP turbine exhaust (MPa),

ρ_2 = steam density at HP turbine exhaust (kg/m^3).

The density ρ_2 is represented using a homogeneous equilibrium model for a two phase mixture:

$$\rho_2 = \frac{1}{x v_g + \left(1 - x\right) v_f} \tag{D.7}$$

where

v_g = specific volume of saturated vapor at HP turbine exhaust pressure (m^3/kg),

v_f = specific volume of saturated liquid at HP turbine exhaust pressure (m^3/kg),

x = quality of steam exiting HP turbine.

The steam quality is expressed in terms of mixture enthalpy h_2 as:

$$x = \frac{h_2 - h_f}{h_{fg}} \tag{D.8}$$

where

h_f = enthalpy of saturated liquid at HP turbine exhaust pressure (J/kg),

h_{fg} = latent heat of vaporization at HP turbine exhaust pressure (J/kg).

The flow rate of saturated steam through the main steam admission valve is represented using conservation of energy and assuming flow dependence only on the steam pressure before the valve [84]. The steam flow rate through the valve may then be expressed as:

$$w_1 = C_1 A_1 \sqrt{P_s \rho_s} \tag{D.9}$$

where

C_1 = valve coefficient for main steam admission valve,

A_1 = main steam admission valve effective flow area (m^2),

P_s = steam pressure in main steam line (MPa),

ρ_s = steam density in main steam line (kg/m^3).

The equations of state representing the latent heat of vaporization, enthalpy of saturated liquid, and specific volumes are represented by the following linear relationships:

$$h_f = 8.2573 \times 10^5 + 0.44\left(P_r - 1.3788\right) \tag{D.10}$$

$$h_{fg} = 1.961 \times 10^6 - 0.4\left(P_r - 1.3788\right) \tag{D.11}$$

$$v_g = 0.1428 - 0.0166\left(P_r - 1.378\right) \tag{D.12}$$

$$v_f = 0.0011, \tag{D.13}$$

while the enthalpy h_2 of the wet steam exiting the HP turbine is represented using the following empirical relationship:

$$\begin{aligned} h_2 = &\left(2.3822\times10^6 + 0.3\left(P_r - 1.3788\right)\right)\eta \\ &-\left(0.0011 + 0.3\left(P_r - 1.3788\right)^2 - 0.1\left(P_c - 6.894\right)\right)\eta \end{aligned} \tag{D.14}$$

where

η = efficiency of expansion process =0.86.

2. HP Turbine

A simple time lag representation for the conservation of mass and momentum is used to model the steam flow rate through the HP turbine. For a control volume encompassing the HP turbine this yields:

$$\tau_{w2}\frac{d}{dt}w_2'' = w_2 - w_{HPB} - w_2'' \tag{D.15}$$

where

τ_{w2} = representative time constant associated with HP turbine (s),

w_2'' = wet steam flow rate from HP turbine to reheater (kg/s),

w_{HPB} = bleed flow rate from HP turbine to HP FWH (kg/s).

The flow rate of bleed steam is represented as a constant fraction of the total steam flow entering the HP turbine and is written as:

$$w_{HPB} = K_{HPB}w_2 \tag{D.16}$$

where

K_{HPB} = fraction of steam flow through HP turbine bled to HP FWH.

3. Moisture Separator

The moisture separator is considered a static element and can be modeled using conservation of mass for a control volume encompassing the moisture separator, which yields:

$$w_{MS} = w_2 - w_{HPB} - w_2' \tag{D.17}$$

where

w_{MS} = condensed steam flow rate out of moisture separator (kg/s),

w_2' = saturated steam flow rate into reheater (kg/s),

In this representation, the mass flow rate entering the control volume is approximated as static, i.e., $w_2'' = w_2 - w_{HPB}$. The steam flow rate out of the moisture separator is then approximated as the vapor constituent entering the unit, which is represented as

$$w_2' = x w_2'' . \tag{D.18}$$

4. Reheater

For purposes of modeling energy transfer characteristics, the reheater is modeled as a point. We first describe the tube-side properties of the reheater using conservation of mass and energy as

$$V_r \frac{d}{dt} \rho_r = w_2' - w_3 \tag{D.19}$$

$$V_r \frac{d}{dt} \left(\rho_r h_r \right) = Q_r + w_2' h_g - w_3 h_r + V_r \frac{dP_r}{dt} . \tag{D.20}$$

If the same assumption is made regarding $\frac{d}{dt}\rho_r$ as was made with $\frac{d}{dt}\rho_c$, then Eq. (D.20) becomes

$$\left(1-k_1\right)\frac{d}{dt}h_r = \frac{Q_r + w_2' h_g - w_3 h_r}{V_r \rho_r} + \frac{P_r\left(w_2' - w_3\right)}{\rho_r^2 V_r}. \tag{D.21}$$

where

V_r = volume of reheater (m^3),

ρ_r = main steam density exiting heater (kg/m^3),

w_3 = main steam flow rate out of reheater to LP turbine (kg/s),

h_r = main steam enthalpy exiting reheater (J/kg),

h_g = saturated vapor enthalpy exiting reheater (J/kg).

Q_r = rate of energy transfer in reheater (W).

For purposes of calculating the steam flow rate leaving the reheater, the reheater tubes are modeled as a throttling valve, and thus the steam flow rate is represented as

$$w_3 = K_3\sqrt{P_r \rho_r} \tag{D.22}$$

where

K_3 = representative valve coefficient.

The equation of state relating the pressure, density and enthalpy is again represented by Callender's equation

$$P_r = \rho_r\left(k_1 h_r - k_2\right) \tag{D.23}$$

where the linear relationship for the enthalpy of saturated vapor is

$$h_g = 2.7875\times 10^6 + 0.04\left(P_r - 1.3788\right). \tag{D.24}$$

For the shell side of the reheater, we use a simple time lag representation for conservation of mass and momentum:

$$\tau_{r1}\frac{d}{dt}w'_{RS} = w_{RS} - w'_{RS} \tag{D.25}$$

and conservation of energy

$$\tau_{r2}\frac{d}{dt}Q_r = \left(\frac{w_{RS} + w'_{RS}}{2}\right)H_{RS}\left(T_s - T_r\right) - Q_r \tag{D.26}$$

where

τ_{r1} = time constant characteristic of tube side steam flow through reheater (s),

τ_{r2} = time constant characteristic of energy transfer from shell to tube side of reheater (s),

w_{RS} = reheat steam flow rate into shell side of reheater (kg/s),

w'_{RS} = condensed reheat steam flow rate out of shell side of reheater (kg/s),

H_{RS} = reheater heat transfer parameter (J/kg-K),

T_s = reheat steam temperature - shell side of reheater (K),

T_r = main steam temperature - tube side of reheater (K).

The flow rate of reheat steam bled from the main steam line through the reheat steam admission valve is modeled in a fashion analogous to the flow of steam through the main steam admission valve, i.e., through a throttling valve, resulting in:

$$w_{RS} = C_2 A_2 \sqrt{P_s \rho_s} \tag{D.27}$$

where

C_2 = valve coefficient – reheat steam valve,

A_2 = reheat steam valve effective flow area (m^2).

The temperature of the shell side steam is represented via the following empirical relationship:

$$T_s = 557.92 + \frac{0.125\left(P_s - 6.894\right) + 459.67}{1.8} \tag{D.28}$$

while the temperature of the tube side steam is represented using the ideal gas law as

$$T_r = \frac{P_r}{\rho_r R}. \tag{D.29}$$

5. LP Turbine

As with the HP turbine, the LP turbine is modeled with a simple time lag representation of mass and momentum. For a control volume encompassing the HP turbine we then have:

$$\tau_{w3}\frac{d}{dt}w_3' = \left(1 - K_{LPB}\right)w_3 - w_3' \tag{D.30}$$

where

τ_{w3} = time constant characteristic of LP turbine (s),

w_3' = wet steam flow rate exiting LP turbine (s),

K_{LPB} = fraction of steam into LP turbine bled to LP FWH.

The flow rate w_{LPB} of steam bled from the LP turbine to the LP FWH is defined to be a fixed fraction of the total steam flow rate entering the turbine and thus is written as

$$w_{LPB} = K_{LPB}w_3. \tag{D.31}$$

6. LP Feedwater Heater

Heat transfer from the shell side to tube side of the LP FWH is represented using a simple correlational model relating the fluid mass flow rates on each side of the heater and a time lag representation of the dynamics. A constant feedwater flow rate is assumed. Conservation of energy for a control volume surrounding the heater may be written as

$$\tau_{LPH} \frac{d}{dt} h_{LPH} = Q_{LPH} + h_0 - h_{LPH} \tag{D.32}$$

where

τ_{LPH} = time constant characteristic of energy transfer in LP FWH (s),

h_{LPH} = enthalpy of feedwater leaving LP FWH – tube side (J/kg),

h_0 = enthalpy of makeup feedwater from condenser to LP FWH – tube side (J/kg),

Q_{LPH} = energy transferred from shell to tube side in LP FWH (J/kg).

A mass conservation relationship will be written for the HP FWH and thus is not needed here (tube side flow from LP FWH feeds into tube side of HP FWH). The energy transfer in the LP FWH is assumed directly proportional to the shell side flow and inversely proportional to the tube side flow and may thus be written as:

$$Q_{LPH} = H_{LPH} \frac{w_{HPH} + w_{LPB}}{w_{FW}}. \tag{D.33}$$

where

H_{LPH} = heat transfer parameter of LP FWH (J/kgK),

w_{HPH} = feedwater flow rate from shell side of HP FWH to shell side LP FWH (kg/s),

w_{FW} = makeup feedwater flow rate from condenser to LP FWH – tube side (kg/s).

7. HP Feedwater Heater

The equations describing the HP FWH are derived in a fashion analogous to those descriptive of the LP FWH. For a control volume encompassing the HP FWH we may express conservation of energy as

$$\tau_{HPH} \frac{d}{dt} h_{HPH} = Q_{HPH} + h_{LPH} - h_{HPH} \tag{D.34}$$

and conservation of mass and momentum as

$$\tau'_{HPH} \frac{d}{dt} w_{HPH} = w_2 - w'_2 + w'_{RS} - w_{HPH} \tag{D.35}$$

where

τ_{HPH} = time constant characteristic of energy transfer in HP FWH (s),

τ'_{HPH} = time constant characteristic of shell side flow rate of HP FWH (s),

h_{HPH} = enthalpy of feedwater exiting tube side HP FWH (J/kg),

Q_{HPH} = energy transferred from shell to tube side in HP FWH (J/kg).

Again energy transfer is assumed directly proportional to shell side flow and inversely proportional to tube side flow resulting in

$$Q_{HPH} = H_{HPH} \frac{w_{HPB} + w_{MS} + w_{RS}}{w_{FW}}. \tag{D.36}$$

where

H_{HPH} = heat transfer parameter of HP FWH (J/kgK),

8. Turbine Work Output

Turbine work expressions are obtained using conservation of energy as

$$E_{HP} = \eta_{HP} w_2 \left(h_2 - h_2'\right) \tag{D.37}$$

$$E_{LP} = \eta_{LP} \left(w_3 - 0.5 w_{LPB}\right)\left(h_r - h_4\right) \tag{D.38}$$

where

E_{HP} = power produced in HP turbine (W),

E_{LP} = power produced in LP turbine (W),

η_{HP} = HP turbine energy conversion efficiency = 0.86,

η_{LP} = LP turbine energy conversion efficiency = 0.83,

h_2' = isentropic enthalpy of wet steam exiting HP turbine (J/kg),

h_4 = isentropic enthalpy of steam exiting LP turbine (J/kg).

The total steam flow through the high and low pressure turbines is represented as w_2 and $\left(w_3 - 0.5 w_{LPB}\right)$, respectively, while $\left(h_s - h_2'\right)$ and $\left(h_r - h_4\right)$ represent the isentropic enthalpy drop across the high and low pressure turbines, respectively. The isentropic exit enthalpy from the LP turbine is assumed constant at

$$h_4 = 2.0887 \times 10^6 \text{ (J/kg)} \tag{D.39}$$

while the wet steam enthalpy exiting the HP turbine is represented with the following empirical state equation:

$$h_2' = 2.3822 \times 10^6 + 0.3\left(P_r - 1.3788\right) - 0.0011\left(P_r - 1.3788\right)^2 - 0.1\left(P_c - 6.894\right). \tag{D.40}$$

The turbine torque can be expressed in terms of the turbine power as:

$$T_{HP} = 120\pi E_{HP} \tag{D.41}$$

$$T_{LP} = 120\pi E_{LP} \tag{D.42}$$

for an assumed angular shaft velocity of 120π rad/s and where

T_{HP} = torque exerted on HP turbine shaft (J),

T_{LP} = torque exerted on LP turbine shaft (J).

APPENDIX D

RELIABILITY DEGRADATION DATABASES FOR THE BALANCE OF PLANT MODEL

Table V. Reliability degradation database for degradation estimation.

Component Number	**Number of Modes**	**Degradation Rate (1/h)**	**Minimum Value**	**Maximum Value**	**PDF Type**
1	3	0.0002	0	100	Gaussian
Nominal Mean	**Nominal Variance**	**Nominal Mode Probability**	**Degradation Mode I Mean**	**Degradation Mode I Variance**	**Degradation Mode I Probability**
8.80	0.20	0.333	8.36	0.20	0.333
Degradation Mode II Mean	**Degradation Mode II Variance**	**Degradation Mode II Probability**			
9.24	0.20	0.333			
Component Number	**Number of Modes**	**Degradation Rate (1/h)**	**Minimum Value**	**Maximum Value**	**PDF Type**
2	3	0.0002	0	100	Gaussian
Nominal Mean	**Nominal Variance**	**Nominal Mode Probability**	**Degradation Mode I Mean**	**Degradation Mode I Variance**	**Degradation Mode I Probability**
23.31	1.36	0.333	22.15	1.36	0.333
Degradation Mode II Mean	**Degradation Mode II Variance**	**Degradation Mode II Probability**			
24.46	1.36	0.333			

Component Number	Number of Modes	Degradation Rate (1/h)	Minimum Value	Maximum Value	PDF Type
3	3	0.0002	0	10.48×10^{-2}	Gaussian
Nominal Mean	**Nominal Variance**	**Nominal Mode Probability**	**Degradation Mode I Mean**	**Degradation Mode I Variance**	**Degradation Mode I Probability**
5.24×10^{-2}	0.68×10^{-2}	0.333	5.50×10^{-2}	0.68×10^{-2}	0.333
Degradation Mode II Mean	**Degradation Mode II Variance**	**Degradation Mode II Probability**			
4.98×10^{-2}	0.68×10^{-2}	0.333			

Component Number	Number of Modes	Degradation Rate (1/h)	Minimum Value	Maximum Value	PDF Type
4	3	0.0002	0	13.34×10^{-4}	Gaussian
Nominal Mean	**Nominal Variance**	**Nominal Mode Probability**	**Degradation Mode I Mean**	**Degradation Mode I Variance**	**Degradation Mode I Probability**
6.67×10^{-4}	0.11×10^{-4}	0.333	7.34×10^{-4}	0.11×10^{-4}	0.333
Degradation Mode II Mean	**Degradation Mode II Variance**	**Degradation Mode II Probability**			
6.00×10^{-4}	0.11×10^{-4}	0.333			

Component Number	Number of Modes	Degradation Rate (1/h)	Minimum Value	Maximum Value	PDF Type
5	3	0.0002	0	88.58	Gaussian
Nominal Mean	**Nominal Variance**	**Nominal Mode Probability**	**Degradation Mode I Mean**	**Degradation Mode I Variance**	**Degradation Mode I Probability**
44.29	4.9	0.333	42.08	4.9	0.333
Degradation Mode II Mean	**Degradation Mode II Variance**	**Degradation Mode II Probability**			
46.50	4.9	0.333			

Component Number	Number of Modes	Degradation Rate (1/h)	Minimum Value	Maximum Value	PDF Type
6	3	0.0002	0	1521.2	Gaussian
Nominal Mean	**Nominal Variance**	**Nominal Mode Probability**	**Degradation Mode I Mean**	**Degradation Mode I Variance**	**Degradation Mode I Probability**
760.6	1446.28	0.333	722.57	1446.28	0.333
Degradation Mode II Mean	**Degradation Mode II Variance**	**Degradation Mode II Probability**			
798.63	1446.28	0.333			

Component Number	Number of Modes	Degradation Rate (1/h)	Minimum Value	Maximum Value	PDF Type
7	3	0.0002	0	1609.4	Gaussian
Nominal Mean	**Nominal Variance**	**Nominal Mode Probability**	**Degradation Mode I Mean**	**Degradation Mode I Variance**	**Degradation Mode I Probability**
804.7	1602.0	0.333	764.47	1602.0	0.333
Degradation Mode II Mean	**Degradation Mode II Variance**	**Degradation Mode II Probability**			
844.94	1602.0	0.333			

Component Number	Number of Modes	Degradation Rate (1/h)	Minimum Value	Maximum Value	PDF Type
8	3	0.0002	0	100	Gaussian
Nominal Mean	**Nominal Variance**	**Nominal Mode Probability**	**Degradation Mode I Mean**	**Degradation Mode I Variance**	**Degradation Mode I Probability**
86.0	18.49	0.333	81.7	18.49	0.333
Degradation Mode II Mean	**Degradation Mode II Variance**	**Degradation Mode II Probability**			
90.3	18.49	0.333			

Component Number	Number of Modes	Degradation Rate (1/h)	Minimum Value	Maximum Value	PDF Type
9	3	0.0002	0	100	Gaussian
Nominal Mean	**Nominal Variance**	**Nominal Mode Probability**	**Degradation Mode I Mean**	**Degradation Mode I Variance**	**Degradation Mode I Probability**
83.0	17.22	0.333	78.85	17.22	0.333
Degradation Mode II Mean	**Degradation Mode II Variance**	**Degradation Mode II Probability**			
87.15	17.22	0.333			

Table VI. Reliability degradation database for degradation detection and isolation.

Component Number	Number of Modes	Degradation Rate (1/h)	Minimum Value	Maximum Value	PDF Type
1	3	0.0002	0	100	Uniform
Nominal Mean	**Nominal Variance**	**Nominal Mode Probability**	**Degradation Mode I Mean**	**Degradation Mode I Variance**	**Degradation Mode I Probability**
8.80	0.20×10^{-4}	0.333	9.68	0.20×10^{-4}	0.333
Degradation Mode II Mean	**Degradation Mode II Variance**	**Degradation Mode II Probability**			
7.92	0.20×10^{-4}	0.333			
Component Number	**Number of Modes**	**Degradation Rate (1/h)**	**Minimum Value**	**Maximum Value**	**PDF Type**
2	3	0.0002	0	100	Uniform
Nominal Mean	**Nominal Variance**	**Nominal Mode Probability**	**Degradation Mode I Mean**	**Degradation Mode I Variance**	**Degradation Mode I Probability**
23.31	1.36×10^{-4}	0.333	23.78	1.36×10^{-4}	0.333
Degradation Mode II Mean	**Degradation Mode II Variance**	**Degradation Mode II Probability**			
22.84	1.36×10^{-4}	0.333			
Component Number	**Number of Modes**	**Degradation Rate (1/h)**	**Minimum Value**	**Maximum Value**	**PDF Type**
3	3	0.0002	0	10.48×10^{-2}	Uniform
Nominal Mean	**Nominal Variance**	**Nominal Mode Probability**	**Degradation Mode I Mean**	**Degradation Mode I Variance**	**Degradation Mode I Probability**
5.24×10^{-2}	0.68×10^{-6}	0.333	5.34×10^{-2}	0.68×10^{-6}	0.333
Degradation Mode II Mean	**Degradation Mode II Variance**	**Degradation Mode II Probability**			
5.14×10^{-2}	0.68×10^{-6}	0.333			

Component Number	Number of Modes	Degradation Rate (1/h)	Minimum Value	Maximum Value	PDF Type
4	3	0.0002	0	13.34×10^{-4}	Uniform
Nominal Mean	**Nominal Variance**	**Nominal Mode Probability**	**Degradation Mode I Mean**	**Degradation Mode I Variance**	**Degradation Mode I Probability**
6.67×10^{-4}	0.11×10^{-8}	0.333	6.80×10^{-4}	0.11×10^{-8}	0.333
Degradation Mode II Mean	**Degradation Mode II Variance**	**Degradation Mode II Probability**			
6.54×10^{-4}	0.11×10^{-8}	0.333			

Component Number	Number of Modes	Degradation Rate (1/h)	Minimum Value	Maximum Value	PDF Type
5	3	0.0002	0	88.58	Uniform
Nominal Mean	**Nominal Variance**	**Nominal Mode Probability**	**Degradation Mode I Mean**	**Degradation Mode I Variance**	**Degradation Mode I Probability**
44.29	4.9×10^{-4}	0.333	45.18	4.9×10^{-4}	0.333
Degradation Mode II Mean	**Degradation Mode II Variance**	**Degradation Mode II Probability**			
43.40	4.9×10^{-4}	0.333			

Component Number	Number of Modes	Degradation Rate (1/h)	Minimum Value	Maximum Value	PDF Type
6	3	0.0002	0	1521.2	Uniform
Nominal Mean	**Nominal Variance**	**Nominal Mode Probability**	**Degradation Mode I Mean**	**Degradation Mode I Variance**	**Degradation Mode I Probability**
760.6	1446.28×10^{-4}	0.333	836.66	1446.28×10^{-4}	0.333
Degradation Mode II Mean	**Degradation Mode II Variance**	**Degradation Mode II Probability**			
684.54	1446.28×10^{-4}	0.333			

Component Number	Number of Modes	Degradation Rate (1/h)	Minimum Value	Maximum Value	PDF Type
7	3	0.0002	0	1609.4	Uniform
Nominal Mean	**Nominal Variance**	**Nominal Mode Probability**	**Degradation Mode I Mean**	**Degradation Mode I Variance**	**Degradation Mode I Probability**
804.7	1602.0×10^{-4}	0.333	885.17	1602.0×10^{-4}	0.333
Degradation Mode II Mean	**Degradation Mode II Variance**	**Degradation Mode II Probability**			
724.23	1602.0×10^{-4}	0.333			

Component Number	Number of Modes	Degradation Rate (1/h)	Minimum Value	Maximum Value	PDF Type
8	3	0.0002	0	100	Uniform
Nominal Mean	**Nominal Variance**	**Nominal Mode Probability**	**Degradation Mode I Mean**	**Degradation Mode I Variance**	**Degradation Mode I Probability**
86.0	18.49×10^{-4}	0.333	94.6	18.49×10^{-4}	0.333
Degradation Mode II Mean	**Degradation Mode II Variance**	**Degradation Mode II Probability**			
77.4	18.49×10^{-4}	0.333			

Component Number	Number of Modes	Degradation Rate (1/h)	Minimum Value	Maximum Value	PDF Type
9	3	0.0002	0	100	Uniform
Nominal Mean	**Nominal Variance**	**Nominal Mode Probability**	**Degradation Mode I Mean**	**Degradation Mode I Variance**	**Degradation Mode I Probability**
83.0	17.22×10^{-4}	0.333	91.3	17.22×10^{-4}	0.333
Degradation Mode II Mean	**Degradation Mode II Variance**	**Degradation Mode II Probability**			
74.7	17.22×10^{-4}	0.333			

REFERENCES

[1] M. D. Carelli, et al., "The Design and Safety Features of the IRIS Reactor," Proceedings of ICONE11 Tokyo, Japan (2003).

[2] R. Isermann, "Integration of Fault Detection and Diagnosis Methods," in *Issues of Fault Diagnosis for Dynamic Systems*, R. J. Patton, P. M. Frank, and R. N. Clark, Eds. London: Springer-Verlag (2000)

[3] V. Venkatasubramanian, R. Rengaswamy, K. Yin, and S. N. Kavuri, "A Review of Process Fault Detection and Diagnosis, Part I: Quantitative Model-Based Methods," *Computers and Chemical Engineering*, **27**, 293 (2003).

[4] R. N. Clark, "The Dedicated Observer Approach to Instrument Fault Detection," Proceedings of 15th IEEE-CDC,237, Fort Lauderdale, FL (1979).

[5] P. M. Frank, "Fault Diagnosis in Dynamic Systems Using Analytical and Knowledge-Based Redundancy - A Survey and Some New Results," *Automatica*, **26**, 3, 459 (1990).

[6] Y. Xiong and M. Saif, "Robust and Nonlinear Fault Diagnosis Using Sliding Mode Observers," Proceedings of IEEE Conference on Decision and Control,567, Orlando, FL (2001).

[7] J. J. Gertler and D. Singer, "A New Structural Framework for Parity Equation-Based Failure Detection and Isolation," *Automatica*, **26**, 381 (1990).

[8] J. J. Gertler, "Analytical Redundancy Methods in Fault Detection and Isolation - Survey and Synthesis," Proceedings of IFAC/IMACS - Symposium on Fault Detection, Supervision and Safety for Technical Processes, SAFEPROCESS'91,9, Baden Baden, FRG (1991).

[9] J. J. Gertler, *Fault Detection and Diagnosis in Engineering Systems*. New York: Marcel Dekker (1998).

[10] A. Hagenblad, F. Gustafsson, and I. Klein, "A Comparison of Two Methods for Stochastic Fault Detection: The Parity Space Approach and Principal Components Analysis," Proceedings of IFAC Symposium on System Identification, Rotterdam, NL (2003).

[11] H. U. Voss, J. Timmer, and J. Kurths, "Nonlinear Dynamical System Identification from Uncertain and Indirect Measurements," *International Journal of Bifurcation and Chaos*, **14**, 6, 1905 (2004).

[12] R. Isermann, "On Fuzzy Logic Applications for Automatic Control, Supervision, and Fault Diagnosis," *IEEE Transactions on Systems, Man, Cybernetics B*, **28**, 221 (1998).

[13] Y. Maki and K. A. Loparo, "A Neural Network Approach to Fault Detection and Diagnosis in Industrial Processes," *IEEE Transactions on Control Systems and Technology*, **5**, 529 (1997).

[14] Q. Zhao and Z. Xu, "Design of a Novel Knowledge-Based Fault Detection and Isolation Scheme," *IEEE Transactions on Systems, Man, Cybernetics B*, **34**, 2, 1089 (2004).

[15] M. Borairi and H. Wang, "Actuator and Sensor Fault Diagnosis of Nonlinear Dynamic Systems via Genetic Neural Networks and Adaptive Parameter Estimation Technique," Proceedings of IEEE International Conference on Control Applications, Trieste, Italy (1998).

[16] S. M. El-Shal and A. S. Morris, "A Fuzzy Expert System for Faut Detection in Statistical Process Control of Industrial Processes," *IEEE Transactions on Systems, Man, Cybernetics C*, **30**, 281 (2000).
[17] R. Burnett, J. F. Watson, and S. Elder, "The Application of Modern Signal Processing Techniques to Rotor Fault Detection and Location within Three Phase Induction Motors," Proceedings of Instrumentation and Measurement Technology,426, Waltham, MA (1995).
[18] R. Dunia and S. J. Qin, "Joint Diagnosis of Process and Sensor Faults Using Principal Component Analysis," *Control Engineering Practice*, **6**, 4, 457469 (1998).
[19] B. Alpay, H. E. Garcia, and T.-S. Yoo, "A Hybrid Model Combining First-Principles and Data Driven Models for On-Line Condition Monitoring," Proceedings of 5th International Topical Meeting on Nuclear Plant Instrumentation Control and Human Machine Interface Technology, Albuquerque, NM (2006).
[20] B. Yildiz, M. W. Golay, K. P. Maynard, and M. Maghraoui, "Development of A Hybrid Intelligent System for On-Line Monitoring of Nuclear Power Plant Operations," Proceedings of 6th International Conference on Probabilistic Safety Assessment and Management (2002).
[21] P. Wang and T. Aldemir, "Some Improvements in State/Parameter Estimation Using the Cell-to-Cell Mapping Technique," *Nuclear Science and Engineering*, **147**, 1 (2004).
[22] I. Munteanu and T. Aldemir, "On-Line Risk Monitoring of Dynamic Systems," Proceedings of International Topical Meeting on Probabilistic Safety Assessment, Detriot, MI (2002).
[23] O. Cappe, E. Moulines, and T. Ryden, *Inference in Hidden Markov Models*. New York ; London: Springer (2005).
[24] Z. Chen, "Bayesian Filtering: From Kalman Filters to Particle Filters, and Beyond," McMaster University, Hamilton, ON Technical Report (2003).
[25] R. F. Stengel, *Optimal Control and Estimation*. New York: Dover Publications (1994).
[26] I. N. Sinitsyn, "Ill-posed problems of Online Conditionally Optimal Filtering," Proceedings of Ill-Posed Problems in Natural Sciences,174, Moscow (1991).
[27] S. Sarkka, "Recursive Bayesian Inference on Stochastic Differential Equations," Ph.D. Dissertation,Helsinki University of Technology (2006).
[28] M. S. Arulampalam, S. Maskell, N. Gordon, and T. Clapp, "A Tutorial on Particle Filters for Online Nonlinear/Non-Gaussian Bayesian Tracking," *IEEE Transactions on Signal Processing*, **50**, 2, 174 (2002).
[29] D. Simon, *Optimal State Estimation : Kalman, H. [infinity] and nonlinear approaches*. New Jersey: John Wiley (2006).
[30] S. Bhaumik, M. Srinivasan, S. Sadhu, and T. K. Ghoshal, "Adaptive Grid Solution of Risk Sensitive Estimator Problems," Proceedings of IEEE Indicon,356, Chennai, India (2005).
[31] R. E. Kalman, "A New Approach to Linear Filtering and Prediction Problems," *Transaction of the ASME - Journal of Basic Engineering*, **82**, 35 (1960).

[32] A. H. Jazwinski, *Stochastic Processes and Filtering Theory*. New York: Academic Press (1970).
[33] S. J. Julier and J. K. Uhlmann, "A New Extension of the Kalman Filter to Nonlinear Systems," Proceedings of SPIE - Int. Soc. Opt. Eng.,182, Orlando, FL (1997).
[34] S. J. Julier and J. K. Uhlmann, "A New Approach for Filtering Nonlinear Systems," Proceedings of Proc. of Am. Contr. Conf., Seattle, WA (1995).
[35] D. Alspach and H. Sorenson, "Nonlinear Bayesian Estimation using Gaussian Sum Approximations," *IEEE Transactions on Automatic Control*, **17**, 4, 439 (1972).
[36] S. Julier, J. Uhlmann, and H. F. Durrant-Whyte, " A New Method for the Nonlinear Transformation of Means and Covariances in Filters and Estimators," *IEEE Transactions on Automatic Control*, **45**, 3, 477 (2000).
[37] D. Tenne and T. Singh, "The Higher Order Unscented Filter," Proceedings of American Control Conference, Denver, CO (2003).
[38] S. J. Julier and J. K. Uhlmann, "A Consistent, Debiased Method for Converting Between Polar and Cartesian Coordinate Systems," Proceedings of Aerosense, 11th Int. Symp. Aerosp./Defense Sensing, Simulat. Contr., Orlando, FL (1997).
[39] B. Alpay, J. P. Holloway, and J. C. Lee, "Degradation Monitoring in IRIS Steam Generators," Proceedings of Joint International Topical Meeting on Mathematics & Computations and Supercomputing in Nuclear Applications, Monterey, CA (2007).
[40] "RELAP5/MOD3.3 Code Manual, Volume 1: Code Structure, Systems Models, and Solution Methods," NUREG/CR-5535, Rev. 1, U.S. Nuclear Regulatory Commission (2001).
[41] T. Bajs, et al., "Development of RELAP5 Nodalization for IRIS Non-LOCA Transient Analysis," Proceedings of Nuclear Mathematical and Computational Sciences, Gatlinburg, TN (2003).
[42] A. Doucet, N. d. Freitas, and N. Gordon, *Sequential Monte Carlo Methods in Practice*. New York: Springer-Verlag (2001).
[43] J. Geweke, "Bayesian Inference in Econometric Models using Monte Carlo Integration," *Econometrica*, **57**, 6, 1317 (1989).
[44] A. Doucet, "On Sequential Monte Carlo Methods for Bayesian Filtering," University of Cambridge, UK, Technical Report (1998).
[45] A. Kong, J. S. Liu, and W. H. Wong, "Sequential Imputations and Bayesian Missing Data Problems," *J. Amer. Stat. Assoc.*, **89**, 425, 278 (1994).
[46] N. J. Gordon, D. J. Salmond, and A. F. M. Smith, "Novel Approach to Nonlinear/Non-Gaussian Bayesian State Estimation," *IEEE Proceedings-F*, **140**, 2, 107 (1993).
[47] J. D. Hol, T. B. Schon, and F. Gustafsson, "On Resampling Algorihms for Particle Filters," Proceedings of Nonlinear Statistical Signal Processing, Cambridge, UK (2006).
[48] S. E. Aumeier, B. Alpay, J. C. Lee, and A. Z. Akcasu, "Probabilistic Techniques for Diagnosis of Multiple Component Degradations," *Nuclear Science and Engineering*, **153** (2006).

[49] S. E. Aumeier, B. Alpay, and J. C. Lee, "Adaptive Kalman Filtering for Diagnosis of Multiple Component Degradations," *Trans. Am. Nucl. Soc.*, **91** (2004).
[50] B. Alpay and J. C. Lee, "Degradation Monitoring through Unscented Kalman Filtering," *Trans. Am. Nucl. Soc.*, **94** (2006).
[51] B. Alpay and J. P. Holloway, "Improved Convergence of a Filter for Degraded State Estimation Using Multiple Data Sources," *Trans. Am. Nucl. Soc.*, **96** (2007).
[52] B. Alpay and J. P. Holloway, "Degradation Estimation by Particle Filtering Using Multiple Data Sources," *Trans. Am. Nucl. Soc.*, **97** (2007).
[53] A. T. Nelson, "Nonlinear Estimation and Modeling of Noisy Time-Series by Dual Kalman Filtering Methods," Ph.D. Dissertation, Oregon Graduate Institute (2000).
[54] M. Basseville and I. V. Nikiforov, *Detection of Abrupt Changes : Theory and Application*. Englewood Cliffs, N.J.: Prentice Hall (1993).
[55] A. H. Jazwinski, "Limited Memory Optimal Filtering," *IEEE Transactions on Automatic Control*, **13**, 558 (1968).
[56] A. S. Willsky, "A Survey of Desing Methods for Failure Detection Systems," *Automatica*, **12**, 601 (1976).
[57] T. J. Tarn and J. Zaborszky, "A Practical Nondiverging Filter," *AIAA*, **8**, 1127 (1970).
[58] Q. Xia, M. Rao, Y. Ying, and X. Shen, "Adaptive Fading Kalman Filter with an Application," *Automatica*, **30**, 8, 1333 (1994).
[59] R. K. Mehra, "Approaches to Adaptive Filtering," *IEEE Transactions on Automatic Control*, **17**, 5, 693 (1972).
[60] P. V. G. Shankar, "Simulation Model of a Nuclear Reactor Turbine," *Nuclear Engineering and Design*, **44**, 269 (1977).
[61] I. Grogorenlo, *Optimal Control and Forecasting of Complex Dynamical Systems*. Singapore: World Scientific (2006).
[62] R. Storm and K. Price, "Differential Evolution - A Simple and Efficient Adaptive Scheme for Global Optimization over Continuous Spaces," *Journal of Global Optimization*, **11**, 341 (1997).
[63] Z. Fathi, W. F. Ramirez, and O. Aarna, "Joint State and Parameter Estimation for a Nuclear Reactor with Fast and Slow Modes," *Optimal Control, Applications and Methods*, **13**, 105 (1992).
[64] J. Liu and M. West, "Combined Parameter and State Estimation in Simulation-Based Filtering," in *Sequential Monte Carlo Methods in Practice*, A. Doucet, N. d. Freitas, and N. Gordon, Eds. New York: Springer-Verlag (2001)
[65] L. Tierney, "Markov Chains for Exploring Posterior Distributions," *The Annals of Statistics*, **22**, 4, 1701 (1994).
[66] W. R. Gilks and C. Berzuini, "Following a Moving Target - Monte Carlo Inference for Dynamic Bayesian Models," *Journal of the Royal Statistical Society B*, **63**, 1, 127 (2001).
[67] R. M. Neal, "Probabilistic Inference Using Markov Chain Monte Carlo Methods," Department of Computer Science, University of Toronto, Technical Report CRG-TR-93-1 (1993).
[68] C. Andrieu, N. d. Freitas, A. Doucet, and M. I. Jordan, "An Introduction to MCMC for Machine Learning," *Machine Learning*, **50**, 5 (2003).

[69] N. Metropolis, et al., "Equations of State Calculations by Fast Computing Machines," *Journal of Chemical Physics*, **21**, 1087 (1953).
[70] W. K. Hastings, "Monte Carlo Sampling Methods Using Markov Chains and Their Applications," *Biometrika*, **57**, 97 (1970).
[71] C. P. Robert and G. Casella, *Monte Carlo Statistical Methods*, 2nd ed. New York: Springer (2004).
[72] C. Berzuini, N. G. Best, W. Gilks, and C. Larizza, "Dynamic Conditional Independent Models and Markov Chain Monte Carlo Methods," *Journal of American Statistical Association*, **92**, 1403 (1997).
[73] P. K. Samantha, W. E. Vesely, F. Hsu, and M. Subudhi, "Degradation Modeling with Application to Aging and Maintenance Effectiveness Evaluations," NUREG/CR-5612 (March 1991).
[74] D. Stock, W. E. Vesely, and P. K. Samantha, "Development and Application of Degradation Modeling to Define Maintenance Practices," NUREG/CR-5967 (1994).
[75] W. E. Vesely and P. K. Samantha, "Applications of Reliability Degradation Analysis," NUREG/CR-6415 (February 1996).
[76] J. Lawless and M. Crowder, "Covariates and Random Effects in a Gamma Process Model with Application to Degradation and Failure," *Lifetime Data Analysis*, **10**, 3, 213 (2004).
[77] J. Prock, "Online Detection and Diagnosis of Sensor and Process Faults in Nuclear Power Plants," in *Issues of Fault Diagnosis for Dynamic Systems*, R. J. Patton, P. M. Frank, and R. N. Clark, Eds. London: Springer-Verlag (2000)
[78] M. Hou, "Fault Detection and Isolation for Descriptor Systems," in *Issues of Fault Diagnosis for Dynamic Systems*, R. J. Patton, P. M. Frank, and R. N. Clark, Eds. London: Springer-Verlag (2000)
[79] P. Li and V. Kadirkamanathan, "Particle Filtering Based Likelihood Ratio Approach to Fault Diagnosis in Nonlinear Stochastic Systems," *IEEE Transactions on Systems, Man, Cybernetics C*, **31**, 337 (2001).
[80] C. Andrieu, A. Doucet, S. S. Singh, and V. B. Tadic, "Particle Methods for Change Dtetection, System Identification, and Control," *Proceedings of the IEEE*, **92**, 3, 423 (2004).
[81] R. K. Mehra and J. Peschon, "An Innovations Approach to Fault Detection and Diagnosis in Dynamic Systems " *Automatica*, **7**, 637 (1971).
[82] R. N. Clark, "A Simplified Instrument Detection Scheme," *IEEE Transactions on Aerospace Electronic Systems*, **14**, 558 (1978).
[83] G. Roberts, A. Gelman, and W. Gilks, "Weak Convergence and Optimal Scaling of Random Walk Metropolis Algorithms " *The Annals of Applied Probability*, **7**, 110 (1997).
[84] W. J. Kearton, *Steam Turbine Theory and Practice*: Pitman and Sons (1961).
[85] S. E. Aumeier, "Probabilistic Techniques for Multi-Component System Diagnostics and Surveillance," Ph.D. Dissertation, Nuclear Engineering, The University of Michigan (1994).